Title
Mechanisms for Adenovirus E1A Evasion of Innate Immunity and Promotion of Cellular De-differentiation

Author
Zemke, Nathan Robert

Publication Date
2018

Peer reviewed|Thesis/dissertation

UNIVERSITY OF CALIFORNIA

Los Angeles

Mechanisms for Adenovirus E1A Evasion of Innate Immunity and Promotion of Cellular De-differentiation

A dissertation submitted in partial satisfaction of the requirements for the degree Doctor of Philosophy in Molecular Biology

by

Nathan Robert Zemke

2019

ABSTRACT OF THE DISSERTATION

Mechanisms for Adenovirus E1A Evasion of Innate Immunity and Promotion of Cellular De-differentiation

By

Nathan Robert Zemke

Doctor of Philosophy in Molecular Biology

University of California, Los Angeles 2019

Professor Arnold J. Berk, Chair

Viruses are ancient pathogens that evolved to exploit cellular processes through sophisticated mechanisms that promote viral replication. Human adenovirus type 2 (Ad2) and the closely related adenovirus 5 (Ad5) are small DNA tumor viruses that infect the exposed, terminally differentiated epithelial cells that line the upper respiratory tract. Normally, these terminally differentiated cells are suboptimal for DNA virus replication since they have low rates of deoxynucleotide synthesis due to their cell cycle arrest in G_0. Ad2 overcomes this obstacle through expression of early region genes immediately after infection that establish a cellular environment suitable for efficient viral replication. The first Ad2 gene expressed upon infection, early-region 1A (E1A). The N-terminal half of adenovirus E1A assembles multimeric complexes with host proteins that repress differentiated cell functions and force host cells into S-phase. In

contrast, the functions of E1A's C-terminal interactions with FOXK, DCAF7 and CtBP are unknown. We found that these interactions modulate RAS signaling, and that a single E1A molecule must bind all three of these host proteins to suppress activation of a subset of IFN-stimulated genes (ISGs). These ISGs were otherwise induced in primary respiratory epithelial cells at 12h p.i. This delayed activation of ISGs required IRF3 and coincided with an ~10-fold increase in IRF3 from protein stabilization. The induced IRF3 bound to chromatin and localized to the promoters of activated ISGs. While IRF3, STAT1/2 and IRF9 all greatly increased in concentration, there were no corresponding mRNA increases, suggesting that E1A regulates the stabilities of these key activators of innate immune responses, as shown directly for IRF3.

As a viral oncogene E1A promotes oncogenic transformation of primary mammalian cells. In cancer differentiated cells are reprogrammed leading to loss of their cell identity. Likewise, expression of E1A suppresses cellular differentiation. We find that eliminating E1A in Ad5-transformed human embryonic kidney cells induces their re-differentiation into cells with characteristics of mesenchymal stem cells (MSC). De-repression of ~1500 genes and a dramatic change in morphology requires chromatin association of Hippo pathway-regulated co-activators YAP and TAZ. E1A causes YAP/TAZ cytoplasmic sequestration. After eliminating E1A, YAP/TAZ are transported into the nucleus where they associate with poised enhancers with DNA-bound TEAD4 and H3K4me1. These complexes induce histone H3 acetylation, chromatin remodeling, and cohesin loading to establish enhancers and eventually super-enhancers. Activation of YAP/TAZ following E1A elimination requires signaling from the actin cytoskeleton. These results together with earlier studies suggest that YAP/TAZ are master regulators of MSC differentiation that function in a developmental check-point controlled by

signaling from the actin cytoskeleton informing the cell if it is in the correct cellular and tissue environment before initiating terminal differentiation.

The dissertation of Nathan Robert Zemke is approved.

Douglas L. Black

Siavash K. Kurdistani

Matteo Pellegrini

Otto O. Yang

Arnold J. Berk, committee chair

University of California, Los Angeles

2019

TABLE OF CONTENTS

LIST OF ILLUSTRATIONS/ FIGURES AND TABLES

Chapter 1

Chapter 2

Chapter 3

Chapter 4

ACKNOWLEDGEMENTS

First and foremost, I must express my deepest gratitude to every member of the Berk lab past and present who has given me help. At the top of this list is my mentor, Arnie Berk. Few people could live up to a reputation as remarkable as the one Arnie possesses, yet he exceeds it. Although I now recognize how little I knew before beginning graduate school, I at least had the good sense to know that the Berk lab was doing important research. The prospect of joining the Berk lab was one of the reasons I chose to come to UCLA. After several other faculty members told me how highly they thought of Arnie, with more than one even referring to him as their hero, I knew my inclination was correct. Thank you Arnie for allowing me to join your lab and for the invaluable scientific training, which will stay with me forever.

Without Carol Eng the Berk lab would not be what it is. Her expertise and motherly guidance went beyond the duties of lab manager. There was never a problem she couldn't fix. Thank you for making everyday easier. Many graduate students and post-docs I worked beside not only helped me at the bench, they also provided friendships that made my graduate school experience markedly more enjoyable. Thank you Sarah Johnson, Miguel Nava, Dawei Gou, and Emily Hsu for your technical and intellectual guidance and cherished companionships.

I have had the extreme fortune of having the expert guidance from high authorities in the field of molecular biology. Thank you to my esteemed thesis committee members: Arnie Berk, Siavash Kurdistani, Doug Black, Matteo Pellegrini, and Otto Yang. Also, thank you Mike Carey, the program director of the gene regulation affinity group for your constructive review of my academic abilities.

Regardless of my pursuit, my family is unconditionally supportive. I thank my parents for filling me with confidence and providing me with a foundation that has allowed me to

accomplish goals that would have otherwise been impossible. Lastly and largely, thank you Sara Fisher for being by my side virtually my entire graduate school career. I can't express how grateful I am to have you in my life.

VITA

2011	B.S., Molecular Biology University of California, San Diego La Jolla, CA
2011 – 2012	Research Project Assistant HHV-6 Foundation Santa Barbara, CA
2012 – 2019	Doctoral Graduate Student Researcher Molecular Biology Interdepartmental Program Gene Regulation Affinity Group University of California, Los Angeles Los Angeles, CA
2013 – 2016	Virology and Gene Therapy Pre-doctoral Trainee University of California, Los Angeles Los Angeles, CA
2014 – 2015	Teaching Assistant Microbiology, Immunology and Molecular Genetics University of California, Los Angeles Los Angeles, CA
2016 – 2017	Whitcome Pre-doctoral Fellowship Trainee University of California, Los Angeles Los Angeles, CA
2018	Teaching Assistant Chemistry and Biochemistry University of California, Los Angeles Los Angeles, CA

PUBLICATIONS AND PRESENTATIONS

Zemke, N.R., Gou, D., Berk, A.J., (2019). Dedifferentiation by adenovirus E1A due to inactivation of Hippo pathway effectors YAP and TAZ. Genes Dev. Published in Advance June 6, 2019, doi: 10.1101/gad.324814.119

Nava, M., Dutta, P., Zemke, N.R., Farias-Eisner, R., Vadgama, J. V., and Wu, Y. (2019). Transcriptomic and ChIP-sequence interrogation of EGFR signaling in HER2+ breast cancer cells reveals a dynamic chromatin landscape and S100 genes as targets. BMC Med. Genomics *12*.

Hsu, E., Pennella, M.A., Zemke, N.R., Eng, C., and Berk, A.J. (2018). Adenovirus E1A Activation Domain Regulates H3 Acetylation Affecting Varied Steps in Transcription at Different Viral Promoters. J. Virol. *92*, 1–18.

Zemke, N.R., and Berk, A.J. (2017). The Adenovirus E1A C Terminus Suppresses a Delayed Antiviral Response and Modulates RAS Signaling. Cell Host Microbe 22, 789–800.e5.

Zemke, N.R., and Berk, A.J., (2017). Adenovirus E1A C-terminal region forms a complex to block the long term interferon response. DNA TUMOUR VIRUS MEETING 2017, *poster presentation*.

Zemke, N.R., and Berk, A.J., (2015). Adenovirus e1a regulates expression of late cell cycle genes through its interactions with DYRK1A/B. MECHANISMS OF EUKARYOTIC TRANSCRIPTION MEETING, 2015.

Ferrari, R., Gou, D., Jawdekar, G., Johnson, S.A., Nava, M., Su, T., Yousef, A.F., Zemke, N.R., Pellegrini, M., Kurdistani, S.K., et al. (2014). Adenovirus small E1A employs the lysine acetylases p300/CBP and tumor suppressor Rb to repress select host genes and promote productive virus infection. Cell Host Microbe *16*, 663–676.

Niesman, I.R., Zemke, N., Fridolfsson, H.N., Haushalter, K.J., Levy, K., Grove, A., Schnoor, R., Finley, J.C., Patel, P.M., Roth, D.M., *et al*. (2013). Caveolin isoform switching as a molecular, structural, and metabolic regulator of microglia. Molecular and cellular neurosciences *56*, 283-297.

Scheurer, M.E., Pritchett, J.C., Amirian, E.S., Zemke, N.R., Lusso, P., and Ljungman, P. (2013). HHV-6 encephalitis in umbilical cord blood transplantation: a systematic review and meta-analysis. Bone marrow transplantation *48*, 574-580.

Niesman, I.R., Saldana, M., Zemke, N., Head, B.P., Patel, H.H., (2012). Cav-3 is associated with and regulates the actin skeleton in BV2 cells. *FASEB J*. **26**:656.18

N.R. Zemke, F.L. Diaz, B.M. Emerson. c-Myc specific defects of TGFβ1/smad signaling in human cancer cells. *Saltman Quarterly*. 8: 51, 2011.

Niesman, I.R., Patton, M., Zemke, N., Levy, K., Ali, S.S., Head, B.P., Patel, H.H., (2011) Caveolin regulation of microglial activation and proliferation. *FASEB J*. **25**:1007.1

I.R. Niesman, J. Bonds, M. Pearn, N. Zemke, D. Roth, H. Patel, P. Patel, B. Head. Caveolin-1 ko mouse represents a novel non-mutational model of Alzheimer's disease (ad). Program No. 855.8. 2010 Neuroscience Meeting Planner. San Diego, CA: Society for Neuroscience, 2010. *poster presentation*.

CHAPTER 1

INTRODUCTION

Human adenoviruses are a family of small DNA tumor viruses consisting of more than 50 unique serotypes classified into seven species/groups based on nucleic acid homology. Since 1962, when it was found that adenovirus serotype 12 (Ad12) caused tumors in inoculated hamsters (Trentin et al., 1962), the oncogenic potential of adenoviruses have been extensively investigated. Others quickly confirmed the tumorigenicity of Ad12 (Huebner et al., 1962), and additionally found that Ad18 and Ad31 also induced tumors in inoculated hamsters (Stich and Yohn, 1967). This observation classified adenoviruses as either oncogenic, if belonging to species A (Ad12, Ad18 and Ad31), while other serotypes were classified as non-oncogenic, except for serotypes belonging to species B (Ad3 and Ad7), which were found to cause slow and infrequent tumor growth (Williams et al., 1995).

In the same decade, adenoviruses were shown to immortalize cultured rodent cells through stable transformation regardless of the serotype's tumorigenic capacity in animals (Freeman et al., 1967; McBride and Wiener, 1964). Furthermore, cultured transformed cells by non-oncogenic Ad2 could induce tumors when introduced into immunosuppressed rats (Gallimore, 1972), and cells transformed by the closely related Ad5 were found to induce tumors in immunodeficient nude mice (Bernards et al., 1983). After it was discovered that adenoviral DNA was retained in the transformed cell (Fujinaga and Green, 1970), researchers looked for which viral genes are required for transformation. It was soon shown that the left end of the adenoviral genome (the first ~15%) was common to Ad2-transformants in independent experiments and is necessary for the transformation phenotype (Gallimore, 1974; Graham et al., 1974). Viral RNA mapping of transcripts expressed from this region became known as early region transcripts (Flint et al., 1975; Sharp et al., 1974), later called early region 1 A and B (E1A and E1B). The first reported isolation of adenovirus transformed human cells came in 1977 by

Graham and colleagues, where they established the commonly used HEK293 cell line by introducing fragmented Ad5 DNA into cells from human embryonic kidney tissue (Graham et al., 1977). It was clear that the cells retained ~4.5% of the left end of the Ad5 genome when the authors performed hybridization of labeled cellular RNA with restriction fragments of Ad5 DNA. Indeed, HEK293 express E1 transforming proteins encoded by E1A and E1B.

More extensive analysis on the transformative properties of E1 genes revealed that E1A alone could induce partial transformation, but both E1A and E1B are necessary for stable transformation (Barker and Berk, 1987; van den Elsen et al., 1983; Houweling et al., 1980). This observation was explained when it was shown that E1B's main function is to block premature lytic phase by inhibiting p53-mediated apoptosis (Sarnow et al., 1982; Yew and Berk, 1992). However, the complementation necessity of E1B for transformation is replaceable by oncogenic Ras (EJ bladder carcinoma Ha-ras-1) (Jochemsen et al., 1986).

The sequences of E1A from different primate adenoviruses reveal four highly homologous regions known as conserved regions 1-4 (CR1 – CR4) (Avvakumov et al., 2004; Kimelman, 1986). Most of E1A's functions can be mapped to one or more of its conserved regions. Early in infection the most abundant E1A messages are two alternatively spliced mRNAs, 12S and 13S, which differ only by the size of the intron removed during mRNA maturation (Svensson et al., 1983). The 12S message encodes the small E1A protein (e1a) of 243 amino acids with CR3 removed by intronic splicing, while the 13S message encodes large E1A, 289 amino acids long consisting of all four conserved regions. CR3 is a C-4 zinc finger containing transcription activation domain (Lillie and Green, 1989). Large E1A, via CR3, mainly functions to activate other early adenoviral genes by recruiting mediator complex and P300/CBP to their promoters to stimulate assembly of transcription pre-initiation complexes (Boyer et al.,

1999; Hsu et al., 2018; Liu and Green, 1994). In the absence of large E1A, the small isoform, e1a, induces DNA synthesis and transformation in growth-arrested cells; therefore CR3 is not necessary for this process (Braithwaite et al., 1983; Spindler et al., 1985). Detailed mutagenesis assays revealed that the transforming activity of E1A requires the first N-terminal 80 amino acids, which encompass CR1 and CR2 (Barbeau et al., 1994; Quinlan et al., 1988).

Co-immunoprecipitation experiments have found several large and small E1A-interacting cellular proteins. The first of which was the retinoblastoma tumor suppressor, Rb1, (Whyte et al., 1988). Shortly after this finding, antigens from unrelated tumor viruses were also found to target Rb1 and its homologues, p107 and p130 (collectively Rbs) (DeCaprio et al., 1988; Dyson et al., 1989). Through these interactions the regulation of the cell cycle by E2F family transcription factors was elucidated. E1A's CR2 (Fig. 1), and other viral antigens, interact with Rbs through an LXCXE high affinity Rb-binding motif (Nevins et al., 1997). E1A displaces Rbs from E2F transcription factors bound at the promoters of several cell cycle regulating genes (Ghosh and Harter, 2003). This exposes E2F activation domains and transcriptionally activates genes that drive cells into S phase. The mechanism of E2F pathway derepression by modulating the activity of the Rbs provides a partial explanation for e1a-mediated transformation. While this process is sufficient to force cells from G_0/G_1 to S phase, it is not, however, sufficient for complete passage around the cell cycle (Stein et al., 1990; Wang et al., 1993).

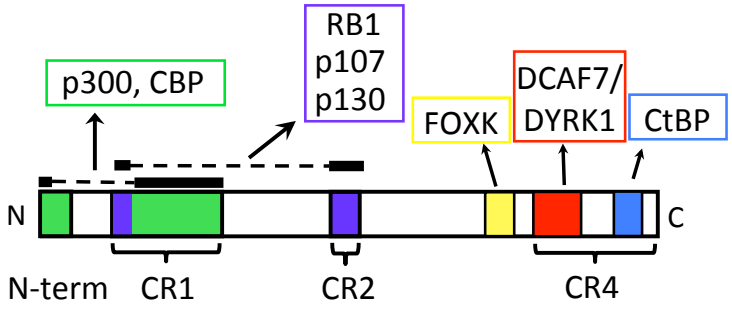

Figure 1 e1a protein interaction map
e1a protein interaction map with p300/CBP (green), RBs (purple), FOXK (yellow), DCAF7 complexes (red), and CtBP (blue), and e1a conserved regions (CR) 1, 2, and 4 (CR3 is uniquely in large E1A).

An interaction of CR1 and e1a's N-terminus with a protein of about 300 kDa, designated p300 (Fig. 1), was found to be necessary for E1A-mediated transformation (Stein et al., 1990). Later determined to be a paralog of CBP (CREB-binding protein), p300, which also binds E1A at the same region, are histone acetyl transferases that function as global transcriptional coactivators by relaxing chromatin structure and interacting with RNA Polymerase II and general transcription factors (Chan and La Thangue, 2001; Vo and Goodman, 2001). Mutations in p300/CBP are common in malignancies, which may relate to their co-regulation of tumor suppression with critical tumor suppressors such as p53 (Iyer et al., 2004). CBP and p300 are found at active enhancer regions and transcription start sites of actively transcribed genes and their enrichment generally correlate with levels of gene activation (Holmqvist and Mannervik, 2013). Small E1A causes a global cellular decrease in histone H3 Lysine 18 and 27 (H3K18 and H3K27) acetylation dependent on its interaction with p300/CBP, suggesting H3K18 and H3K27 to be substrates of p300/CBP (Horwitz et al., 2008). Furthermore, e1a redirects p300 to E2F-enriched promoters where H3K18ac is selectively increased and transcription is activated (Ferrari et al., 2008, 2014).

While e1a only needs to interact with either Rbs or P300/CBP to drive quiescent baby rat kidney cells into S-Phase (Howe et al., 1990), it must retain both interactions to achieve immortalization in cooperation with E1B or oncogenic Ras (Stein et al., 1990). Since these discoveries, several other E1A interacting proteins have been described, although the functional consequences of these interactions are not as well understood (Berk, 2005).

The less studied C-terminal region (exon 2 encoded) of E1A was demonstrated to suppress transformation. Ras-cooperative transformation experiments revealed that e1a with C-terminal deletions enhanced transformation (Subramanian et al., 1989; Boyd et al., 1993). A deletion of amino acids 225-238 gave a hypertransforming phenotype comparable to a large deletion removing most of the C-terminus. This construct deleted a conserved PXDLS motif and corresponded with the loss of interaction with the first discovered small E1A C-terminal binding protein, C-teriminal binding protein (CtBP). While it is presently unknown why these E1A deletion mutants cause these phenotypes, it is likely due to the loss of interaction with proteins such as CtBP1/2 (collectively CtBP), the DDB1- and CUL4-associated factor 7 (DCAF7), Dual specificity tyrosine-phosphorylation-regulated kinase 1A and 1B (DYRK1A/B) and Forkhead box protein K1 and K2 (FOXK1/2) (Fig. 1).

CtBP binds directly to proteins with a PXDLS amino acid motif, located in E1A CR4 (Fig. 1; Schaeper et al., 1995). This region is highly conserved amongst the different serotypes of human and simian adenoviruses. Repressors with PXDLS-like motifs such as Zeb1/2 and Znf217 recruit CtBP dimers to target promoters (Postigo and Dean, 1999; Quinlan et al., 2006). CtBP acts as a corepressor by inhibiting transcription of tumor suppressor genes like *INK4* and *CDH1* as well as proapoptotic genes like *PERP*, *BAX* and *PMAIP1* (Yousef et al., 2012). CtBP promotes repression through its association with chromatin-modifying enzymes such as histone

deactylases and demethylases (Shi et al., 2003). Small molecule inhibition of CtBP has been shown to specifically target transformed and cancer cells for apoptosis (Straza et al., 2010). It was reported that e1a mediates the acetylation of CtBP by p300/CBP which eliminates CtBP repression of *PMAIP1* (E-Cadherin) (Zhao et al., 2006). The derepression of tumor suppressors through e1a inhibition of normal CtBP activity may help explain the Ras-cooperative hypertransformation phenotype when PXDLS is deleted. However, how e1a modulates CtBP activity has yet to be determined.

DCAF7 (a.k.a. HAN11 or WDR68) directly interacts with a broad region of E1A's CR4 (Fig. 1; Glenewinkel et al., 2016). E1A mutations that interfere with DCAF7 binding also exhibit hypertransformation in cooperation with oncogenic Ras (Komorek et al., 2010). DCAF7 is a CLR4 E3 ubiquitin ligase substrate receptor (Jin et al., 2006). DCAF7 binds to the dual specificity tyrosine-regulated kinases, DYRK1A and DYRK1B (collectively DYRK1) as well as the homeodomain interacting protein kinase 2, HIPK2 (Miyata and Nishida, 2011; Ritterhoff et al., 2010). Through its direct binding to E1A, DCAF7 is responsible for E1A's indirect association with DYRK1 and HIPK2 (Glenewinkel et al., 2016). Genetic studies in zebrafish and *Drosophila* indicate that DCAF7 orthologs are necessary for normal organismal development (Morriss et al., 2013; Nissen et al., 2006). The *DYRK1A* locus is present on the Down syndrome critical region of Chromosome 21 (Shapiro, 1999). *DYRK1A* kinase activity is believed to be involved in cell cycle control and differentiation through activating transcription factors such as NFAT, Gli and Foxo1 and the Notch signaling pathway (Arron et al., 2006; Fernandez-Martinez et al., 2009; Woods et al., 2001). DYRK1A activates p53-mediated cell death by directly phosphorylating p53 at Ser15 and promoting activation of *CDKN1A* (p21) in embryonic neuronal cells (Park et al., 2010). Also, DYRK1A has been shown to promote formation of the DREAM

complex, which represses E2F-regulated cell cycle-dependent genes during quiescence (Sadasivam and DeCaprio, 2013). DYRK1A achieves this through phosphorylation of Lin52, a component of the MuvB core, which increases its affinity for p130, p107 and repressive E2Fs to form the DREAM complex. Inhibition of DYRK1A causes derepression of DREAM-regulated genes and formation of Myb-MuvB (MMB) complex, which activates many G2/M-phase genes (Litovchick et al., 2011).

The forkhead (FKH) family transcription factors regulate genes involved in cell cycle progression, apoptosis and differentiation. Two FKH members FOXK1 and FOXK2 (collectively FOXK) have been identified to interact with a serine/threonine rich region of E1A just upstream of CR4 in its C-terminal half (Fig. 1; Komorek et al., 2010). This region is conserved among the human adenoviruses classified in "species C" and is highly similar to a domain of the human papillomavirus E6 protein, also known to bind FOXK (Komorek et al., 2010). This interaction is mediated through a Forkhead association (FHA) domain that is unique to FOXK and facilitates an interaction with phosphorylated residues (Durocher and Jackson, 2002; Komorek et al., 2010). *Foxk1* knockout mice show a severe growth defect as well as impairment of myogenic cell proliferation (Garry et al., 2000). This may be due to its repression of *FOXO4* in myogenic progenitors (Shi et al., 2010). Furthermore, synchronous U2OS cells lose cell cycle oscillations when FOXK1 is knocked down (Grant et al., 2012). While FOXK1 has been the more extensively studied homolog, FOXK2, was found to co-regulate AP-1 activated genes by recruiting AP-1 to chromatin (Ji et al., 2012). Furthermore, ChIP-seq experiments have found that FOXK1 is also enriched at AP-1 binding sites (Grant et al., 2012). Little is known about the functional consequences of the FOXK1-E1A interaction, though E1A mutants that disrupt this interaction present a Ras-cooperative hypertransformation phenotype (Komorek et al., 2010).

Bibliography

Arron, J.R., Winslow, M.M., Polleri, A., Chang, C.-P., Wu, H., Gao, X., Neilson, J.R., Chen, L., Heit, J.J., Kim, S.K., et al. (2006). NFAT dysregulation by increased dosage of DSCR1 and DYRK1A on chromosome 21. Nature *441*, 595–600.

Avvakumov, N., Kajon, A.E., Hoeben, R.C., and Mymryk, J.S. (2004). Comprehensive sequence analysis of the E1A proteins of human and simian adenoviruses. Virology *329*, 477–492.

Barbeau, D., Charbonneau, R., Whalen, S.G., Bayley, S.T., and Branton, P.E. (1994). Functional interactions within adenovirus E1A protein complexes. Oncogene *9*, 359–373.

Barker, D.D., and Berk, A.J. (1987). Adenovirus proteins from both E1B reading frames are required for transformation of rodent cells by viral infection and DNA transfection. Virology *156*, 107–121.

Berk, A.J. (2005). Recent lessons in gene expression, cell cycle control, and cell biology from adenovirus. Oncogene *24*, 7673–7685.

Bernards, R., Schrier, P.I., Bos, J.L., and Van der Eb, A.J. (1983). Role of adenovirus types 5 and 12 early region 1b tumor antigens in oncogenic transformation. Virology *127*, 45–53.

Boyd, J.M., Subramanian, T., Schaeper, U., La Regina, M., Bayley, S., and Chinnadurai, G. (1993). A region in the C-terminus of adenovirus 2/5 E1a protein is required for association with a cellular phosphoprotein and important for the negative modulation of T24-ras mediated transformation, tumorigenesis and metastasis. EMBO J. *12*, 469–478.

Boyer, T.G., Martin, M.E., Lees, E., Ricciardi, R.P., and Berk, A.J. (1999). Mammalian Srb/Mediator complex is targeted by adenovirus E1A protein. Nature *399*, 276–279.

Braithwaite, A.W., Cheetham, B.F., Li, P., Parish, C.R., Waldron-Stevens, L.K., and Bellett, A.J. (1983). Adenovirus-induced alterations of the cell growth cycle: a requirement for expression of E1A but not of E1B. J. Virol. *45*, 192–199.

Chan, H.M., and La Thangue, N.B. (2001). p300/CBP proteins: HATs for transcriptional bridges and scaffolds. J. Cell Sci. *114*, 2363–2373.

DeCaprio, J.A., Ludlow, J.W., Figge, J., Shew, J.Y., Huang, C.M., Lee, W.H., Marsilio, E., Paucha, E., and Livingston, D.M. (1988). SV40 large tumor antigen forms a specific complex with the product of the retinoblastoma susceptibility gene. Cell *54*, 275–283.

Durocher, D., and Jackson, S.P. (2002). The FHA domain. FEBS Lett. *513*, 58–66.

Dyson, N., Howley, P.M., Munger, K., and Harlow, E. (1989). The human papilloma virus-16 E7 oncoprotein is able to bind to the retinoblastoma gene product. Science *243*, 934–937.

van den Elsen, P., Klein, B., Dekker, B., van Ormondt, H., and van der Eb, A. (1983). Analysis of virus-specific mRNAs present in cells transformed with restriction fragments of adenovirus type 5 DNA. J. Gen. Virol. *64*, 1079–1090.

Fernandez-Martinez, J., Vela, E.M., Tora-Ponsioen, M., Ocana, O.H., Nieto, M.A., and Galceran, J. (2009). Attenuation of Notch signalling by the Down-syndrome-associated kinase DYRK1A. J. Cell Sci. *122*, 1574–1583.

Ferrari, R., Pellegrini, M., Horwitz, G.A., Xie, W., Berk, A.J., and Kurdistani, S.K. (2008). Epigenetic reprogramming by adenovirus e1a. Science *321*, 1086–1088.

Ferrari, R., Gou, D., Jawdekar, G., Johnson, S.A., Nava, M., Su, T., Yousef, A.F., Zemke, N.R., Pellegrini, M., Kurdistani, S.K., et al. (2014). Adenovirus small E1A employs the lysine acetylases p300/CBP and tumor suppressor Rb to repress select host genes and promote productive virus infection. Cell Host Microbe *16*, 663–676.

Flint, S.J., Gallimore, P.H., and Sharp, P.A. (1975). Comparison of viral RNA sequences in adenovirus 2-transformed and lytically infected cells. J. Mol. Biol. *96*, 47–68.

Freeman, A.E., Vanderpool, E.A., Black, P.H., Turner, H.C., and Huebner, R.J. (1967). Transformation of primary rat embryo cells by a weakly oncogenic adenovirus--type 3. Nature *216*, 171–173.

Fujinaga, K., and Green, M. (1970). Mechanism of viral carcinogenesis by DNA mammalian viruses. VII. Viral genes transcribed in adenovirus type 2 infected and transformed cells. Proc. Natl. Acad. Sci. U. S. A. *65*, 375–382.

Gallimore, P.H. (1972). Tumour production in immunosuppressed rats with cells transformed in vitro by adenovirus type 2. J. Gen. Virol. *16*, 99–102.

Gallimore, P.H. (1974). Viral DNA in transformed cells. II. A study of the sequences of adenovirus 2 DNA IN NINE LINES OF TRANSFORMED RAT CELLS USING SPECIFIC FRAGMENTS OF THE VIRAL GENOME;. J. Mol. Biol. *89*, 49–72.

Garry, D.J., Meeson, A., Elterman, J., Zhao, Y., Yang, P., Bassel-Duby, R., and Williams, R.S. (2000). Myogenic stem cell function is impaired in mice lacking the forkhead/winged helix protein MNF. Proc. Natl. Acad. Sci. U. S. A. *97*, 5416–5421.

Ghosh, M.K., and Harter, M.L. (2003). A viral mechanism for remodeling chromatin structure in G0 cells. Mol. Cell *12*, 255–260.

Glenewinkel, F., Cohen, M.J., King, C.R., Kaspar, S., Bamberg-Lemper, S., Mymryk, J.S., and Becker, W. (2016). The adaptor protein DCAF7 mediates the interaction of the adenovirus E1A oncoprotein with the protein kinases DYRK1A and HIPK2. Sci. Rep. *6*, 28241.

Graham, F.L., van der Eb, A.J., and Heijneker, H.L. (1974). Size and location of the transforming region in human adenovirus type 5 DNA. Nature *251*, 687–691.

Graham, F.L., Smiley, J., Russell, W.C., and Nairn, R. (1977). Characteristics of a human cell line transformed by DNA from human adenovirus type 5. J. Gen. Virol. *36*, 59–74.

Grant, G.D., Gamsby, J., Martyanov, V., Brooks, L. 3rd, George, L.K., Mahoney, J.M., Loros, J.J., Dunlap, J.C., and Whitfield, M.L. (2012). Live-cell monitoring of periodic gene expression in synchronous human cells identifies Forkhead genes involved in cell cycle control. Mol. Biol. Cell *23*, 3079–3093.

Holmqvist, P.-H., and Mannervik, M. (2013). Genomic occupancy of the transcriptional co-activators p300 and CBP. Transcription *4*, 18–23.

Horwitz, G.A., Zhang, K., McBrian, M.A., Grunstein, M., Kurdistani, S.K., and Berk, A.J. (2008). Adenovirus small e1a alters global patterns of histone modification. Science *321*, 1084–1085.

Houweling, A., van den Elsen, P.J., and van der Eb, A.J. (1980). Partial transformation of primary rat cells by the leftmost 4.5% fragment of adenovirus 5 DNA. Virology *105*, 537–550.

Howe, J.A., Mymryk, J.S., Egan, C., Branton, P.E., and Bayley, S.T. (1990). Retinoblastoma growth suppressor and a 300-kDa protein appear to regulate cellular DNA synthesis. Proc. Natl. Acad. Sci. U. S. A. *87*, 5883–5887.

Hsu, E., Pennella, M.A., Zemke, N.R., Eng, C., and Berk, A.J. (2018). Adenovirus E1A Activation Domain Regulates H3 Acetylation Affecting Varied Steps in Transcription at Different Viral Promoters. J. Virol. *92*, 1–18.

Huebner, R., Rowe, W., and Lane, W. (1962). Oncogenic effects in hamsters of human adenovirus types 12 and 18. Proc Natl Acad Sci U S A *48*, 2051–2058.

Iyer, N.G., Ozdag, H., and Caldas, C. (2004). p300/CBP and cancer. Oncogene *23*, 4225–4231.

Ji, Z., Donaldson, I.J., Liu, J., Hayes, A., Zeef, L.A.H., and Sharrocks, A.D. (2012). The forkhead transcription factor FOXK2 promotes AP-1-mediated transcriptional regulation. Mol. Cell. Biol. *32*, 385–398.

Jin, J., Arias, E.E., Chen, J., Harper, J.W., and Walter, J.C. (2006). A Family of Diverse Cul4-Ddb1-Interacting Proteins Includes Cdt2, which Is Required for S Phase Destruction of the Replication Factor Cdt1. Mol. Cell *23*, 709–721.

Jochemsen, A.G., Bernards, R., van Kranen, H.J., Houweling, A., Bos, J.L., and van der Eb, A.J. (1986). Different activities of the adenovirus types 5 and 12 E1A regions in transformation with the EJ Ha-ras oncogene. J. Virol. *59*, 684–691.

Kimelman, D. (1986). A novel general approach to eucaryotic mutagenesis functionally identifies conserved regions within the adenovirus 13S E1A polypeptide. Mol. Cell. Biol. *6*, 1487–1496.

Komorek, J., Kuppuswamy, M., Subramanian, T., Vijayalingam, S., Lomonosova, E., Zhao, L.-J., Mymryk, J.S., Schmitt, K., and Chinnadurai, G. (2010). Adenovirus type 5 E1A and E6 proteins of low-risk cutaneous beta-human papillomaviruses suppress cell transformation through interaction with FOXK1/K2 transcription factors. J. Virol. *84*, 2719–2731.

Lillie, J.W., and Green, M.R. (1989). Transcription activation by the adenovirus E1a protein. Nature *338*, 39–44.

Litovchick, L., Florens, L.A., Swanson, S.K., Washburn, M.P., and DeCaprio, J.A. (2011). DYRK1A protein kinase promotes quiescence and senescence through DREAM complex assembly. Genes Dev. *25*, 801–813.

Liu, F., and Green, M.R. (1994). Promoter targeting by adenovirus E1a through interaction with different cellular DNA-binding domains. Nature *368*, 520–525.

McBride, W.D., and Wiener, A. (1964). IN VITRO TRANSFORMATION OF HAMSTER KIDNEY CELLS BY HUMAN ADENOVIRUS TYPE 12. Proc. Soc. Exp. Biol. Med. *115*, 870–874.

Miyata, Y., and Nishida, E. (2011). DYRK1A binds to an evolutionarily conserved WD40-repeat protein WDR68 and induces its nuclear translocation. Biochim. Biophys. Acta - Mol. Cell Res. *1813*, 1728–1739.

Morriss, G.R., Jaramillo, C.T., Mikolajczak, C.M., Duong, S., Jaramillo, M.S., and Cripps, R.M. (2013). The Drosophila wings apart gene anchors a novel, evolutionarily conserved pathway of neuromuscular development. Genetics *195*, 927–940.

Nevins, J.R., Leone, G., DeGregori, J., and Jakoi, L. (1997). Role of the Rb/E2F pathway in cell growth control. J. Cell. Physiol. *173*, 233–236.

Nissen, R.M., Amsterdam, A., and Hopkins, N. (2006). A zebrafish screen for craniofacial mutants identifies wdr68 as a highly conserved gene required for endothelin-1 expression. BMC Dev. Biol. *6*, 28.

Park, J., Oh, Y., Yoo, L., Jung, M.-S., Song, W.-J., Lee, S.-H., Seo, H., and Chung, K.C. (2010). Dyrk1A phosphorylates p53 and inhibits proliferation of embryonic neuronal cells. J. Biol. Chem. *285*, 31895–31906.

Postigo, A.A., and Dean, D.C. (1999). ZEB represses transcription through interaction with the corepressor CtBP. Proc. Natl. Acad. Sci. U. S. A. *96*, 6683–6688.

Quinlan, K.G.R., Nardini, M., Verger, A., Francescato, P., Yaswen, P., Corda, D., Bolognesi, M., and Crossley, M. (2006). Specific recognition of ZNF217 and other zinc finger proteins at a surface groove of C-terminal binding proteins. Mol. Cell. Biol. *26*, 8159–8172.

Quinlan, M.P., Whyte, P., and Grodzicker, T. (1988). Growth factor induction by the adenovirus type 5 E1A 12S protein is required for immortalization of primary epithelial cells. Mol. Cell. Biol. *8*, 3191–3203.

Ritterhoff, S., Farah, C.M., Grabitzki, J., Lochnit, G., Skurat, A. V, and Schmitz, M.L. (2010). The WD40-repeat protein Han11 functions as a scaffold protein to control HIPK2 and MEKK1 kinase functions. EMBO J. *29*, 3750–3761.

Sadasivam, S., and DeCaprio, J.A. (2013). The DREAM complex: master coordinator of cell cycle-dependent gene expression. Nat. Rev. Cancer *13*, 585–595.

Sarnow, P., Ho, Y.S., Williams, J., and Levine, A.J. (1982). Adenovirus E1b-58kd tumor antigen and SV40 large tumor antigen are physically associated with the same 54 kd cellular protein in transformed cells. Cell *28*, 387–394.

Schaeper, U., Boyd, J.M., Verma, S., Uhlmann, E., Subramanian, T., and Chinnadurai, G. (1995). Molecular cloning and characterization of a cellular phosphoprotein that interacts with a conserved C-terminal domain of adenovirus E1A involved in negative modulation of oncogenic transformation. Proc. Natl. Acad. Sci. U. S. A. *92*, 10467–10471.

Shapiro, B.L. (1999). The Down syndrome critical region. J. Neural Transm. Suppl. *57*, 41–60.

Sharp, P.A., Pettersson, U., and Sambrook, J. (1974). Viral DNA in transformed cells. I. A study of the sequences of adenovirus 2 DNA in a line of transformed rat cells using specific fragments of the viral genome. J. Mol. Biol. *86*, 709–726.

Shi, X., Bowlin, K.M., and Garry, D.J. (2010). Fhl2 interacts with Foxk1 and corepresses Foxo4 activity in myogenic progenitors. Stem Cells *28*, 462–469.

Shi, Y., Sawada, J., Sui, G., Affar, E.B., Whetstine, J.R., Lan, F., Ogawa, H., Luke, M.P.-S., Nakatani, Y., and Shi, Y. (2003). Coordinated histone modifications mediated by a CtBP co-repressor complex. Nature *422*, 735–738.

Spindler, K.R., Eng, C.Y., and Berk, A.J. (1985). An adenovirus early region 1A protein is required for maximal viral DNA replication in growth-arrested human cells. J. Virol. *53*, 742–750.

Stein, R.W., Corrigan, M., Yaciuk, P., Whelan, J., and Moran, E. (1990). Analysis of E1A-mediated growth regulation functions: binding of the 300-kilodalton cellular product correlates with E1A enhancer repression function and DNA synthesis-inducing activity. J. Virol. *64*, 4421–4427.

Stich, H.F., and Yohn, D.S. (1967). Mutagenic capacity of adenoviruses for mammalian cells. Nature *216*, 1292–1294.

Straza, M.W., Paliwal, S., Kovi, R.C., Rajeshkumar, B., Trenh, P., Parker, D., Whalen, G.F., Lyle, S., Schiffer, C.A., and Grossman, S.R. (2010). Therapeutic targeting of C-terminal binding protein in human cancer. Cell Cycle *9*, 3740–3750.

Svensson, C., Pettersson, U., and Akusjarvi, G. (1983). Splicing of adenovirus 2 early region 1A mRNAs is non-sequential. J. Mol. Biol. *165*, 475–495.

Trentin, J.J., Yabe, Y., and Taylor, G. (1962). The Quest for Human Cancer Viruses: A new approach to an old problem reveals cancer induction in hamsters by human adenovirus. Science (80-.). *137*, 835–841.

Vo, N., and Goodman, R.H. (2001). CREB-binding protein and p300 in transcriptional regulation. J. Biol. Chem. *276*, 13505–13508.

Wang, H.G., Rikitake, Y., Carter, M.C., Yaciuk, P., Abraham, S.E., Zerler, B., and Moran, E. (1993). Identification of specific adenovirus E1A N-terminal residues critical to the binding of cellular proteins and to the control of cell growth. J. Virol. *67*, 476–488.

Whyte, P., Buchkovich, K.J., Horowitz, J.M., Friend, S.H., Raybuck, M., Weinberg, R.A., and Harlow, E. (1988). Association between an oncogene and an anti-oncogene: the adenovirus E1A proteins bind to the retinoblastoma gene product. Nature *334*, 124–129.

Williams, J., Williams, M., Liu, C., and Telling, G. (1995). Assessing the role of E1A in the differential oncogenicity of group A and group C human adenoviruses. Curr. Top. Microbiol. Immunol. *199 (Pt 3*, 149–175.

Woods, Y.L., Rena, G., Morrice, N., Barthel, A., Becker, W., Guo, S., Unterman, T.G., and Cohen, P. (2001). The kinase DYRK1A phosphorylates the transcription factor FKHR at Ser329 in vitro, a novel in vivo phosphorylation site. Biochem. J. *355*, 597–607.

Yew, P.R., and Berk, A.J. (1992). Inhibition of p53 transactivation required for transformation by adenovirus early 1B protein. Nature *357*, 82–85.

Yousef, A.F., Fonseca, G.J., Cohen, M.J., and Mymryk, J.S. (2012). The C-terminal region of E1A: a molecular tool for cellular cartography. Biochem. Cell Biol. *90*, 153–163.

Zhao, L.-J., Subramanian, T., and Chinnadurai, G. (2006). Changes in C-terminal binding protein 2 (CtBP2) corepressor complex induced by E1A and modulation of E1A transcriptional activity by CtBP2. J. Biol. Chem. *281*, 36613–36623.

CHAPTER 2

The Adenovirus E1A C Terminus Suppresses a Delayed Antiviral Response and Modulates RAS Signaling

e1a mutants defective for C-terminal region-host protein interactions

We constructed Ad vectors expressing mutant e1as defective for interacting with FOXK, DCAF7 or CtBP (FOXKb$^-$, DCAF7b$^-$ and CtBPb$^-$, respectively). Multi-site combinations of individual mutations that had been previously shown to reduce these interactions were constructed in order to generate strong phenotypes that simplify genomic level analysis. To eliminate the FOXK interaction with the e1a ser/thr-rich region just N-terminal of CR4 (Fig. 1), two e1a amino acid substitutions T183A and S185A were introduced (Fig. 2.1A), previously reported to individually interfere with e1a's ability to bind FOXK (Komorek et al., 2010). Immunoprecipitation of e1a followed by western blotting validated that these amino acid substitutions inhibited e1a-association with FOXK1 but not with CtBP, DCAF7 or DYRK1A (Fig. 2.1B,C). To prevent e1a binding to DCAF7 complexes we constructed a four amino acid substitution, R212E, D225K, L226A and L227A (Fig. 2.1A), mutations previously shown to individually reduce association with DYRK1A (Cohen et al., 2013). This mutant failed to co-IP DCAF7 and one of its associated kinases, DYRK1A (Fig. 2.1C), however e1a's interactions with FOXK1 and CtBP remained intact (Fig. 2.1B). Lastly, we mutated the previously characterized e1a CtBP binding motif (Zhao et al., 2007), PLDLS, to ALAAA spanning amino acids 233-237 (Fig. 2.1A). These mutations completely eliminate e1a's ability to co-IP CtBP (Fig. 2.1B). The mutations introduced in FOXKb$^-$, DCAF7b$^-$ and CtBPb$^-$ did not interfere with e1a's ability to bind RB1 or p300 (Fig. 2.1C).

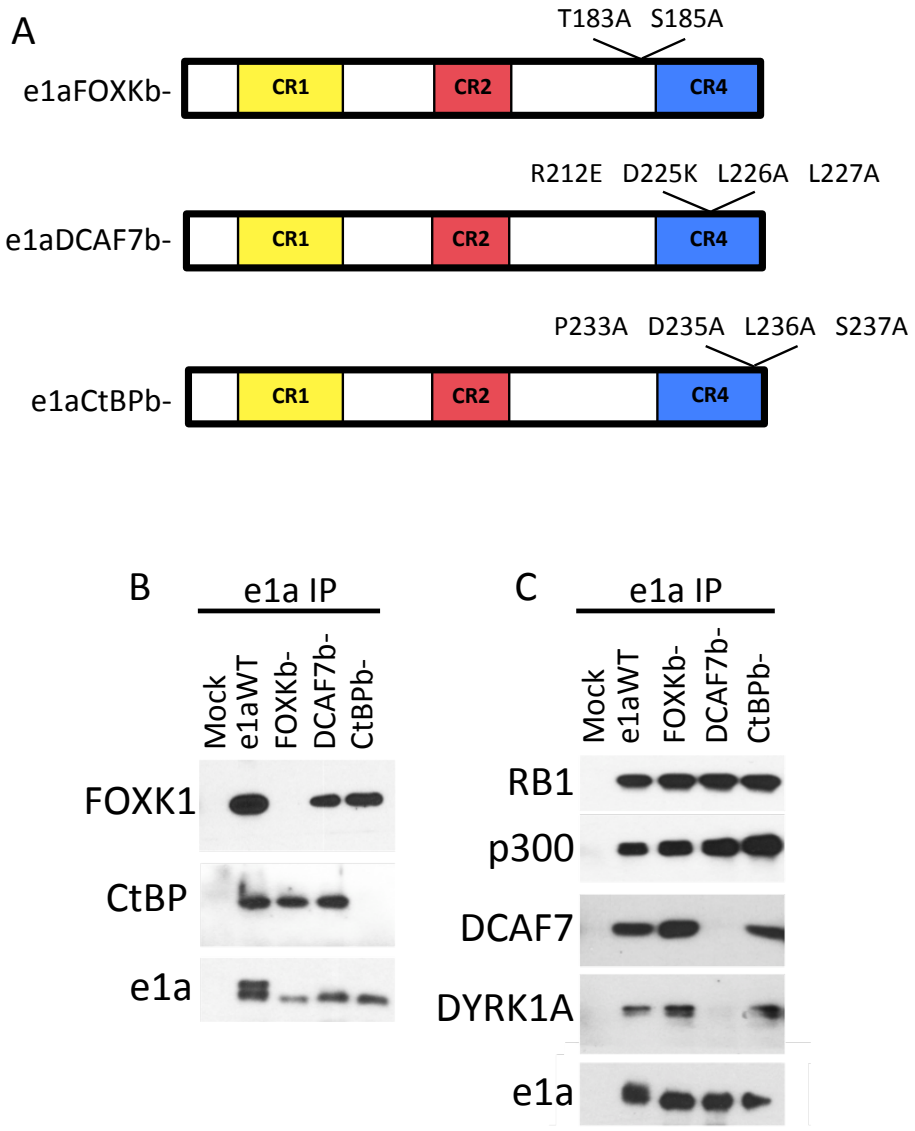

Figure 2.1 Mutations in e1a's C-terminal Region that Disrupt Interactions with Host Proteins
(A) Amino acid substitutions in e1a to disrupt FOXK binding (e1aFOXKb-), DCAF7 binding (e1aDCAF7b-), or CtBP binding (e1aCtBPb-).
(B) Extracts of HeLa cells 24h p.i. with the indicated mutant e1a expression vectors were immunoprecipitated with anti-e1a mAb (M58) and immunoprecipitates were subjected to western blotting with the indicated antibodies. **(C)** Same as (B) but with A549 cells.

WT e1a from whole cell lysate can be resolved into two differentially migrating bands by SDS-PAGE; however, the e1a C-terminal mutants exhibited primarily the faster migrating form (Fig. 2.1B, 2.2). The slower migrating form is due to phosphorylation at Ser89 (Dumont et al., 1989). Although pSer89 is reduced in the C-terminal mutants, phosphorylation at Ser173, the major site of e1a phosphorylation (Tsukamoto et al., 1986), was similar to WT e1a (Fig. 2.2).

To assay the effects of these mutations following infection, we incorporated these E1A mutants into *dl1500* background human Ad5 vectors, previously described (Ferrari et al., 2014), that do not express the large E1A isoform making them defective for activation of other adenoviral promoters and viral replication (Montell et al., 1984).

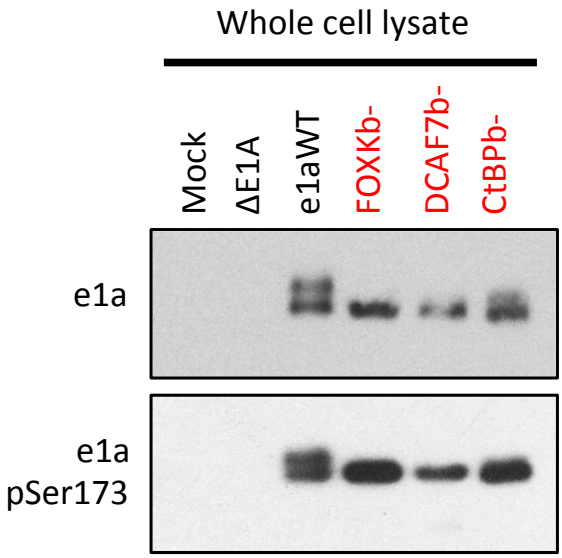

Figure 2.2 The e1a C-terminal mutations interfere with phosphorylation at Ser89 but not Ser173
Western blot of protein extract from HBTEC 24h p.i. with the indicated vectors using monoclonal antibodies against e1a (M58, top) and e1a pSer173 (bottom).

Consequences of defects in e1a interactions on regulation of cellular mRNAs and virus replication

Contact-inhibited, G1-arrested human primary bronchial/tracheal epithelial cells (HBTEC), derived from the natural host tissue for Ad2 and the closely related Ad5, were infected with FOXKb$^-$, DCAF7b$^-$, CtBPb$^-$, or a WT e1a expressing Ad5 vector (e1aWT). To control for the effects of the infectious process on cellular gene expression, cells were also mock-infected or infected with an Ad5 E1A deletion mutant (ΔE1A), *dl*312 (Jones and Shenk, 1979). For comparison, we included infections with two Ad5 vectors expressing e1a N-terminal multi-site mutants, a p300/CBP-binding mutant, e1aP300b$^-$, and an RB1/p107/p130-binding mutant, e1aRBb$^-$ (Ferrari et al., 2014). e1aP300b$^-$ and e1aRBb$^-$ were found previously to misregulate hundreds of genes that are activated or repressed by e1aWT in primary human fibroblasts (Ferrari et al., 2014).

RNA-seq was performed with RNA isolated at 24 h p.i. to determine which expressed genes (FPKM>1) were differentially expressed 2-fold or more by the e1a mutant expressing cells compared to cells expressing WT e1a. Relatively small numbers of genes were expressed differently in cells producing e1a C-terminal mutants compared to cells expressing e1aWT (105 – 146 genes overexpressed by the different C-terminal mutants compared to e1aWT, and 68 – 138 genes underexpressed (Fig. 2.3A, Table 2.1). Since the genes expressed at higher level in the e1a mutant compared to e1aWT expressing cells were also expressed at higher level than in mock-infected cells (Fig. 2.4A), they were activated by infection with the vectors expressing the e1a C-terminal mutants. The same genes were only slightly activated by theΔE1A mutant (Fig. 2.4A). Similarly, genes expressed at lower level by the C-terminal mutants than in cells expressing WT e1a were expressed at lower level than in mock-infected cells, and were reduced

less by the ΔE1A mutant (Fig. 2.4B). Consequently, these genes were more repressed by the e1a C-terminal mutants than by WT e1a. The number of genes differentially expressed by the C-terminal mutants compared to e1aWT was much lower than the number of differentially expressed genes comparing e1aP300b$^-$ and e1aRBb$^-$ to e1aWT (Fig. 2.3B, Table 2.1). These data show that the e1a-p300/CBP and e1a-RB family protein interactions regulate many more cellular genes than the e1a C-terminal interactions.

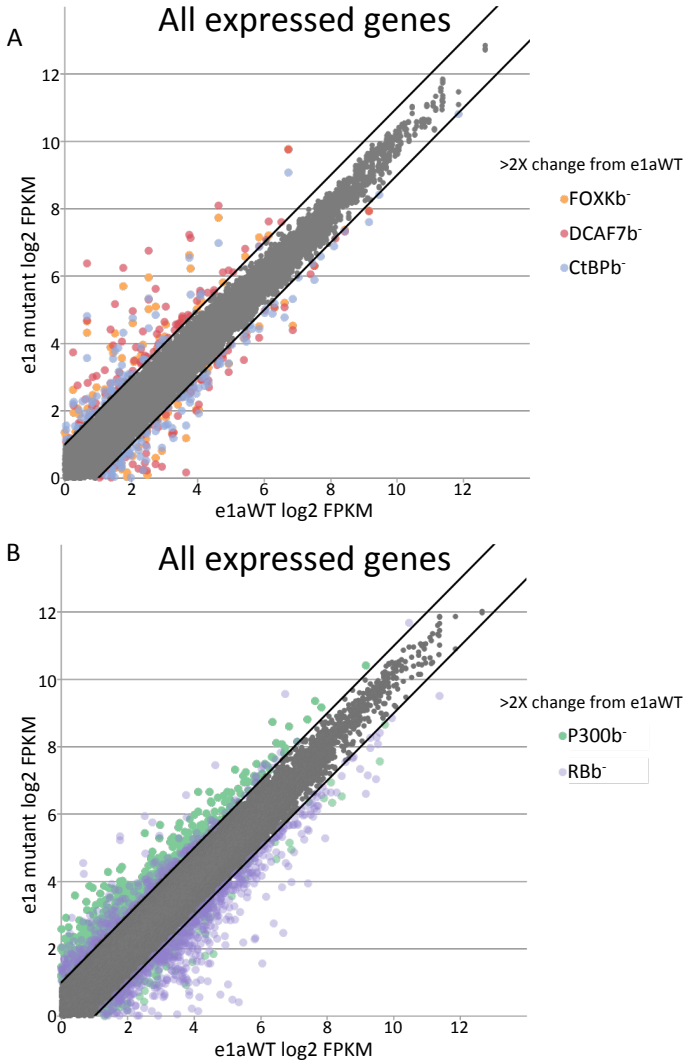

Figure 2.3 Cellular Gene Expression in HBTEC Expressing WT e1a or e1a Mutants
(A) Scatter plot of log2 FPKM values for all expressed cellular genes (>1 FPKM) in cells expressing e1a mutants (y-axis), (FOXKb$^-$, orange; DCAF7b$^-$, purple; CtBPb$^-$, blue), and e1aWT (x-axis). Colored dots above and below the black lines show the FPKMs of genes expressed at two times higher (above) or 2-fold lower (below) than the level from e1aWT. FPKMs of genes expressed within 2-fold of the mock-infected levels are shown in gray. **(B)** Same as (A) but for cells expressing the e1a p300b$^-$ mutant (green) or the RBb$^-$ mutant (purple).

Table 2.1 Number of host cell genes expressed greater than two times higher and less than two times lower than in HBTECs infected with the e1aWT vector

e1a mutant	Genes 2X > e1aWT	Genes 2X < e1aWT
P300b-	728	241
RBb-	454	790
FOXKb-	105	68
DCAF7b-	146	105
CtBPb-	119	138

Unexpectedly, there was a large overlap in the genes overexpressed in response to each of the C-terminal mutants (Fig. 2.4A,C). Most of these genes were overexpressed 2-fold or more by two or more C-terminal mutants with 52 genes being overexpressed by all three. Furthermore, when considering the three groups of genes overexpressed in response to the FOXKb$^-$, DCAF7b$^-$, and CtBPb$^-$ e1a mutants, changes in their expression relative to that in cells expressing WT e1a were similar for each of the mutants (Fig. 2.4A). These results suggest that each of the e1a C-terminal interactions influence host cell gene expression similarly. Gene ontology analysis of the 52 genes overexpressed ≥2-fold by all three mutants showed overwhelming enrichment for interferon (IFN) response genes (p=7.2 E-47) (Fig. 2.4C). Several of these genes are known to have antiviral functions (Schoggins, 2014). Motif analysis of the promoter regions of the 52 genes overexpressed by all three C-terminal mutants shows that they are highly enriched for the well-characterized IFN-stimulated response element (ISRE) (p-value 1 E-22) (Fig. 2.4C) bound by IFN-signaling activated transcription factors such as IRFs and STATs (Borden et al., 2007).

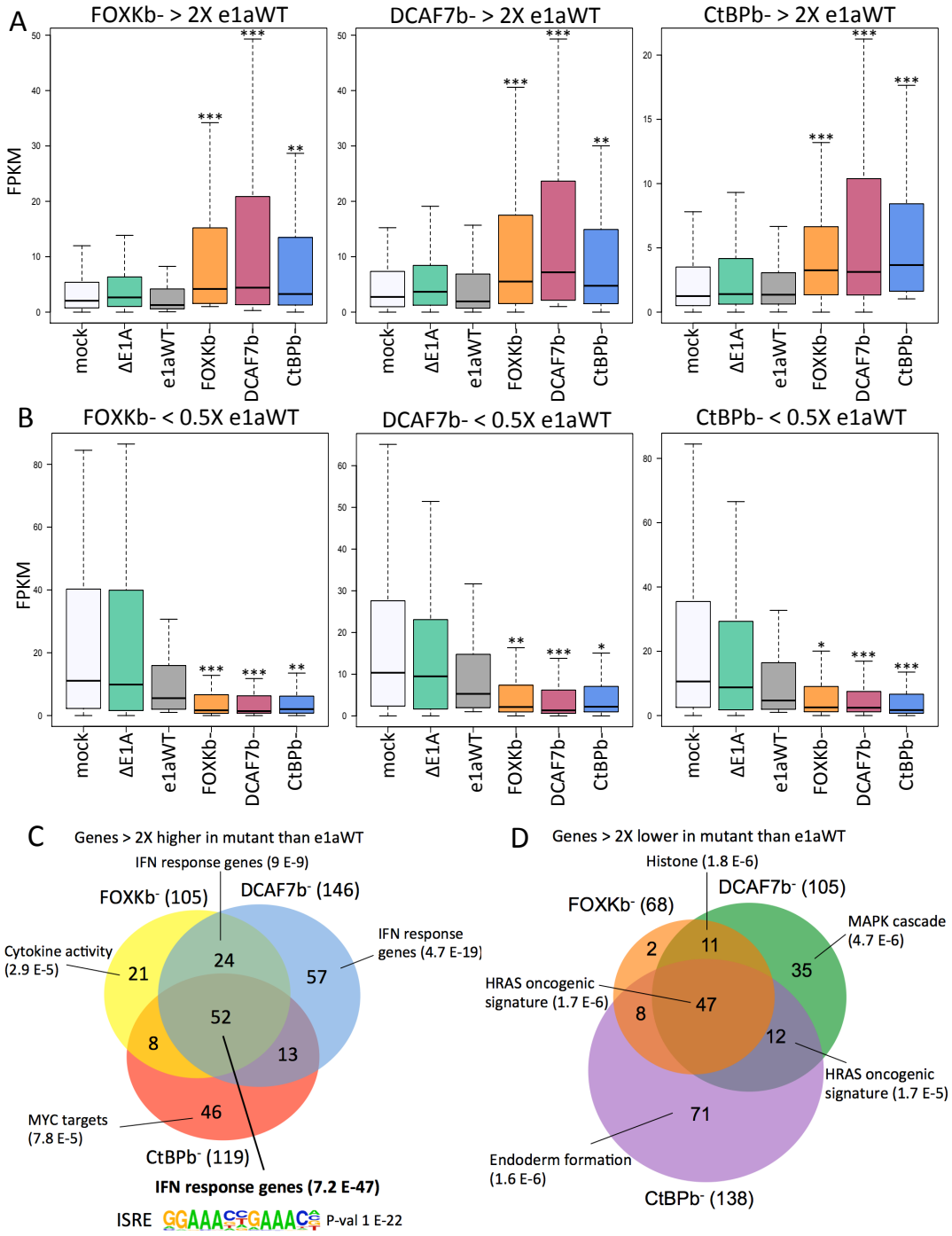

Figure 2.4 Genes Differentially Expressed by e1a C-terminal Mutants
(A) Distributions of FPKMs plotted as boxplots for the genes expressed 2-fold higher by HBTEC expressing FOXKb$^-$ (left, 105 genes), DCAF7b$^-$ (middle, 146 genes) or CtBPb$^-$ (right, 119 genes) compared to e1aWT. **(B)** Distributions of FPKM values for genes expressed 2-fold lower by HBTECs expressing FOXKb- (68 genes, left), DCAF7b- (105 genes, middle) or CtBPb- (138 genes, right) compared to e1aWT. (A,B) * $p<0.005$, ** $p<0.001$, *** $p<0.0001$ Kolmogorov-Smirnov test for significant differences from the distribution in e1aWT expressing HBTECs. **(C-D)** Venn diagrams showing overlap and gene ontologies for genes expressed 2-fold higher (C) or 2-fold lower (D) by each e1a mutant compared to e1aWT. The ISRE motif enriched in promoters of genes expressed 2-fold higher by all three e1a mutants is shown in (C).

As with the genes overexpressed by the C-terminal mutants, the genes expressed 2-fold lower in cells expressing a C-terminal mutant compared to e1aWT also showed a surprisingly high degree of overlap (Fig. 2.4B,D). Again, the distributions of expression for the three sets of genes 2-fold lower for each C-terminal mutant, were significantly lower for all three C-terminal mutants compared to e1aWT (Fig. 2.4B). These results further demonstrate that all three of the e1a C-terminal interactions regulate a similar set of cellular genes. The genes that were expressed at lower level when e1a was defective for any one of its C-terminal interactions are enriched for genes related to the HRAS oncogenic signature (Fig. 2.4D).

To test if the loss of e1a's C-terminal interactions affect virus replication through the activation of this subset of ISGs we infected separate plates of HBTEC with vectors for each of the mutants to induce the C-terminal mutant activated genes. 12h later the cells were superinfected with WT Ad5. 48h later, virus was harvested and WT Ad5 was assayed by plaque formation on HeLa cells. (The recombinant Ad5 vectors cannot form plaques on HeLa cells because they do not express the large E1A protein required to activate transcription from the other viral early promoters.) Cells initially infected with the e1a FOXKb$^-$ and CtBPb$^-$ vectors produced ~12 fold less WT Ad5 than cells pre-infected with an e1aWT expressing vector, while cells initially infected with the DCAF7b$^-$ vector produced ~28 fold less (Fig. 2.5A). These data indicate that activation and/or repression of host genes by the e1a C-terminal mutants greatly interfere with Ad5 replication. This interference with viral replication correlates with the level of the ISGs induced by the C-terminal mutants (Fig. 2.4A, 2.5A).

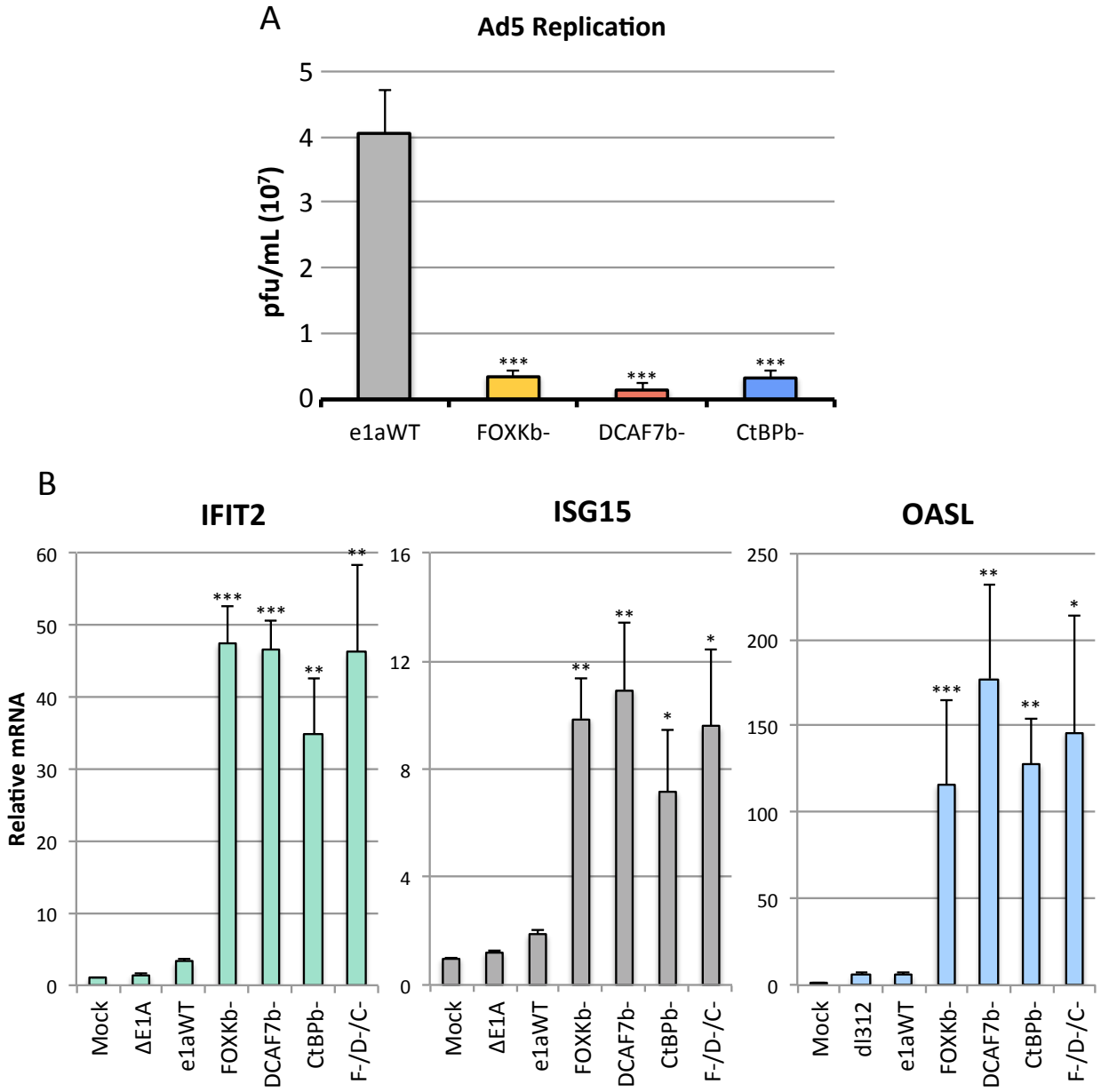

Figure 2.5 e1a Protein Complexes and Phosphorylation
(A) HBTEC were infected with vectors expressing WT e1a or the indicated C-terminal mutants. 12h later, the same cells were superinfected with WT Ad5 virus at an moi of 5 for 48h before harvesting virus. Virus titers were quantified by plaque assays on a HeLa monolayer. Data are represented as averages + S.D. **(B)** Relative levels of indicated mRNAs in HBTEC infected with vectors for the indicated e1a C-terminal mutants, as assayed by qRT-PCR. F-/D-/C- refers to cells coinfected with all three of the e1a C-terminal mutants. Data are represented as averages + S.D. **(A,B)** Data are represented as averages of three separate experiments + S.D. * $p<0.05$, ** $p<0.01$, *** $p<0.001$

The same e1a molecule must make all three C-terminal region interactions to block transcriptional activation of a subset of IFN-stimulated genes

e1a has been postulated to function as a molecular hub (Pelka et al., 2008) due to its intrinsically disordered flexible structure (Ferreon et al., 2009), allowing it to form functional multimeric complexes by simultaneously binding to multiple proteins that would otherwise not interact. While the RNA-seq results indicate that e1a must make all three C-terminal interactions with host cell proteins to reduce expression of certain ISGs, they do not address the question of whether one e1a molecule must make two or three of the three possible interactions to prevent activation of these ISGs. To address this question we performed a coinfection with vectors for all three C-terminal mutants to determine if there would be complementation of the defect in suppressing overexpression of these ISGs. Expression of IFIT2, ISG15 and OASL were similar in the coinfected cells as in cells expressing the individual mutants (Fig. 2.5B). The e1a mutants expressed in the coinfected cells can make each of the three possible bi-molecular interactions between e1a and FOXK, e1a and the DCAF7 complex, and e1a and CtBP (Fig. 2.1B,C). Yet these ISGs continued to be overexpressed, phenocopying cells expressing the single mutants. These results suggest that e1a prevents activation of these ISGs, dependent on the same e1a molecule interacting with all three C-terminal binding proteins, either simultaneously or in series. Coinfection of cells with vectors that produced equal amounts of WT e1a and the DCAF7b$^-$ mutant showed that DCAF7b$^-$ is partially dominant to e1aWT (Fig. 2.6A).

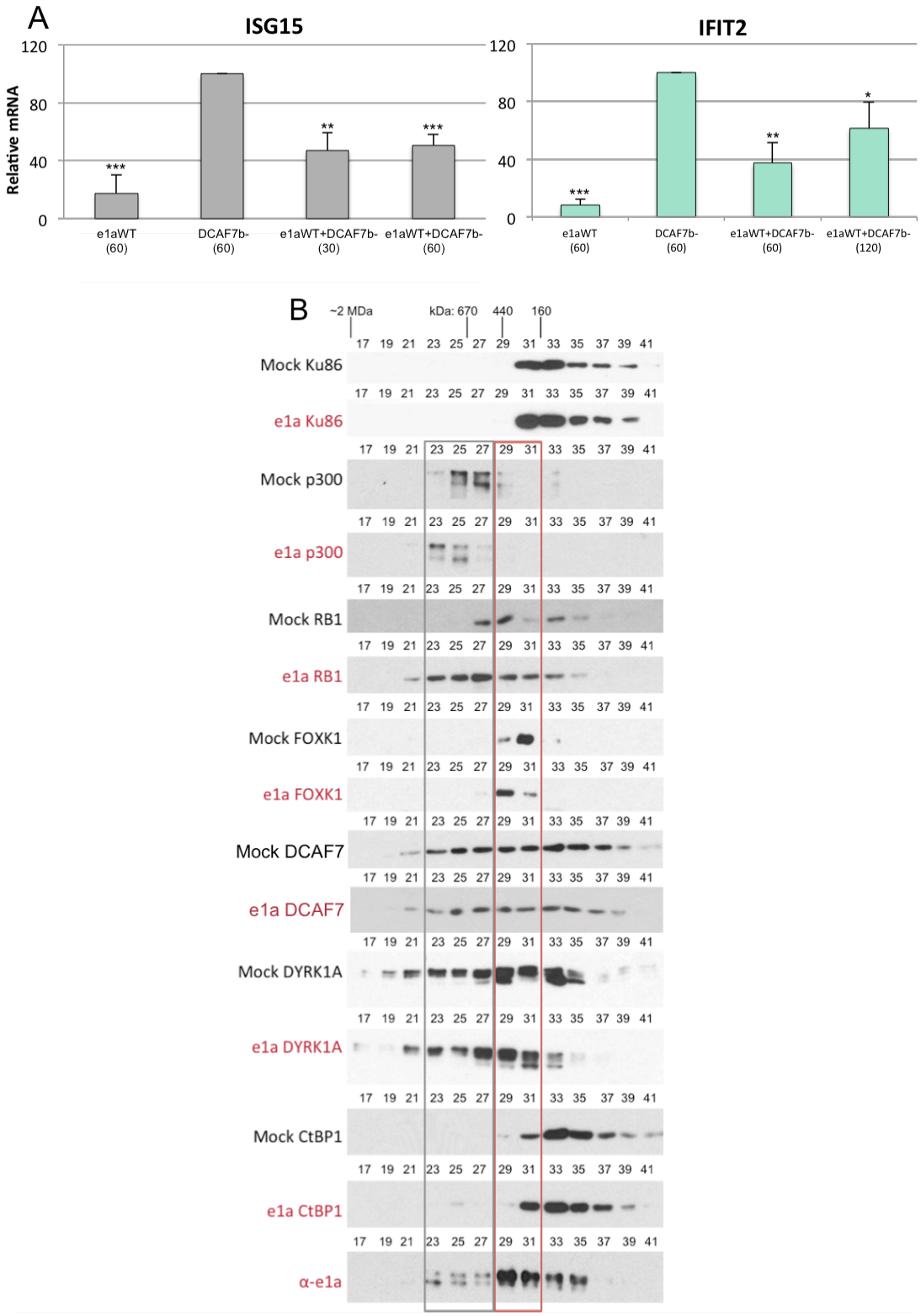

Figure 2.6 e1aWT and DCAF7b$^-$ coinfection and e1a nuclear protein complexes
(**A**) Relative levels of ISG15 and IFIT2 mRNA as assayed by qRT-PCR from HBTECs infected or coinfected with indicated vectors. moi for individual vectors indicated in parentheses. Data are represented as averages of percent of DCAF7b- (moi 60) activation + S.D. (**B**) Western blots of Superose 6 column fractions from mock or e1aWT-vector infected HeLa nuclear extract (24 h p.i.). Non-e1a interacting nuclear factor Ku86 is shown as a control.

To further explore the complexes e1a forms with cellular proteins, nuclear extracts from mock or e1aWT vector-infected HeLa cells were subjected to gel filtration on a Superose 6 column capable of resolving globular protein complexes of 0.1 to 2 MDa. In the presence of e1a, p300, RB1 and FOXK1 were shifted to earlier eluting fractions indicating incorporation into higher molecular weight complexes (Fig. 2.6B). The most dramatic shift was with RB1; a large fraction of RB1 co-eluted with p300 in the presence of e1a, consistent with our previous observations (Ferrari et al., 2014) and an earlier report of an e1a-p300-RB1 trimeric complex (Wang et al., 1995). Eluted fractions containing FOXK1 and CtBP1 were distinct from fractions containing p300-e1a-RB1 complexes (Fig. 2.6B, compare red and purple boxes). DCAF7 and DYRK1A eluted heterogeneously from high molecular weight fractions ~1 MDa, consistent with a recent report (Vona et al., 2015), through lower molecular weight fractions down to ~150 kD. These data indicate that most of the e1a-p300-RB1 complexes in the nucleus are distinct from e1a complexes containing FOXK1 and CtBP1.

Increased transcription of overexpressed ISGs

An increase in mRNA expression can be due to a higher level of transcription or increased stability of the transcript. To test if the increased expression of *IFIT2* and *ISG15* in cells expressing the C-terminal e1a mutants was due to increased transcription, we designed primers for qRT-PCR that only amplify intron-containing pre-mRNA. The higher levels of *IFIT2* and *ISG15* pre-mRNA induced by expression of the C-terminal e1a mutants (Fig. 2.7A) indicates that these genes were activated at the level of transcription. Transcriptional activation was further confirmed by the observation of activating chromatin signatures. ChIP-seq for RNA polymerase II (pol2) revealed that *ISG15* had an increase in pol2 association near the transcription start site

(TSS) as well as through the gene body after infection with the C-terminal mutant vectors but not with the e1aWT vector (Fig. 2.7B). Another ISG, *MX1* also had peaks of pol2 near the alternative TSSs that increased after infection with the C-terminal mutant vectors compared to the e1aWT vector, correlating with the increased level of mRNA (Fig. 2.7B). A similar profile was seen for *OASL* (Fig. 2.8A) and other activated ISGs (not shown). ChIP-seq was also performed on two histone modifications that correlate with levels of active transcription, acetylated (ac) H3K18 and H3K27. Both *ISG15* and *MX1* exhibited increases in H3K18ac near their TSSs after expression of the e1a C-terminal mutants but not e1aWT, while H3K27ac increased only slightly or not at all (Fig. 2.7B). *OASL* gained acetylation on both H3K18 and H3K27 near its TSS in response to the C-terminal mutants (Fig. 2.8A). The average profile of pol2 and H3K18ac near the TSS for the 52 genes overexpressed by all three C-terminal mutants showed that on average pol2 and H3K18ac were higher in cells expressing the mutants compared to e1aWT (Fig. 2.8B). The higher levels of pre-mRNA, pol2 and H3 acetylation demonstrate a transcriptional activation of these ISGs induced by the e1a C-terminal mutants.

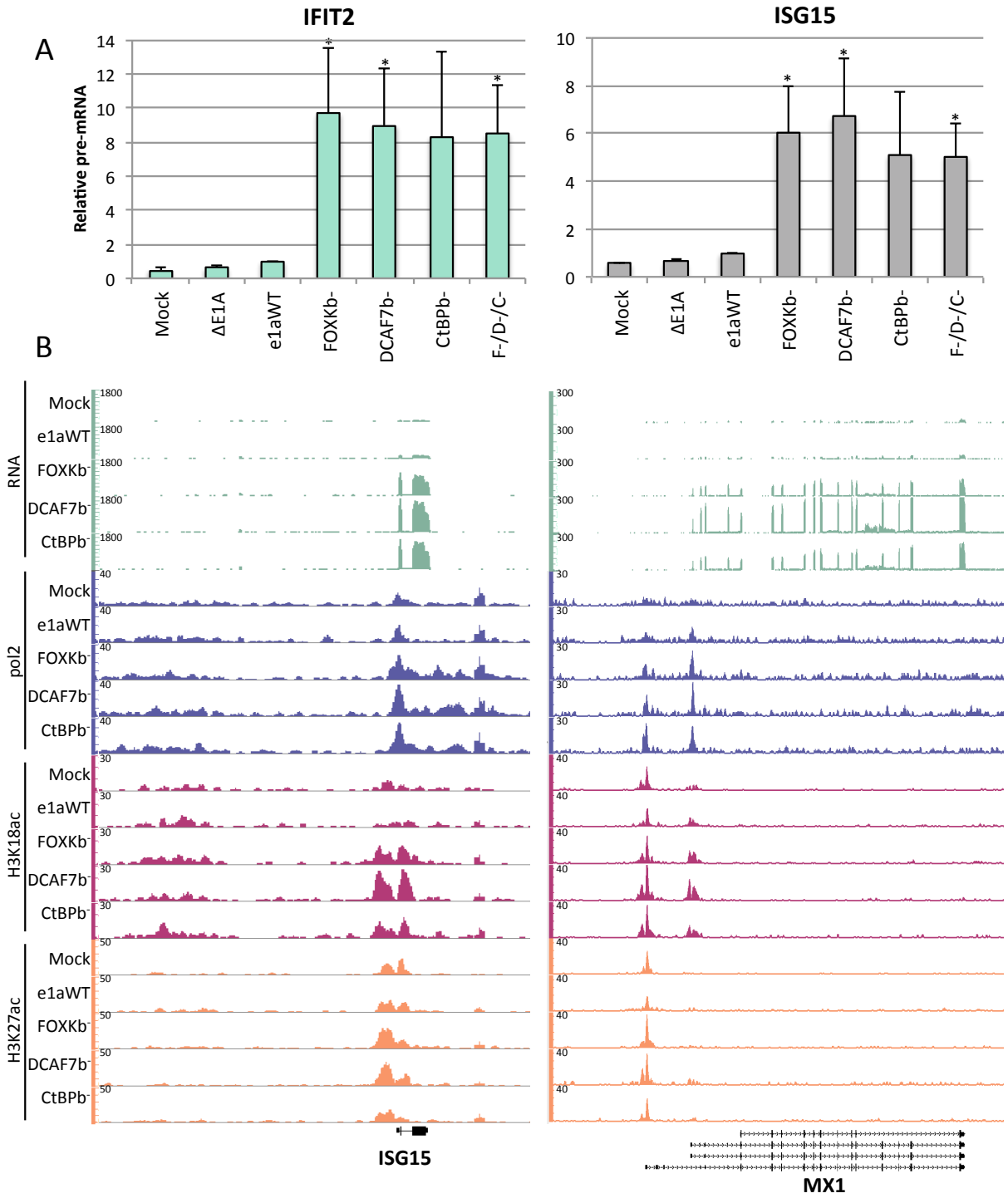

Figure 2.7 Transcriptional Activation of ISGs by e1a C-terminal Mutants
(A) Relative levels of IFIT2 and ISG15 pre-mRNAs following infection with the indicated vectors or coinfected with the vectors for e1a mutants for each of the three e1a C-terminal mutants (F-/D-/C-). Data are represented as averages of three separate experiments + S.D. * $p<0.05$, ** $p<0.01$, *** $p<0.001$. **(B)** Genome browser plots of RNA- or ChIP-seq normalized sequence tags.

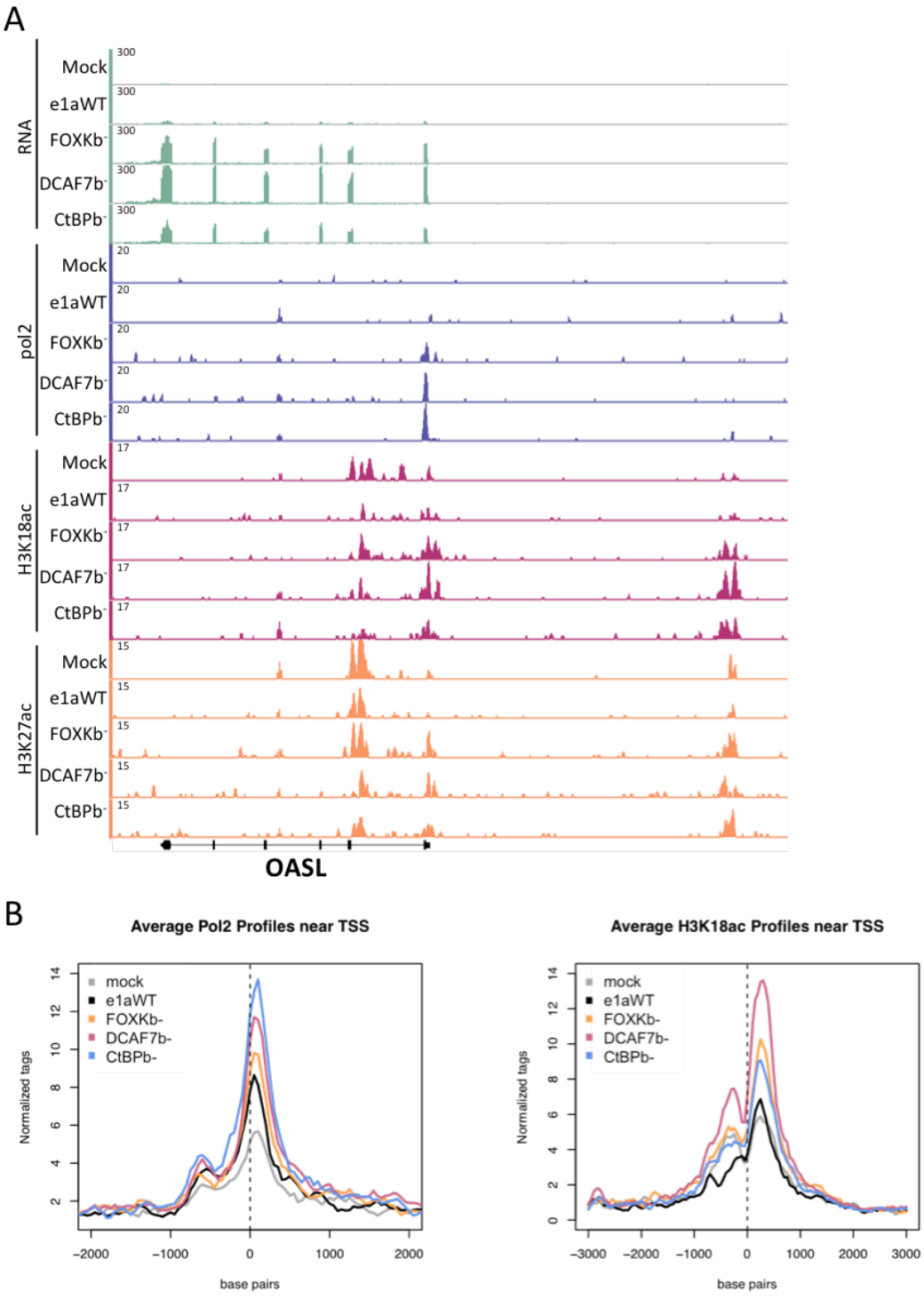

Figure 2.8 Chromatin marks related to transcriptional activation at e1a C-terminal-induced ISGs
(**A**) Genome browser track of RNA-seq and ChIP-seq enrichment upstream of and across the OASL gene from HBTEC infected for 24h. (**B**) Metagene plots showing average tag density of Pol2 or H3K18ac ChIP-seq enrichment around TSS of 52 genes expressed 2-fold higher by all three e1a C-terminal mutants using chromatin from cells mock-infected or infected with indicated e1a expressing Ad5 vector for 24 h. Data was normalized so there were equal numbers of mapped reads across samples.

e1a C-terminal mutants cause increases in IRFs and STATs, but only IRF3 is necessary for ISG activation

STAT1 and STAT2 are phosphorylated following Type I IFN receptor activation resulting in formation of transcription factor ISGF3 composed of p-STAT1, p-STAT2 and IRF9 (Borden et al., 2007; Darnell et al., 1994). We noted that many of the 52 genes overexpressed by all three C-terminal e1a mutants are also in a list of genes activated by the transcription factor unphosphorylated ISGF3 (U-ISGF3), a complex of unphosphorylated STAT1 (U-STAT1) and STAT2 (U-STAT2) with IRF9 that reach high concentrations and drive a secondary prolonged response to IFNβ-stimulation lasting for days (Cheon and Stark, 2009; Cheon et al., 2013). 21 out of the 29 U-ISGF3 activated genes (72%) reported in Cheon et al. (2013) were overexpressed 2-fold or more by all three e1a C-terminal mutants (Fig. 2.9A) and 26 (90%) were overexpressed by at least one e1a C-terminal mutant. Given this striking overlap, we examined levels of total and phosphorylated STAT1, STAT2, and IRF9 protein following infection to determine if we could attribute ISG activation by the C-terminal e1a mutants to increased U-ISGF3.

Indeed, by 24h p.i. the C-terminal e1a mutants caused a substantial increase in the concentrations of STAT1, STAT2 and IRF9 compared to mock-infected cells (Fig. 2.10A). Infection with the ΔE1A vector also increased STAT1/2, although to a lesser extent than vectors for the C-terminal mutants, but IRF9 was increased to a comparable level. While U-ISGF3 subunits have been reported to increase in concentration following activation of the type I IFN receptors and JAK/STAT signaling pathway, we did not detect any phosphorylated STAT1 following infection from 2-24h with any of the Ad5 vectors (Fig. 2.9B). Importantly, the type I IFN encoding mRNAs were not significantly increased as measured by RNA-seq. These observations indicate that ISG activation is not due to an autocrine response to IFN production

by the infected cells, but rather, may result from the large increase in the U-ISGF3 subunits, independent of JAK/STAT pathway activation.

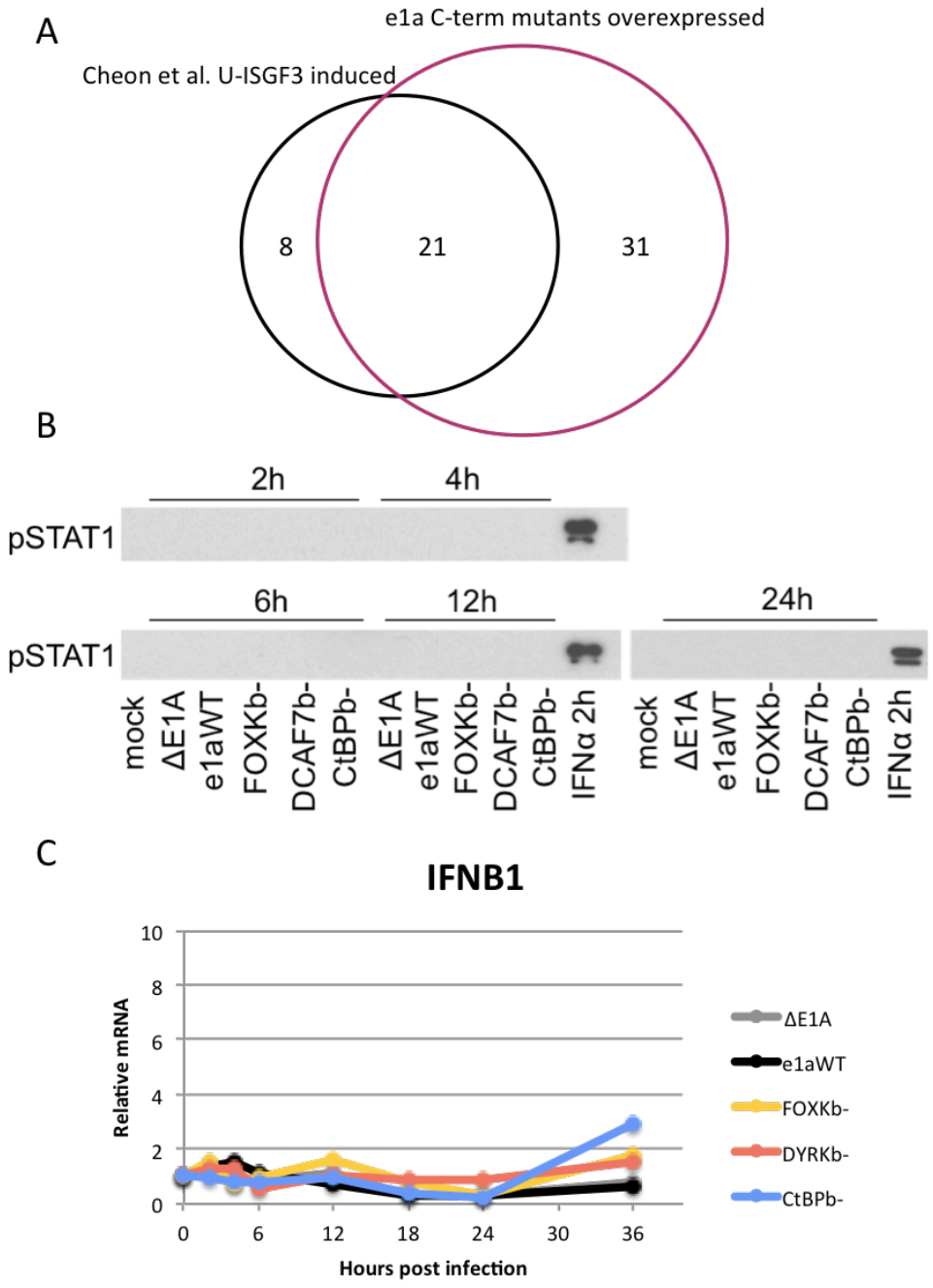

Figure 2.9 STAT1 is not phosphorylated at its activating site following infection
(**A**) Venn diagram showing overlap of U-ISGF3 induced genes (Cheon et al., 2013) and e1a C-terminal mutant overexpressed genes. (**B**) Western blots for phosphorylated Y701 STAT1 from lysates of infected HBTEC at various times p.i. An extract from HTBEC treated with 10ng/mL IFNα for 2h was used as a positive control for STAT1 phosphorylated at Y701. (**C**) IFNB1 mRNA assayed by qRT-PCR during a time course of infection of HBTEC.

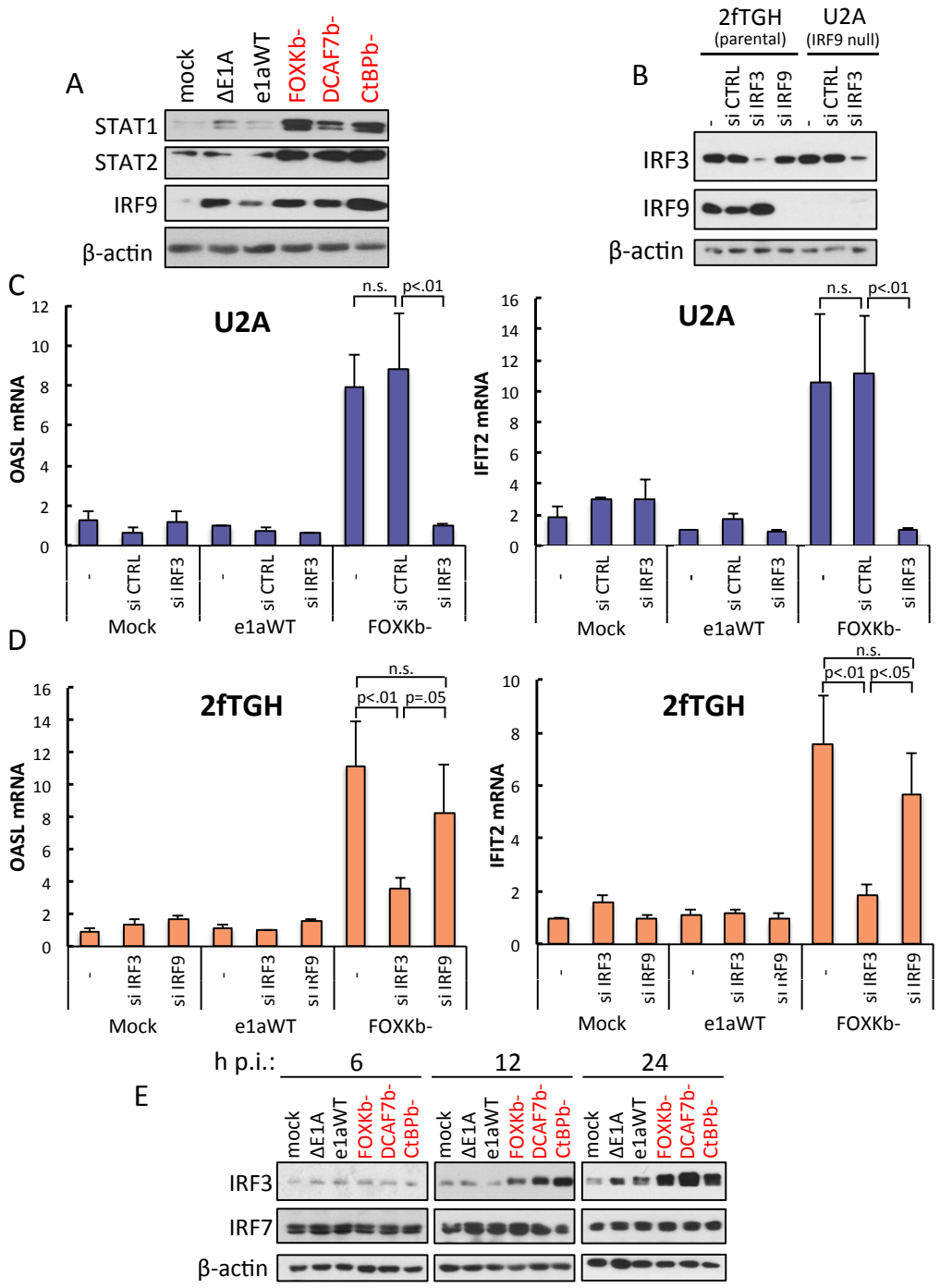

Figure 2.10 e1a C-terminal mutants increase STAT1/2, IRF9 and IRF3 but only IRF3 is necessary for ISG activation

(A) Western blots of HBTEC extract from 24h p.i., with the indicated expression vectors. (**B**) Western blots with extract from 2fTGH and U2A cells transfected with indicated siRNAs for 72h and immunoblotted for KD efficiency of IRF3 and IRF9. (**C**) qRT-PCR assaying OASL and IFIT2 mRNA from U2A cells transfected with a negative control siRNA with no known targets (si CTRL), siRNA targeting IRF3 (si IRF3) or no siRNA (-). Data are represented as averages of three separate experiments + S.D. (**D**) Same as with (C) but in 2fTGH and including siRNA targeting IRF9. Data are represented as averages of three separate experiments + S.D. **(E)** Western blots of HBTEC extract from 6, 12 or 24 h p.i., with the indicated expression vectors.

To determine if the U-ISGF3 complex was responsible for ISG activation by the e1a C-terminal mutants, we infected U2A cells, which do not express IRF9 (McKendry et al., 1991), the principal DNA binding subunit (Fink and Grandvaux, 2013). Inconsistent with a requirement for U-ISGF3, the FOXKb$^-$ e1a mutant activated *OASL* and *IFIT2* to a similar level as in the parental cells, 2fTGH (Fig. 2.10C,D), which express IRF9 (Fig. 2.10B). Similar results were observed in STAT1 mutant U3A and STAT2 mutant U6A cells (Stark, 2007) (Fig. 2.11). Therefore U-ISGF3 is not necessary for activation of these ISGs by the e1a C-terminal mutants.

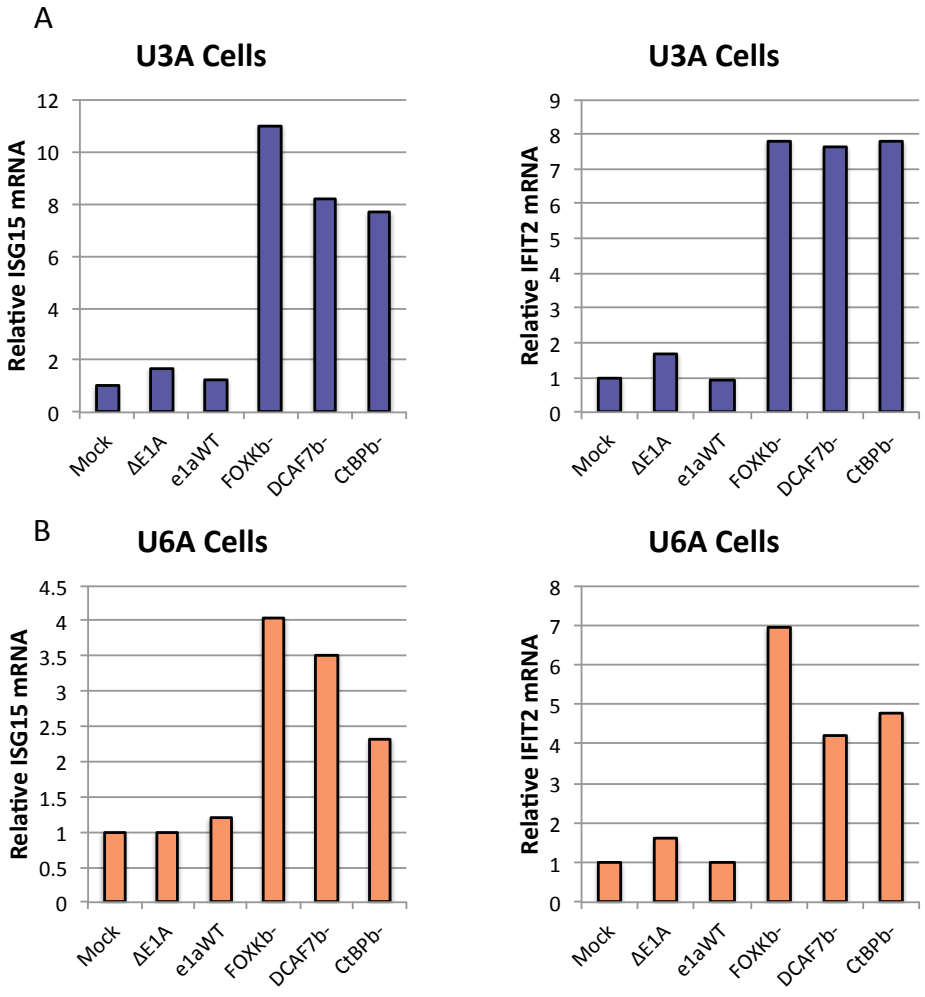

Figure 2.11 STAT1 and STAT2 are not necessary for e1a C-terminal activation of ISGs
(**A**) STAT1 mutant U3A cells were infected for 24h with the indicated vectors prior to RNA isolation and qRT-PCR to determine relative ISG15 and IFIT2 mRNA levels. (**B**) Same as with **A** but in STAT2 mutant U6A cells.

Since, the promoters of the activated ISGs contain ISREs bound by all the IRFs, we analyzed changes in expression of other IRFs in addition to IRF9. IRF3 is the principal effector activating the IFN response pathway following cellular detection of viral DNA during infection (Ikushima et al., 2013). When we analyzed IRF3 protein following infection of HBTEC by the C-terminal mutants, we observed an increase over mock-infected cells by 12h p.i. that became still greater by 24h p.i. (Fig. 2.10E). The structurally related IRF7, however, did not change. IRF3 is regulated by cytoplasmic restriction until phosphorylated to allow nuclear entry (Lin et al., 1998). Consequently we analyzed the phosphorylation status of IRF3 at activating site Ser396. Cells expressing the e1a C-terminal mutants but not WT e1a had high IRF3 Ser396 phosphorylation at 24h p.i., comparable to the level induced by poly(I:C), a TLR3 ligand, after 3h (Fig. 2.12A). Although we observed increased total IRF3 by 12h p.i. (Fig. 2.10E), phosphorylation was not induced until 24h p.i. (Fig. 2.12A); therefore the increase in IRF3 preceded its phosphorylation at Ser396.

Unlike IRF9, IRF3 siRNA knockdowns in U2A cells did prevent e1a-FOXKb$^-$ from activating *OASL* and *IFIT2* (Fig. 2.10B,C). IRF3 siRNA KD In the parental 2fTGH cells also prevented activation of these genes, while siRNA KD of IRF9 had no significant effect (Fig. 2.10B,D). Taken together, these results indicate that IRF3, but not U-ISGF3, is necessary for e1a C-terminal mutant activation of these ISGs.

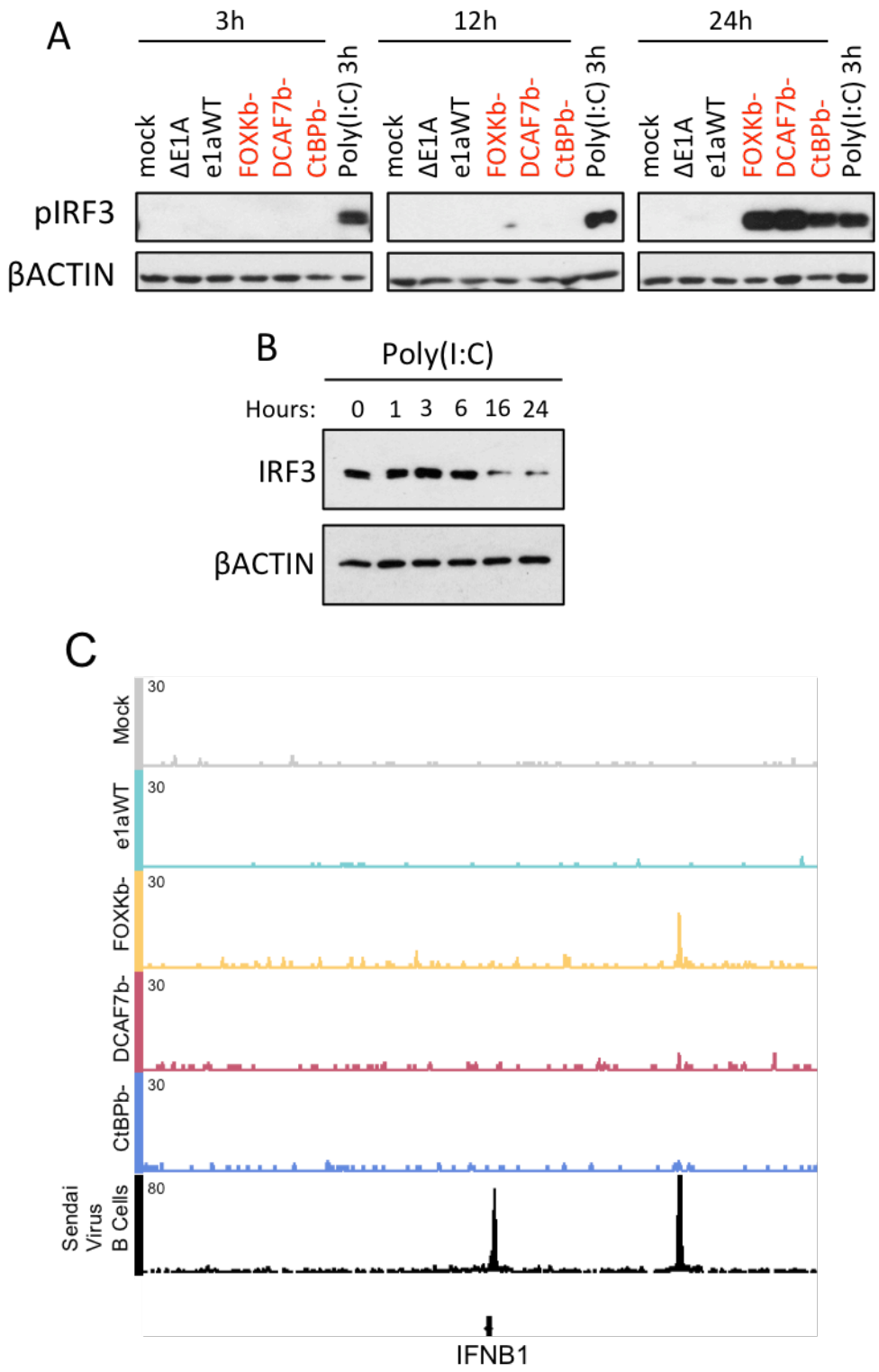

Figure 2.12 Phosphorylation of IRF3 protein by infections and Poly(I:C)
(**A**) HBTEC were infected for the indicated times or transfected with poly(I:C) 20ug/mL for 3h as a positive control for pIRF3. Level of pSer396 IRF3 was assayed by western blot. (**B**) HBTEC were transfected with Poly(I:C) 20ug/mL for the indicated times and total IRF3 protein was assayed by western blot. (**C**) Genome Browser image demonstrating the absence of IRF3 binding at its promoter following Ad5 vector infection/e1a expression, while Sendai virus infected B lymphocytes induces binding. GEO: GSE44939 (Freaney et al., 2013).

IRFs and STATs increase post-transcriptionally leading to IRF3 accumulation on chromatin independent of phosphorylation to activate a subset of ISGs

Following the observation that IRF3, and not IRF9, was required for ISG activation by the e1a C-terminal mutants, we analyzed chromatin associated levels of these proteins as well as STAT1/2. We observed a dramatic increase in IRF3 association with chromatin at 12h p.i. that persisted to 36h p.i., specifically in response to the C-terminal mutants (Fig. 2.13A). Furthermore, IRF3 ChIP-seq in C-terminal mutant, but not mock-infected or e1aWT expressing HBTEC revealed IRF3 binding to the promoters of activated ISGs such as *ISG15* and *MX1* (Fig. 2.13B). Inconsistent with phosphorylation being required for IRF3's nuclear entry, we did not observe IRF3 phosphorylation at 12h p.i. when IRF3 had increased on chromatin. However, an increase in pIRF3 was observed at later time points. STAT1 also accumulated on chromatin in e1a C-terminal mutant expressing cells, but with slower kinetics than IRF3 (Fig. 2.13A). STAT2 and IRF9 showed only modest increases in association with chromatin. The observed increase of IRF3 on chromatin 12h p.i. is consistent with the kinetics of ISG activation induced in cells expressing e1a C-terminal mutants. In these cells *OASL*, *ISG15* and *IFIT2* were activated by 12h p.i. and ISG15 and IFIT2 mRNAs continued to increase until or past 24h (Fig. 2.13C, left).

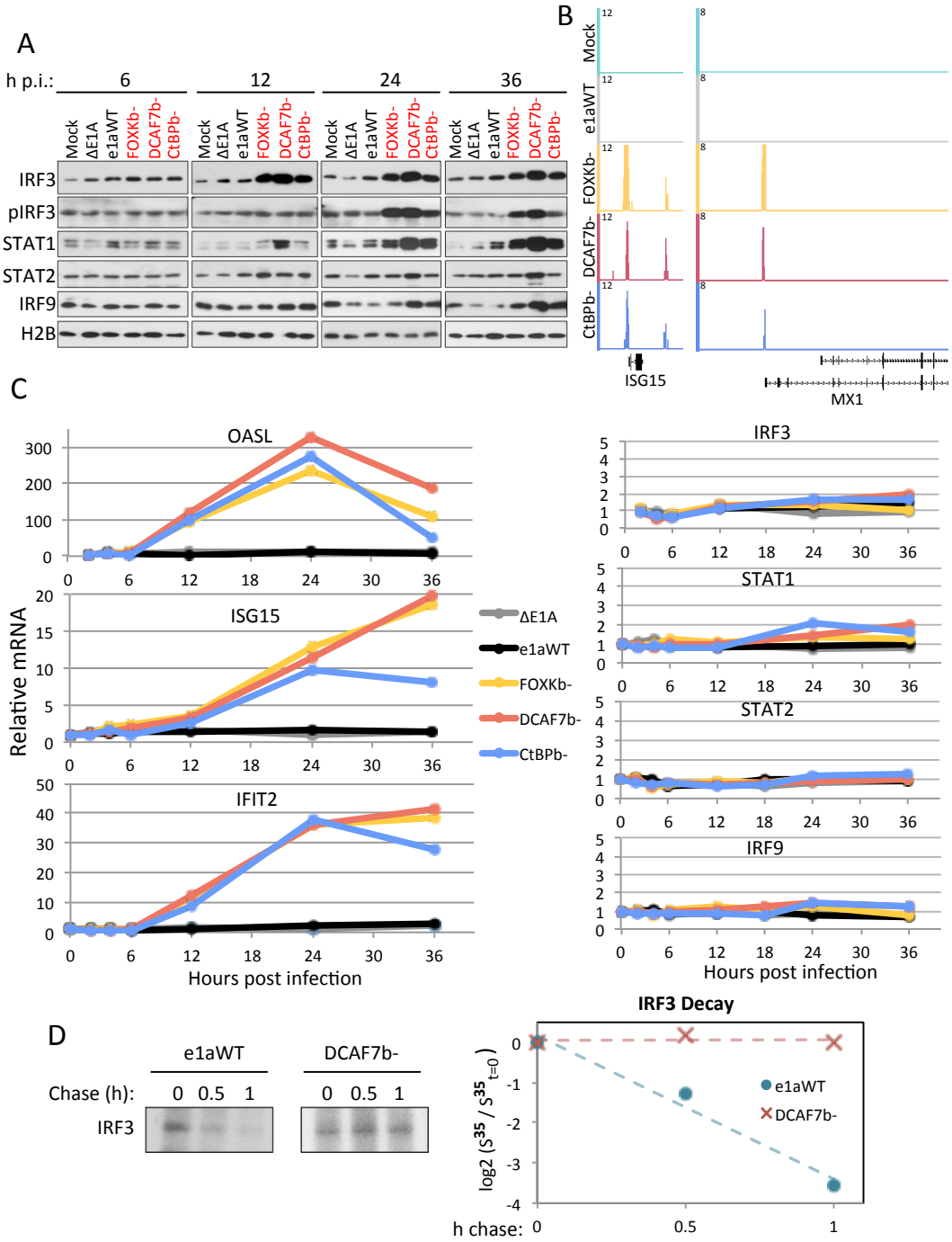

Figure 2.13 e1a C-terminal mutants induce stabilization and IRF3 binding to chromatin prior to phosphorylation

(A) Western blot of chromatin associated proteins from HBTEC 6, 12, 24 or 36h p.i. with the indicated vectors. **(B)** Genome browser plots of IRF3 ChIP-seq normalized sequence tags. **(C)** qRT-PCR of OASL, ISG15, IFIT2, IRF3, STAT1, STAT2 and IRF9 mRNA from HBTEC during a time course of infection with the indicated vectors. Data are plotted as relative to mock-infected. (**D**) S^{35}-Met –Cys pulse-chase followed by IRF3 IP SDS-PAGE and autoradiography from HBTEC infected with either e1aWT or DCAF7b-. Left is autoradiogram displaying IRF3 band and right is graph of log2 of the relative intensities of the bands measured by densitometry from the autoradiogram. The least squares line through the points indicates a $t_{1/2} \approx 0.33$ h.

The increased levels of IRFs and STATs could be due to an increase in their respective mRNAs, accelerated translation or stabilization of the proteins. To determine which mechanism occurs under these conditions, *IRF3*, *STAT1/2* and *IRF9* mRNA were assayed by qRT-PCR from 0-36h p.i. (Fig. 2.13C, right). The levels of these mRNAs increased 2-fold or less, whereas their encoded proteins increased much more by 24h p.i. (Fig. 2.10A,E). Therefore, the increase in these proteins is not a result of their mRNAs increasing, whether from transcription or message stabilization. To determine if IRF3 is stabilized we performed S^{35} protein labeling pulse-chase experiments followed by IRF3 immunopreciptitaion and autoradiography. In e1aWT expressing HBTEC IRF3 had a short half-life, ~20 min. In contrast, in cells expressing e1aFOXKb$^-$ there was no observed IRF3 decay (Fig. 2.13D). Taken together, our data suggest that the e1a C-terminal mutants activate transcription of a subset of ISGs through an increase in IRF3 by protein stabilization, leading to selective ISG promoter binding and transcription activation. Furthermore, the phosphorylation of IRF3 induced by poly(I:C) activation of TLR3 signaling, did not lead to an increase in total IRF3 in HBTEC (Fig. 2.12B). Therefore a mechanism that increases IRF3 protein level independently of phosphorylation at the activating site operates in the e1a C-terminal mutant expressing cells. We note that the well-characterized IRF3 target *IFNB1* (Ikushima et al., 2013), was not activated throughout a timecourse of infection (Fig. 2.9C), and IRF3 was not found to bind the *IFNB1* promoter following infection with the e1a C-terminal mutant expressing Ad vectors (Fig. 2.12C), while IRF3 is recruited to *IFNB1* following infection with other viruses as seen in Sendai virus infected human B lymphocytes (Freaney et al., 2013). Taken together this suggests a noncanonical mechanism of activation by IRF3 with restricted gene targets.

Methods

Experimental Model and Subject Details

Cell Culture

Male human Bronchial/Tracheal Epithelial Cells (HBTEC, Lifeline Cell Technology Cat# FC-0035; lot# 02196) were grown at 37°C in BronchiaLife Medium Complete Kit (Lifeline Cell Technology catalog number: LL-0023) in a 5% CO2 incubator until they reached confluence. Cells were then incubated 3 days more without addition of fresh media and were either mock infected or infected with the indicated Ad5-based vectors in the conditioned medium. All other cell lines were grown in Dulbecco's Modified Eagle Medium (DMEM) with 10% fetal bovine serum.

Method Details

Ad Vectors, Infection, Interferon Treatment

Ad5 vectors expressed Ad2 WT or mutant e1a's from the normal E1A promoter with the dl1500 deletion removing the 13S E1A mRNA 5' splice site (Montell et al.,1984). The vectors were constructed using the Ψ5 vector and in vivo Cre24 mediated recombination (Hardy et al., 1997),and consequently contain an out of frame insertion of a LoxP site at the Bgl II site in the region encoding the carboxy-terminus of E1B-55K. All infections were for 24 h at an moi of 60, unless otherwised indicated. These multiplicities of infection yielded approximately equal amounts of WT and C-terminal mutant e1a proteins and mRNA as judged by western blotting,

qRT-PCR of E1A message and mapping of RNA-seq reads to the Ad2 genome. Human interferon-α 1 (IFNα) from Cell Signaling Technology (Cat#8927) was added to the conditioned media of HBTEC cultures at a concentration of 10 ng/mL for indicated times. The ΔE1A mutant was dl312 (Jones and Shenk, 1979).

RNA-seq Procedure and Data Analysis

$1X10^6$ Low-passage HBTEC were mock-infected or infected with Ad5 E1A-E1B-substituted, E3-deleted vectors expressing WT Ad2 small E1A proteins from the dl1520 deletion removing the 13S E1A mRNA 50 splice site (Montell et al., 1984), 3 days after reaching confluence. RNA was isolated 24h p.i. using QIAGEN RNeasy Plus Mini Kit. Eluted RNA was treated with Ambion DNA-free™ DNA Removal Kit and then Ambion TRIzol reagent, precipitated with isopropanol, and dissolved in sterile water. RNA concentration was measured with a Qubit fluorometer. One microgram of RNA was fragmented and copied into DNA then PCR amplified with bar-coded primers for separate samples to prepare sequencing libraries using the Illumina TruSeq RNA Sample Preparation procedure. Libraries were sequenced using the Illumina HIseq-2000 to obtain single end 50-base-long reads. Sequences were aligned to the hg19 human genome sequence using TopHat v2. FPKM (fragments per kb per million mapped reads) for each annotated hg19 RefSeq gene ID was determined using Cuffdiff v2 from Cufflinks RNA-Seq analysis tools at http://cufflinks.cbcb.umd.edu. Homer (http://homer.salk.edu/homer PMID: 20513432) gene ontology enrichment analysis was performed on indicated gene lists. Homer motif discovery algorithm was used to look for transcription factor motifs +/- 1 kb from the TSS of genes expressed 2X or more by all three e1a C-terminal mutants compared to e1aWT. RNA-seq results from mock, ΔE1A, e1aWT and e1a C-terminal mutants were validated with

three replicate experiments. One representative experiment was used for further analysis and presentation of the data.

ChIP-Seq

Pol2, H3K18ac and H3K27ac ChIP-seq was performed using $1x10^7$ low-passage HBTEC were mock-infected or infected with indicated Ad vector 3 days after reaching confluence. 24h p.i. cells were cross-linked for 1% formaldehyde for 10 minutes at room temperature on rotator. Formaldehyde crosslinking was quenched with 0.14M glycine for 30 minutes at room temperature on rotator. Cells were washed with PBS and scraped from plates in PBS with Roche protease inhibitor cocktail. Cells were pelleted and lysed in 400uL lysis buffer (1% SDS, 50mM Tris-HCl pH8, 20mM EDTA, Roche complete protease inhibitors) and sonicated at 4°C using the Qsonica Q800R2 at 20% amplitude 10s on 30s off until DNA fragments from sheared chromatin were mostly between the sizes of 200-600 base pairs. 100uL of sonicated chromatin was diluted in 10X lysis dilution buffer (16.7 mM Tris-HCl, 1.1% Triton X-100, 1.2mM EDTA, 167mM NaCl) and precleared for 1h 4°C with 30uL of protein A dynabeads washed 10X lysis dilution buffer on nutator. IPs were performed O/N at 4°C on nutator with precleared chromatin and 2ug of anti-Pol2, -H3K27ac or 5uL of H3K18ac anti-rabbit sera. 50uL of protein A dynabeads were added for 4h on nutator at 4°C. Bead-immunocomplexes were washed for 5min 2X with each of the following buffers in order: wash buffer A (50mM Hepes pH 7.9, 0.1% SDS, 1% Triton X-100, 0.1% Deoxycholate, 1mM EDTA, 140mM NaCl), wash buffer B (50mM Hepes pH 7.9, 0.1% SDS, 1% Triton X-100, 0.1% Deoxycholate, 1mM EDTA, 500mM NaCl), LiCl buffer (20mM Tris-HCl pH8, 0.5% NP-40, 0.5% Deoxycholate, 1mM EDTA, 250mM LiCl), TE (50mM Tris-HCl pH8, 1mM EDTA). Elution was performed in 150uL of elution

buffer (50mM Tris HCl pH8, 1mM EDTA, 1% SDS) then ChIP samples and inputs (10uL of precleared chromatin lysis plus 140uL elution buffer) were reverse crosslinked O/N at 65°C. Samples were RNase A treated for 1h at 37°C and DNA was purified and extracted with phenol/chloroform and ethanol precipitated. DNA pellets were resuspended in 12uL of TE and measured using Qubit fluorometer. IRF3 ChIP-seq was performed similarly with the following modifications: cells were double crosslinked with 4mM DSG in PBS for 30min then 1% formaldehyde for 10 min, crosslinking was quenched in 500mM Tris pH7.9 for 20min and cell pellets were lysed in 1mL lysis buffer 1 (50mM HEPES-KOH, pH 7.5, 140mM NaCl, 1mM EDTA, 10% glycerol, 0.5% NP-40, 0.25% Triton X-100, Roche complete protease inhibitors) for 10min on ice. Lysate was pelleted at 3000 rpm 5min 4°C then resuspended in 1mL lysis buffer 2 (10mM Tris-HCl, pH 8.0, 200mM NaCl, 1mM EDTA, 0.5mM EGTA, Roche complete protease inhibitors) and placed on nutator 10min 4°C and pelleted as before, then resuspended in 125uL of lysis buffer 3 (10mM Tris-HCl, pH 8.0, 100mM NaCl, 1mM EDTA, 0.5mM EGTA, 0.1% Na-Deoxycholate, 0.5% N-lauroylsarcosine, Roche complete protease inhibitors) and sonicated, 5ug of anti-IRF3 (Cat#sc-9082; Lot#31515) was used, magnetic beads were washed and blocked in 0.5% BSA in PBS. Sequencing libraries were constructed from 1 ng of immunoprecipitated and input DNA using the KAPA Hyper Prep Kit from KAPA Biosystems and NEXTflex ChIP-Seq barcodes purchased from Bioo Scientific.

Data Analysis of ChIP-seq

ChIP-seq libraries were sequenced using Hiseq-2000 or 4000 systems for single-end 50 base pair reads. Reads were mapped to the hg19 human genome reference using Bowtie2 software. Only reads that aligned to a unique position in the genome with no more than two sequence

mismatches were retained for further analysis. Duplicate reads that mapped to the same exact location in the genome were counted only once to reduce clonal amplification effects. A custom algorithm executed by MATLAB was used for further processing. The genome was tiled into 50 base pair windows and each read was extended by 150 bases and was counted as one read to each window to which it partially or fully matched. The total counts of the input and ChIP samples were normalized to each other. Normalization was done across samples for equal number of uniquely mapped reads. The input sample was used to estimate the expected counts in a window. Wiggle files were generated using a custom algorithm and present the data as normalized tag density as seen in all figures with genome browser shots and average tag density for the indicated TSSs generated by CEAS software.

siRNA and Poly(I:C) Transfections

siRNA KD was performed in U2A or 2fTGH using Invitrogen RNAiMAX reverse transfection protocol. 500,000 cells were plated in 6cm^2 plates in antibiotic free 10% FBS DMEM containing siRNA for a final concentration of 10nM that was preincubated in 7.5uL of lipofectamine RNAiMAX reagent in 750uL of Opti-MEM. Ambion siRNAs used were IRF3 s7505, IRF9 s2029 and negative control no.1 AM4611. After 48h of transfections cells were infected for 24h in U2A cells and 12h in 2fTGH with Ad5 vectors or mock-infected. Poly(I:C) purchased from Sigma-Aldrich was transfected into cells at 20ug/mL final concentration using 20uL of lipofectamine 2000 Invitrogen diluted in 1mL of Opti-Mem into 10cm^2 plates of confluent HBTECs. RNA was isolated using QIAGEN RNeasy Plus Mini Kit. Cells were lysed for protein in EBC lysis buffer (120mM NaCl, 0.5% NP-40, 50mM Tris-Cl pH 8.0, Roche cOmplete protease inhibitor). Transfections were performed in triplicate. Data are represented as an

average of n=3 experimental replicates.

Cellular Biochemical Fractionation

For chromatin associated protein $4x10^6$ HBTEC were infected for indicated times collected and washed in PBS and resuspended in 100uL of Buffer A (10mM HEPES [pH 7.9], 10mM KCl, 1.5mM MgCl2, 0.34 M sucrose, 10% glycerol, 1mM dithiothreitol, and Roche protease inhibitor cocktail) and triton X-100 was added for 0.1% final concentration. Cells were incubated on ice for 8 minutes then nuclei were pelleted by centrifugation 5 min, 1,300 × g , 4°C. Supernatant extract was collected as cytoplasmic extract. The pellet was washed 1X in buffer A and lysed in buffer B (3mM EDTA, 0.2mM EGTA, 1mM dithiothreitol, and Roche protease inhibitor cocktail), and insoluble chromatin was pelleted from soluble (nucleoplasmic supernatant) by centrifugation (5 min, 1,700 × g, 4°C). The chromatin pellet was washed once with buffer B and resuspended in 1% SDS Laemmli buffer and denatured for 10 min at 65°C. HeLa cell nuclear extract for Superose 6 gel filtration was isolated as described in (Dignam et al., 1983). $15x10^7$ HeLa cells were mock or e1aWT infected for 24h then pelleted in PBS. Cells were resuspended in 5 volumes to pellet size with Buffer A (10mM HEPES (pH 7.9 at 4C), 1.5mM MgCl2, 10mM KC1 and 0.5mM DTT). Cells were transferred to B-type pestle dounce homogenizer and lysed with 10 strokes then centrifuged for 20 min at 10,000 rpm. Nuclei pellets were resuspended in buffer C (20mM HEPES (pH 7.9), 25% (v/v) glycerol, 0.42M NaCl, 1.5mM MgCl2, 0.2mM EDTA, 0.5mM PMSF and 0.5mM DTT) and stirred gently for 30 min at 4°C. Nuclei were spun at 10,000 rpm for 30min. Supernatant was collected and used for Superose 6 gel filtration.

Co-Immunoprecipitation

Co-IPs were performed using M58 crosslinked to protein G agarose beads. 1mL of clarified M58 hybridoma supernatant was incubated with 50uL of 50% slurry protein G agarose beads on nutator for 4h at 4°C. Beads were washed 3X with 0.2M sodium borate pH 9 then antibody was crosslinked to protein G beads in 20mM DMP in 0.2M sodium borate pH 9 for 40 min on nutator at room temperature. Beads were then washed once with 0.2M ethanolamine pH 8 then quenched in 1mL ethanolamine pH 8 on nutator for 2h at room temperature. To remove uncoupled IgGs beads were washed 3X with 0.58% acetic acid and 150mM NaCl, then washed 3X with PBS. Cells were lysed in EBC lysis buffer (120 mM NaCl, 0.5% NP-40, 50 mM Tris-Cl pH 8.0, and Roche cOmplete protease inhibitors) l on ice. 2-4 mg of supernatant lysate from infected HeLa or A549 cells was precleared with 30uL agarose G beads for 1h then immunoprecipitated overnight at 4°C with M58 cross-linked to agarose G beads. Immuno-bead complexes were washed 3 times with cold EBC buffer and eluted in Laemmli buffer and incubated 10 min at 65°C.

Western blot

Proteins were extracted from indicated cells by lysis in EBC (120 mM NaCl, 0.5% NP-40, 50 mM Tris-Cl pH 8.0, and Roche cOmplete protease inhibitors). Protein concentration was quantified by Bradford assay and normalized in Laemmli buffer and heated for 10min at 65°C then resolved in a 9% SDS-polyacrylamide gel. Proteins were electrotransferred to a polyvinylidene difluoride (PVDF) membrane then blocked in 5% milk in TBS-Tween 0.1% (blocking buffer) for 30 minutes. Primary antibody was added at manufacturer recommended dilutions for 1h at room temperature or O/N at 4°C. Membranes were washed 3X in TBS-Tween (0.1%) then anti-mouse or anti-rabbit secondary antibodies were added for 1h room temperature in blocking buffer. Membranes were then washed 3X in TBS-Tween (0.1%) prior to addition of

ECL reagent for detection of chemiluminescence. Western blots were validated with replicates of two or more with representative western blots presented.

qRT-PCR

Cells were collected at indicated times following transfection or infection and RNA was isolated as described above. 1ug of RNA, as measured by Qubit fluorometer, was used for reverse transcription with SuperScript III First-Strand Synthesis SuperMix using random hexamer primers. qRT-PCR was performed with 5uL of cDNA, diluted 1:10 or 1:10000 for 18s rRNA. Runs were done using an ABI 7500 Real Time Thermocycler and reactions took place in optical-grade, 96-well plates (Applied Biosystems, Carlsbad, CA, USA) 25uL total volume with primers at a concentration of 900nM and 12.5uL of 2X FastStart Universal SYBR Green Master (Rox). Relative mRNA levels were calculated as $2^{\Delta Ct}$ and normalized to relative values of 18s rRNA. Data are presented as average of three or more experimental replicates ± standard deviation.

Plaque Assay

$6cm^2$ confluent HBTEC plates were infected for 12h at moi 60 with the indicated e1a-expressing recombinant Ad5 vectors then superinfected with WT Ad5 virus for 48h. Cells were lysed with 3 cycles of freeze/thaw/vortex in 1mL of PBS and the cellular debris was pelleted. The supernatant, containing released Ad particles, was serially diluted to 10^{-4} - 10^{-6} and 100uL of the dilutions used to infect $6cm^2$ 80% confluent HeLa monolayer. After 1h absorption of virus 5mL of 0.7% agarose in DMEM with 10% fetal bovine serum was overlayed. 1 day later 3mL of 0.7% agarose and DMEM with 10% fetal bovine serum was overlayed. Cells were stained with neutral red stain on day 6 p.i. and plaques were counted on day 7 to determine Ad5 titers. Data are

represent the average plaque forming units from three replicate superinfections ± standard deviation.

S^{35} Pulse-Chase Protein Labeling and Autoradiography

Confluent $3x10^6$ HBTEC were mock-infected or infected for 22h with the indicated Ad vectors. Cells were washed 2X with room temperature PBS and DMEM Met-Cys-free (Gibco Cat#21013) pulse media with 250uCi/mL EasyTag EXPRESS 35S Protein Labeling Kit was added to cells for 2h and placed in cell culture incubators. After labeling, labeling media was removed and cells were washed 2X with room temperature PBS and Fresh HBTEC media was added for indicated chase times. Upon harvesting cells were washed with cold PBS and collected and lysed in 500uL of EBC lysis buffer (120 mM NaCl, 0.5% NP-40, 50 mM Tris-Cl pH 8.0, and Roche cOmplete protease inhibitors). Cell lysate was used for IRF3 immunoprecipitation as described above in co-immunoprecipitation section with 2uL of anti-IRF3 (D6I4C) from Cell Signaling Technology. Eluted protein was run on 9% SDS polyacrylamide gels. Gels were fixed in 10% acetic acid and 20% methanol in water on rotator for 30 minutes. Gels were washed for 30 minutes in DI water on rotator and incubated in 1M sodium salicylate on rotator for 30 minutes prior to being dried on a gel drying vacuum system. Exposed films were scanned and band intensities were quantified using ImageJ software.

Quantification and Statistical Analysis

Relative mRNA values as determined by qRT-PCR from experiments of three independent biological replicates were used to determine significance between conditions using a one-way

ANOVA statistical tests. Statistical differences in the distributions of expression (FPKM values) of a given set of genes between conditions were determined using Kolmogorov-Smirnov tests.

Data and Software Availability

The accession number for the sequencing data reported in this paper is GEO: GSE105040

Key Resources Table

REAGENT or RESOURCE	SOURCE	IDENTIFIER
Antibodies		
Rabbit polyclonal anti-FOXK1	Bethyl	Cat#A301-728A; RRID:AB_1211446
Rabbit monoclonal anti-WDR68 a.k.a. DCAF7	Abcam	Cat#ab138490
Mouse monoclonal anti-DYRK1A	Abcam	Cat#ab54944; RRID:AB_941372
Rabbit polyclonal anti-CtBP (H-440)	Santa Cruz	Cat#sc-11390; RRID:AB_2086634
Rabbit polyclonal anti-CtBP1	Bethyl	Cat#A300-338A; RRID:AB_420970
Rabbit polyclonal anti-H3K18ac (814)	Grunstein/Kurdistani laboratories (Suka et al., 2001)	N/A
Rabbit polyclonal anti-H3K27ac	Active Motif	Cat#39133; RRID:AB_2561016; Lot#31814008
Rabbit polyclonal anti-KU-86 (H-300)	Santa Cruz	Cat#sc-9034; RRID:AB_2218743
Rabbit polyclonal anti-Pol2 (N20)	Santa Cruz	Cat#sc-899; RRID:AB_632359
Rabbit monoclonal anti-STAT1 (D1K9Y)	Cell Signaling Technology	Cat#14994S
Rabbit monoclonal anti-Phospho-STAT1 Tyr701 (58D6)	Cell Signaling Technology	Cat#9167S
Rabbit monoclonal anti-STAT2 (D9J7L)	Cell Signaling Technology	Cat#72604S
Rabbit monoclonal anti-IRF9 (D2T8M)	Cell Signaling Technology	Cat#76684S
Rabbit polyclonal anti-p300 (N15)	Santa Cruz	Cat#sc-584; RRID:AB_2293429
Mouse monoclonal anti-Rb1	Abcam	Cat#ab24; RRID:AB_303042
Rabbit polyclonal anti-IRF7	Cell Signaling Technology	Cat#4920S; RRID:AB_2127551
Rabbit monoclonal anti-IRF3 (D6I4C)	Cell Signaling Technology	Cat#11904S

Rabbit monoclonal anti-Phospho-IRF-3 (Ser396) (4D4G)	Cell Signaling Technology	Cat#4947S; RRID:AB_823547
Rabbit polyclonal anti-H2B	Millipore	Cat#07-371; Lot#2617640; RRID:AB_310561
Mouse monoclonal anti-E1A (M58) hybridoma supernatant	Produced in house; (Harlow et al., 1985)	N/A
Mouse monoclonal anti-p-Adenovirus-2 E1A (C-9), specific for pSer219 in E1A, equivalent to Ser173 in e1a	Santa Cruz	Cat#sc-374663; RRID:AB_10986401
Rabbit polyclonal anti-Beta-Actin	GeneTex	Cat#GTX16039; RRID:AB_367276
Rabbit polyclonal anti-IRF3 (FL-425)	Santa Cruz	Cat#sc-9082; RRID:AB_2264929; Lot#31515
Bacterial and Virus Strains		
e1aWT Ad5 recombinant vector	(Ferrari et al., 2014)	N/A
*dl*312	(Jones and Shenk, 1979)	N/A
FOXKb- Ad5 recombinant vector	This paper	N/A
DCAF7b- Ad5 recombinant vector	This paper	N/A
CtBPb- Ad5 recombinant vector	This paper	N/A
P300b- Ad5 recombinant vector	(Ferrari et al., 2014)	N/A
RBb- Ad5 recombinant vector	(Ferrari et al., 2014)	N/A
Chemicals, Peptides, and Recombinant Proteins		
Human Interferon-α1 (hIFN-α1)	Cell Signaling Technology	Cat#8927
Poly(I:C)	Sigma-Aldrich	P9582
Proteinase K	Roche/Sigma-Aldrich	Cat#3115887001
RNase A	Roche/Sigma-Aldrich	Cat#10109142001
Lipofectamine RNAiMAX Transfection Reagent	Thermo Fisher	Cat#13778075
Complete Protease inhibitor Cocktail	Roche	Cat#04693132001
Critical Commercial Assays		
EasyTag EXPRESS 35S Protein Labeling Kit	Perkin-Elmer	NEG772014MC
TruSeq Stranded mRNA Library Prep Kit	illumina	Cat#RS-122-2101
Kapa Hyper Prep Kit	Kapa biosystems	Cat#KK8504
NEXTflex ChIP-Seq barcodes	BIOO	Cat#NOVA-514121
RNeasy Plus Mini Kit	Qiagen	Cat#74134
SuperScript III First-Strand Synthesis SuperMix	ThermoFisher	Cat#18080400
FastStart Universal SYBR Green Master (Rox)	Roche	Cat#04913850001
Dynabeads Protein A	Thermo Fisher	Cat#10001D
DNA-free™ DNA Removal Kit	Ambion/ThermoFisher	Cat#1906
Deposited Data		
Raw and aligned data	This paper	GEO: GSE105040
Experimental Models: Cell Lines		
Male Human Bronchial/Tracheal Epithelial Cells (HBTEC)	Lifeline Cell Technologies	Cat#FC-0035; lot#02196
A549	ATCC	RRID:CVCL_0023
HeLa	Cold Spring Harbor Laboratory	RRID:CVCL_0030

2fTGH	George Stark Lab	RRID:CVCL_0115
U2A	George Stark Lab	RRID:CVCL_M019
U3A	George Stark Lab	RRID:CVCL_9469
U6A	George Stark Lab	RRID:CVCL_D316
Oligonucleotides		
See table S3	This Paper	N/A
Software and Algorithms		
Bowtie2	http://bowtie-bio.sourceforge.net/bowtie2/index.shtml	RRID: SCR_005476
Samtools	http://samtools.sourceforge.net/	RRID:SCR_002105
Tophat2.2.1	https://ccb.jhu.edu/software/tophat/index.shtml	RRID:SCR_000691
HOMER	http://homer.salk.edu/homer	RRID:SCR_010881
CEAS	http://liulab.dfci.harvard.edu/CEAS/	RRID:SCR_010946
cuffdiff2.0.2	http://cole-trapnell-lab.github.io/cufflinks/cuffdiff/	RRID:SCR_001647

Bibliography

Borden, E.C., Sen, G.C., Uze, G., Silverman, R.H., Ransohoff, R.M., Foster, G.R., and Stark, G.R. (2007). Interferons at age 50: past, current and future impact on biomedicine. Nat. Rev. Drug Discov. *6*, 975–990.

Cheon, H., and Stark, G.R. (2009). Unphosphorylated STAT1 prolongs the expression of interferon-induced immune regulatory genes. Proc. Natl. Acad. Sci. U. S. A. *106*, 9373–9378.

Cheon, H., Holvey-Bates, E.G., Schoggins, J.W., Forster, S., Hertzog, P., Imanaka, N., Rice, C.M., Jackson, M.W., Junk, D.J., and Stark, G.R. (2013). IFNβ-dependent increases in STAT1, STAT2, and IRF9 mediate resistance to viruses and DNA damage. EMBO J. *32*, 2751–2763.

Cohen, M.J., Yousef, A.F., Massimi, P., Fonseca, G.J., Todorovic, B., Pelka, P., Turnell, A.S., Banks, L., and Mymryk, J.S. (2013). Dissection of the C-terminal region of E1A redefines the roles of CtBP and other cellular targets in oncogenic transformation. J. Virol. *87*, 10348–10355.

Darnell, J.E., Kerr, I.M., and Stark, G.R. (1994). Jak-STAT pathways and transcriptional activation in response to IFNs and other extracellular signaling proteins. Science *264*, 1415–1421.

Dignam, J.D., Martin, P.L., Shastry, B.S., and Roeder, R.G. (1983). Eukaryotic gene transcription with purified components. Methods Enzymol. *101*, 582–598.

Dumont, D.J., Tremblay, M.L., and Branton, P.E. (1989). Phosphorylation at serine 89 induces a shift in gel mobility but has little effect on the function of adenovirus type 5 E1A proteins. J. Virol. *63*, 987–991.

Ferrari, R., Gou, D., Jawdekar, G., Johnson, S.A., Nava, M., Su, T., Yousef, A.F., Zemke, N.R., Pellegrini, M., Kurdistani, S.K., et al. (2014). Adenovirus small E1A employs the lysine acetylases p300/CBP and tumor suppressor Rb to repress select host genes and promote productive virus infection. Cell Host Microbe *16*, 663–676.

Ferreon, J.C., Martinez-Yamout, M.A., Dyson, H.J., and Wright, P.E. (2009). Structural basis for subversion of cellular control mechanisms by the adenoviral E1A oncoprotein. Proc. Natl. Acad. Sci. U. S. A. *106*, 13260–13265.

Fink, K., and Grandvaux, N. (2013). STAT2 and IRF9: Beyond ISGF3. Jak-Stat *2*, e27521.

Freaney, J., Kim, R., Mandhana, R., and Horvath, C. (2013). Extensive cooperation of immune master regulators IRF3 and NF??B in RNA Pol II recruitment and pause release in human innate antiviral transcription. Cell Rep. *4*, 959–973.

Hardy, S., Kitamura, M., Harris-Stansil, T., Dai, Y., and Phipps, M.L. (1997). Construction of adenovirus vectors through Cre-lox recombination. J. Virol. *71*, 1842–1849.

Harlow, E., Franza, B.R., and Schley, C. (1985). Monoclonal antibodies specific for adenovirus early region 1A proteins: extensive heterogeneity in early region 1A products. J. Virol. *55*, 533–546.

Ikushima, H., Negishi, H., and Taniguchi, T. (2013). The IRF family transcription factors at the interface of innate and adaptive immune responses. Cold Spring Harb. Symp. Quant. Biol. *78*, 105–116.

Jones, N., and Shenk, T. (1979). Isolation of adenovirus type 5 host range deletion mutants defective for transformation of rat embryo cells. Cell *17*, 683–689.

Komorek, J., Kuppuswamy, M., Subramanian, T., Vijayalingam, S., Lomonosova, E., Zhao, L.-J., Mymryk, J.S., Schmitt, K., and Chinnadurai, G. (2010). Adenovirus type 5 E1A and E6 proteins of low-risk cutaneous beta-human papillomaviruses suppress cell transformation through interaction with FOXK1/K2 transcription factors. J. Virol. *84*, 2719–2731.

Lin, R., Heylbroeck, C., Pitha, P.M., and Hiscott, J. (1998). Virus-Dependent Phosphorylation of the IRF-3 Transcription Factor Regulates Nuclear Translocation, Transactivation Potential, and Proteasome-Mediated Degradation. Mol. Cell. Biol. *18*, 2986–2996.

McKendry, R., John, J., Flavell, D., Müller, M., Kerr, I.M., and Stark, G.R. (1991). High-frequency mutagenesis of human cells and characterization of a mutant unresponsive to both alpha and gamma interferons. Proc. Natl. Acad. Sci. U. S. A. *88*, 11455–11459.

Montell, C., Courtois, G., Eng, C., and Berk, A. (1984). Complete transformation by adenovirus 2 requires both E1A proteins. Cell *36*, 951–961.

Pelka, P., Ablack, J.N.G., Fonseca, G.J., Yousef, A.F., and Mymryk, J.S. (2008). MINIREVIEW Intrinsic Structural Disorder in Adenovirus E1A: a Viral Molecular Hub Linking Multiple Diverse Processes. J. Virol. *82*, 7252–7263.

Schoggins, J.W. (2014). Interferon-stimulated genes: Roles in viral pathogenesis. Curr. Opin. Virol. *6*, 40–46.

Stark, G.R. (2007). How cells respond to interferons revisited: From early history to current complexity. Cytokine Growth Factor Rev. *18*, 419–423.

Suka, N., Suka, Y., Carmen, A.A., Wu, J., and Grunstein, M. (2001). Highly specific antibodies determine histone acetylation site usage in yeast heterochromatin and euchromatin. Mol. Cell *8*, 473–479.

Tsukamoto, a S., Ponticelli, a, Berk, a J., and Gaynor, R.B. (1986). Genetic mapping of a major

site of phosphorylation in adenovirus type 2 E1A proteins. J. Virol. *59*, 14–22.

Vona, C.D., Bezdan, D., Islam, A.B.M.M.K., Salichs, E., López-Bigas, N., Ossowski, S., and Luna, S.D.L. (2015). Chromatin-wide profiling of DYRK1A reveals a role as a gene-specific RNA polymerase II CTD kinase. Mol. Cell *57*, 506–521.

Wang, H.G., Moran, E., and Yaciuk, P. (1995). E1A promotes association between p300 and pRB in multimeric complexes required for normal biological activity. J. Virol. *69*, 7917–7924.

Zhao, L.-J., Subramanian, T., Vijayalingam, S., and Chinnadurai, G. (2007). PLDLS-dependent interaction of E1A with CtBP: regulation of CtBP nuclear localization and transcriptional functions. Oncogene *26*, 7544–7551.

CHAPTER 3

De-differentiation during oncogenic transformation caused by YAP/TAZ inactivation

Introduction

Compromised differentiation is a hallmark of oncogenic transformation and tumor progression (Roy and Hebrok, 2015). Likewise, expression of viral oncogenes often inhibit differentiation. Adenovirus E1A, in addition to forcing quiescent cells into S-phase by inhibiting Retinoblastoma (Rb) family proteins (DeCaprio, 2009) and repressing expression of CDK inhibitors (Ferrari et al., 2014), also represses cellular differentiation (Frisch and Mymryk, 2002). For example, E1A blocks differentiation of rodent myoblasts by interfering with the function of developmentally regulated *cis*-acting transcription control regions (Webster et al., 1988). Yet, how E1A represses differentiation of various cell types has not been fully clarified. While most E1A-induced transcriptional repression requires its interaction with the closely related lysine acetyltransferases CBP and p300 (Ferrari et al., 2014; Stein et al., 1990), it is unclear how particular genes, mainly cell-type specific genes, are targeted for repression.

A consequence of E1A's interaction with CBP and p300 is a dramatic reduction in total cellular histone H3 lysines 27 and 18 acetylation (H3K27/18ac) (Ferrari et al., 2014; Horwitz et al., 2008; Jin et al., 2011). H3K27/18ac are highly enriched at enhancers and promoters of active genes, and their presence correlates with enhancer activity (Creyghton et al., 2010). Enhancers are critical for establishing the diversity between different cell types necessary for the complex multi-tissue development of a metazoan (Bulger and Groudine, 2011; Carey, 1998; Levine, 2010). More recently, a new classification of enhancers, termed super-enhancer, was described that includes ~1.5-4% of enhancers in differentiated mammalian cells (Whyte et al., 2013). Super-enhancers are clusters of neighboring enhancers with a high density of transcription factor (TF) binding, activating histone marks and co-activator association (Whyte et al., 2013). Super-

enhancers often are controlled by cell-type-specific TFs and regulate key cell identity genes important for normal mammalian development.

The Hippo pathway regulates organ size across metazoans (Pan, D., 2013; Yu et al., 2015; Zanconato et al., 2016;) and is essential for the first tissue differentiation during mammalian embryonic development: the differentiation of cells on the surface of the 16-32 cell embryo (morula) into trophectoderm which will develop into the early placenta, and cells in the interior of the morula which develop into the embryo and adult (Sasaki, 2017). In mammals, paralogous transcription co-activators, YAP (aka YAP1) and TAZ (aka WWTR1), are the terminal effectors for Hippo signaling and activate target genes mainly through binding TEAD family TFs (Zhao et al., 2008). *YAP/TAZ* are considered to be oncogenes because they are frequently over-expressed in a variety of human cancers, are often amplified in squamous cell carcinoma, and over-expression of *YAP/TAZ* target genes correlates with poor prognosis (Wang et al., 2018). YAP is indispensable for early embryonic development (Sasaki, 2017), and is expressed at some point during the development of almost all mammalian cell types (Varelas, 2014). During active Hippo signaling, a kinase cascade results in phosphorylation and activation of kinases LATS1/2 which phosphorylate YAP/TAZ leading to their cytoplasmic retention and ubiquitin-mediated degradation (Yu et al., 2015). Crucially, the hippo pathway regulates expression of multiple genes in response to mechanical cues generated by interactions with neighboring cells and the extracellular matrix (ECM) (Dupont et al., 2011; Meng et al., 2018). The AMOT family proteins (AMOTs) enhance Hippo signaling by activating LATS1/2 at adherens junctions between cells in preimplantation embryos (Hirate et al., 2013). Hippo signaling is suppressed when AMOTs are sequestered away from adherens junctions by binding to filamentous actin (F-actin) (Hirate et al., 2013). AMOTs also inhibit YAP/TAZ through direct

interactions (Chan et al., 2011; Zhao et al., 2011). YAP/TAZ also are regulated by alternative Wnt signaling in addition to Hippo pathway signaling (Park et al., 2015).

We began this study pursuing the mechanism of how adenovirus E1A causes preferential hypoacetylation of H3K27/18 at enhancers and super-enhancers compared to promoters (TSSs). Unexpectedly, we found that most of this regulation of H3 acetylation occurs at sites of TEAD TF association, leading us to the discovery that E1A inactivates the TEAD co-activators YAP and TAZ by causing their sequestration in the cytoplasm. Further analyses showed that YAP/TAZ inactivation contributes greatly to the de-differentiated phenotype of adenovirus-transformed cells. Despite hundreds of generations of E1A-induced de-differentiation, when E1A was eliminated from HEK293 cells, they retained the ability to re-differentiate into cells resembling normal human mesenchymal stem cells (MSC), the cell type from which they were likely derived. This re-differentiation was dependent on activation by both YAP and TAZ. Mechanistically, following E1A loss, YAP and TAZ translocate from the cytoplasm to the nucleus, dependent on F-actin assembly and signaling through Rho-family small GTPases. In the nucleus they associate with TEAD TFs and establish enhancers and then super-enhancers that strongly activate MSC-specific genes necessary for a drastic change in cell morphology. Virtually all the MSC-specific gene activation and enhancer establishment after removal of E1A depends on YAP/TAZ. These results, together with earlier studies, suggest that YAP/TAZ operate in a developmental check-point regulated by signals from the actin cytoskeleton generated through indirect interactions with adherens junctions between neighboring cells and with the surrounding extracellular matrix. Such signaling from the actin-cytoskeleton is required for MSC differentiation because YAP/TAZ associate with and activate virtually all MSC-specific enhancers.

RESULTS

E1A represses principally cell-type specific genes

To analyze E1A repression of cell-type specific genes as opposed to ubiquitously expressed genes, we performed RNA-seq on three cultured primary human cell types at 24 h post-infection with adenovirus type 5 (Ad5) mutant *dl*1500 (Montell et al., 1984). This mutant has a nine base-pair deletion of the 5' splice-site of the mRNA encoding the large E1A isoform, and consequently expresses only the small E1A protein isoforms. Since large E1A is required to activate transcription from all other viral RNA Polymerase II promoters (Montell et al., 1984; Winberg and Shenk, 1984), *dl*1500 expresses only the small E1A isoforms and very low levels of other viral proteins. Considering genes with a greater than 2-fold change in FPKM comparing *dl*1500-infected to control, mock-infected cells and a q-value <0.05 at 24h p.i., 495 genes were repressed by small E1A in primary human foreskin fibroblasts (HFF), 755 in primary human fetal lung fibroblasts (IMR90), and 1869 in primary human bronchial/tracheal epithelial cells (HBTEC) (Fig. 3.1A), considerably more than in the IMR90 and HFF fibroblasts. This may be because HBTECs are derived from the natural host tissue for Ad5. The genes repressed in the HBTECs are expressed at higher level in these epithelial cells compared to the fibroblasts, while the genes repressed uniquely in the fibroblasts are expressed at higher level in the fibroblasts than in the epithelial cells (Fig. 3.1B). The gene ontologies of genes repressed uniquely in IMR90 fibroblasts are enriched for fibroblast functions, while the genes repressed uniquely in HBTECs are enriched for epithelial differentiation and development (Fig. 3.1C). Therefore, E1A preferentially represses highly expressed cell type-specific genes, potentially explaining E1A's ability to repress differentiation of various cell types (Frisch and Mymryk, 2002).

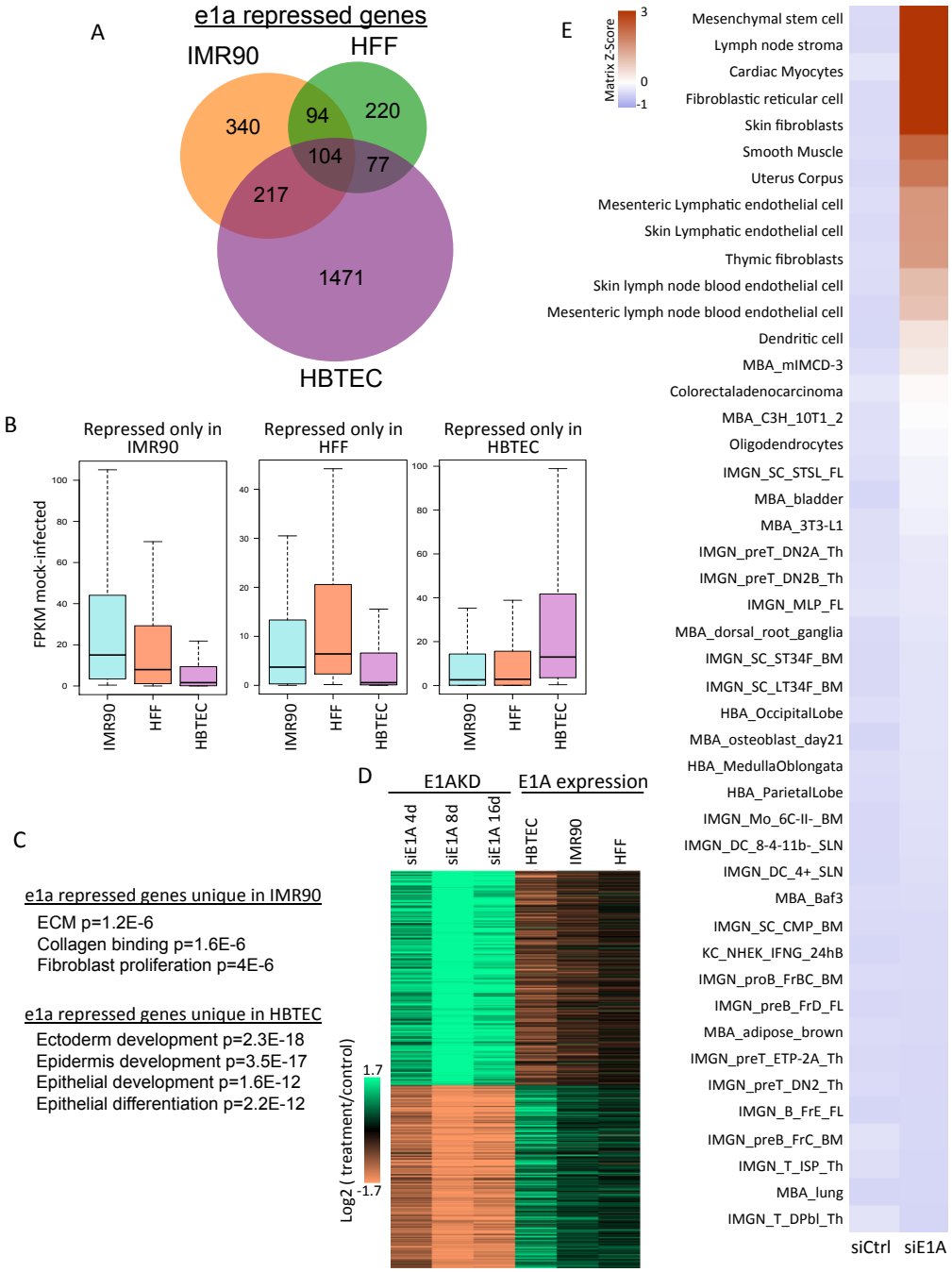

Figure 3.1 E1A represses cell specific gene expression and differentiation
(**A**) Venn diagram representing number of overlapping and non-overlapping significantly repressed genes from mRNA-seq in IMR90 (Ferrari et al. 2014), HFF, or HBTEC (Zemke and Berk, 2017) infected for 24 hours with Ad5 small E1A vector at multiplicity of infection (MOI) 40 for IMR90 and 60 for HFF and HBTEC. (**B**) Boxplots represent expression distributions (FPKM) in mock-infected cells of genes uniquely repressed by small E1A in the cell types indicated at the top. (**C**) Gene ontology (DAVID) enriched terms of genes uniquely repressed by small E1A in IMR90 or HBTEC. (**D**) Heatmap comparing expression change for all genes activated and repressed by E1AKD in HEK293 cells to expression change of the same genes in HBTEC, IMR90, or HFF 24 h post infection with Ad5 *dl*1500 expressing small E1A compared to mock-infected cells. (**E**) SaVanT analysis heatmap displaying Z-scores for similarity of expression values of HEK293 siRNA transfected cells to gene signatures in various cell types. Z-scores for cell types most similar to E1AKD293 are: MSC 3.9, lymph node stroma 3.8, cardiac myocytes 3.3, fibroblastic reticular cell 3.3, skin fibroblasts 3.1, smooth muscle 2.3.

Following loss of E1A, HEK293 cells re-differentiate into cells with properties of MSCs

To determine if removing E1A from adenovirus-transformed cells would reverse repression of cellular differentiation, we performed E1A siRNA knockdown (E1AKD) in the Ad5-transformed human embryonic kidney cell line HEK293 (Graham et al., 1977) followed by RNA-sequencing (RNA-seq). E1A protein levels were reduced to <1% by four days post E1A siRNA transfection (Fig. 3.2A). Considering genes with expression changes >2-fold and q-value <0.05 compared to cells transfected with a negative control siRNA (siCtrl) at eight days post siRNA-transfection, E1AKD repressed 2203 genes and activated 2584 genes (Fig. 3.2B). E1AKD-repressed genes were highly enriched for cell cycle function (Fig. 3.2C), and were likely repressed by re-activation of Rb family proteins. In contrast, the genes activated following E1AKD were enriched for MSC functions such as ECM synthesis, components of focal adhesions, collagen catabolism, and mesodermal cell differentiation (Fig. 3.2C). Genes activated by E1AKD in HEK293 cells are repressed by E1A in normal primary human cells, while genes repressed by E1AKD in HEK293 cells are activated by E1A in normal primary human cells (Fig. 3.1D). Consequently, most genes regulated by E1A in HEK293 cells are bona fide E1A-regulated genes in acutely infected primary human cells. Consequently, it is probably more accurate to consider genes "activated by E1AKD" to be repressed by E1A in the transformed HEK293 cells, and **de-repressed** when E1A is virtually eliminated by E1A siRNA.

By 4 days of E1AKD, the cells underwent a dramatic change in morphology, expanding to a larger surface area, mostly due to an increased cytoplasmic compartment accompanied by dense newly formed actin filaments (F-actin) stained with fluorescent-phalloidin (Fig. 3.2D). These "E1AKD293 cells" also assumed a much flatter morphology than the siCtrl cells, which were similar to untreated HEK293 cells and had a more globular shape with scant cytoplasm,

indicative of rapidly proliferating cells (Fig. 3.2D). The bioinformatic Signature Visualization Tool (SaVanT), which compares gene expression profiles of multiple human and mouse cell types and tissues (Lopez et al., 2017), scored E1AKD293 cells as most similar to normal mesenchymal stem cells (MSCs), and slightly less so to fibroblasts which have a similar pattern of gene expression to MSCs (Driskell and Watt, 2015) (Fig. 3.1E). HEK293 cells did not have a gene expression profile similar to any normal human cell type (Fig. 3.1E). HEK293 were derived by stable transformation of cultured primary human embryonic kidney cells with fragmented Ad5 DNA (Graham et al., 1977). Consequently, the cell type originally transformed was likely one of the most abundant cell types in the developing embryonic kidney, including MSC, the most abundant (Little and McMahon, 2012). Taken together, the RNA-seq data and morphological changes indicate that following loss of E1A, the E1AKD293 cells re-differentiate into cells with properties of MSCs.

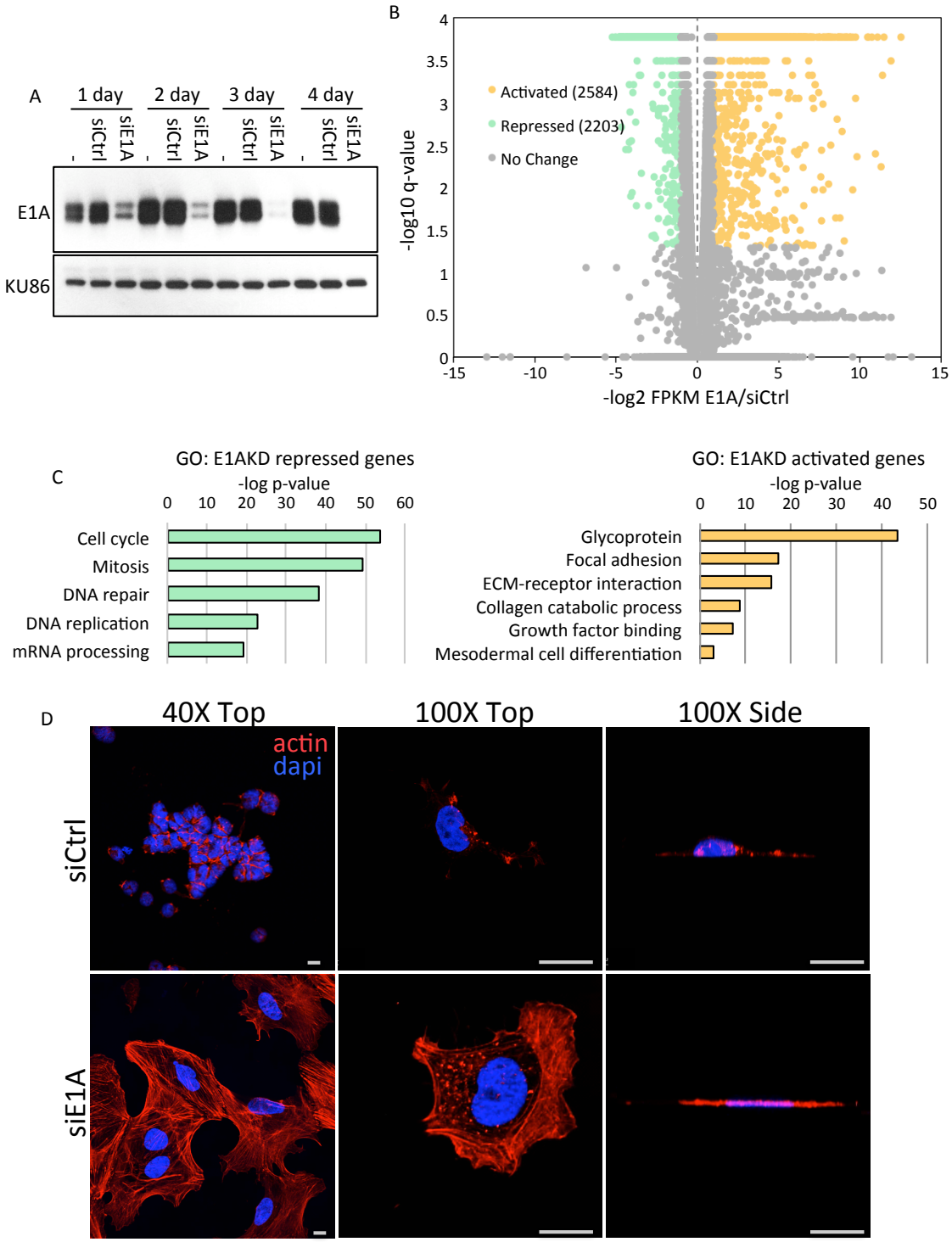

Figure 3.2 E1AKD in HEK293 cells reverses oncogenic transformation associated gene expression and morphology

(A) Expression of E1A proteins after 1-4 days of indicated siRNA transfections or mock-transfected (-) in HEK293 cells. Nuclear protein KU86 serves as a loading control. **(B)** XY scatter plot displaying genes as dots and indicating genes significantly changed ($q<0.05$) with >2X activated (yellow) or repressed (green) by E1AKD compared to siCtrl in HEK293 cells following 8 days of siRNA treatment. **(C)** Gene ontology (DAVID) enriched terms of activated or repressed E1AKD genes from analysis from Fig. 3.2B. **(D)** Confocal microscopy of siRNA transfected HEK293 cells for 4 days fixed and stained with phalloidin-iFluor and DAPI.

E1AKD establishes typical and super-enhancers to activate MSC-specific gene expression

E1A's principle mechanism of repression is associated with inhibition of CBP and p300 acetyltransferase activity (Ferrari et al., 2014; Stein et al., 1990), and a reduction in total cell H3K18ac and H3K27ac to ~30% the level in control cells (Ferrari et al., 2014; Horwitz et al., 2008). Consistent with this, E1AKD in HEK293 reciprocally resulted in an increase in total H3K27/18ac (Fig. 3.3A). To identify the genomic regions that gained H3 acetylation we performed ChIP-seq at 1 and 4 days post siRNA transfection. By 4 days, H3K27ac increased 5-fold or more at 3,657 peaks; 90% of these are more than 5 kb from a transcription start site (TSS), indicative of enhancers (Fig. 3.3B). Only 220 H3K27ac peaks showed a greater than 5-fold reduction with 53% being within 5 kb of a TSS. These peaks are enriched for E2F motifs (p=1E-17) and likely were hypoacetylated because the return of Rb family protein activity after loss of E1A repressed E2F-directed H3 acetylation. Most of the E1AKD-induced H3 acetylation was gained at enhancers while promoters were largely unaffected (Fig. 3.3B). Consistently, in normal primary HBTECs, E1A induced H3K27/18 hypoacetylation at enhancers to a much greater extent than promoters (Fig. 3.4A).

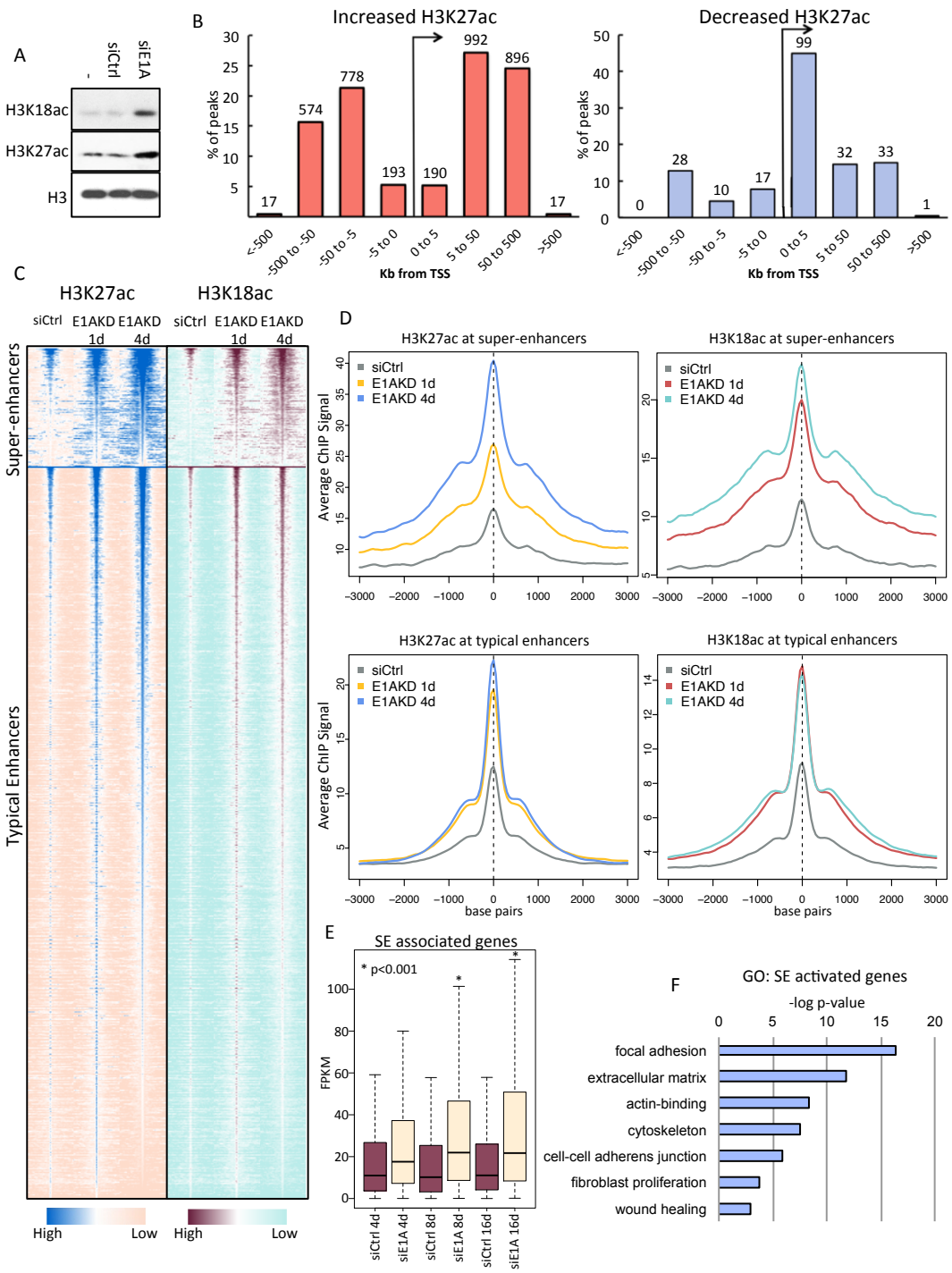

Figure 3.3 E1AKD in HEK293 cells stimulates H3 acetylation at enhancers genome-wide
(A) Levels of total H3K18 and H3K27 acetylation following 1 day of siRNA transfection or mock-transfection (-) in HEK293 cells. **(B)** Bars represent percentage of significant H3K27ac or H3K18ac ChIP-seq peaks found within indicated distance to nearest TSS. **(C)** Heat maps representing relative ChIP-seq read density for each significant peak that was located > 2.5kb from a TSS and subdivided into super-enhancer or typical enhancer peaks from siRNA transfected HEK293 cells. Base pair span is +/-3kb from center of peak. **(D)** Averages of ChIP-seq read density centered at all significant peaks of either typical enhancers or within super- enhancers following indicated siRNA transfections in HEK293 cells. **(E)** Boxplots represent expression distributions (FPKM) of SE-associated gene expression following indicated siRNA transfections in HEK293 cells. * p<0.001 as compared to siCtrl of same transfection length. **(F)** Gene ontology (DAVID) enriched terms of E1AKD293 activated SE-associated genes.

To determine how super-enhancers respond to E1A we used the Ranking of Super-Enhancers (ROSE) algorithm (Hnisz et al., 2013) with H3K27ac ChIP-seq data from 4-day siRNA transfected cells. This identified 272 super-enhancers in HEK293 transfected with control siRNA, compared to 668 in E1AKD293 cells (Fig. 3.4B). 477 new super-enhancers formed in E1AKD293 cells. H3K27/18ac increased within typical enhancers after 1 day of E1AKD then remained stable, while levels in super-enhancers continued to increase for 4 days (Fig. 3.3C,D). Super-enhancer associated genes (assigned by proximity) were significantly de-repressed after E1AKD (Fig. 3.3E), and their gene ontologies are enriched for MSC functions, focal adhesion, ECM and adherens junctions, also enriched in normal MSC (Fig. 3.3F). Therefore, E1AKD de-represses genes that promote differentiation of HEK293 into MSC-like cells by establishing typical and super-enhancers that activate them. Since cell type-specific genes tend to be the genes most reliant on enhancers for expression (Heinz et al., 2015), E1A's preferential targeting of H3K27/18 hypoacetylation to typical and super-enhancers may explain why cell-type specific genes are targeted for repression.

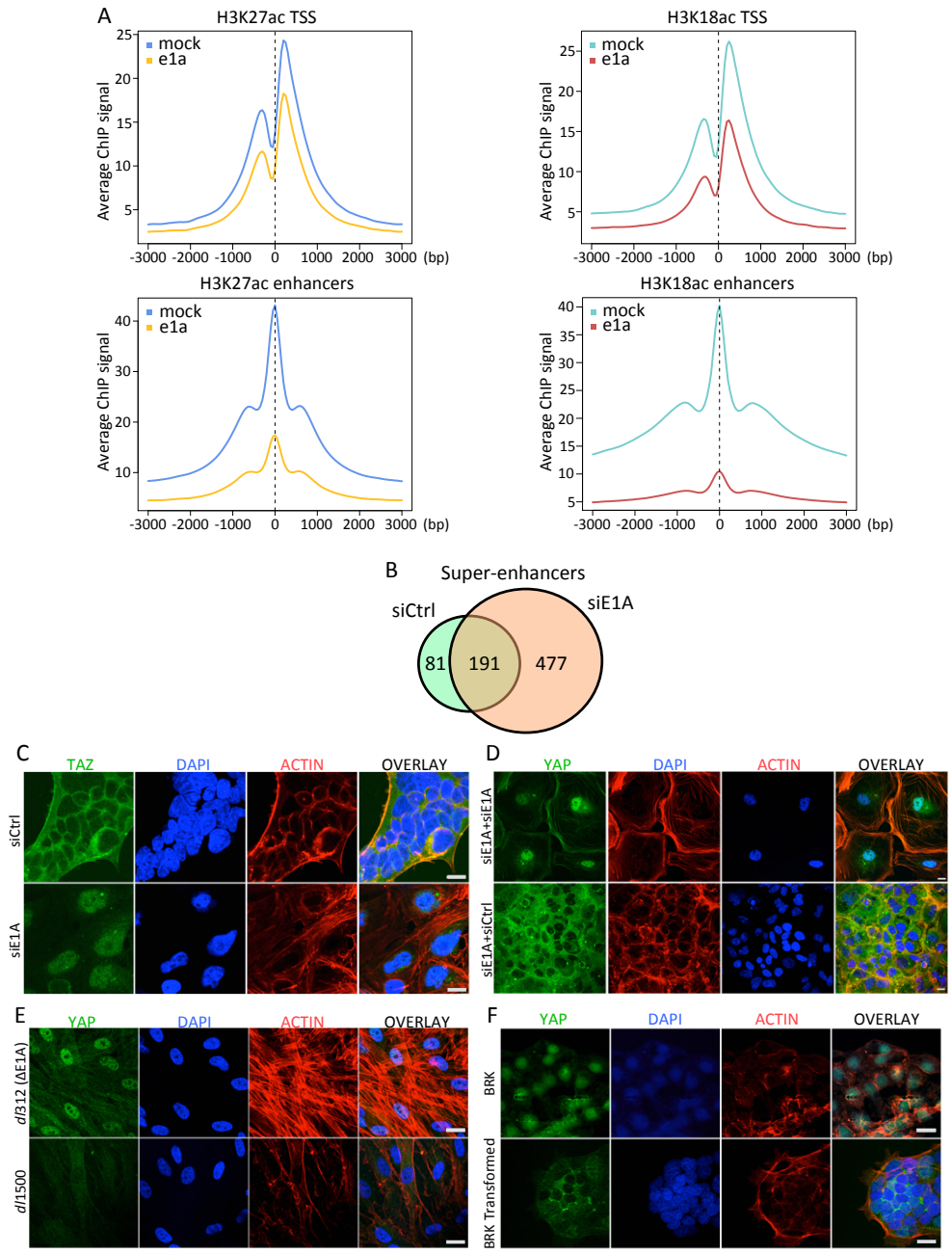

Figure 3.4 Enhancers are most sensitive to E1A-induced hypoacetylation and YAP is inactivated by E1A in different cell types

(A) Average ChIP-seq signal centered at all TSS (top) or enhancers (H3K27ac peaks >2.5kb from a TSS) in HBTEC following 24 hours of mock-infection or infection with Ad5 dl1500 mutant expressing small E1A (e1a). MOI 60. **(B)** Venn diagram of super-enhancers in HEK293 transfected with siCtrl (green) or siE1A (orange). **(C)** Confocal microscopy of 4 day siRNA transfected HEK293 cells fixed and immunostained with anti-TAZ (CL0371) and stained with phalloidin-iFluor and DAPI. Scale bars represent 20 µM. **(D)** HEK293 cells were transfected with siE1A RNA. Four days later, the media was changed to media with siE1A RNA (top row, siE1A+siE1A), or media with siCtrl RNA (siE1A+siCtrl). 4 days later cells were fixed and stained with anti-YAP antibody (DH81X), phalloidin-iFluor and DAPI and confocal micrographs were prepared. **(E)** Confocal microscopy of IMR90 cells infected for 4 days with Ad5 dl312 (ΔE1A) or dl1500 (expressing small E1A) at MOI 10. Fixed and immunostained with anti-YAP (DH81X) phalloidin-iFluor and DAPI. **(F)** Confocal microscopy of normal BRK cells or BRK transformed with E1A and E1B. Fixed and immunostained with anti-YAP (DH81X) and stained with phalloidin-iFluor and DAPI.

E1AKD induces YAP association with chromatin-bound TEADs, chromatin remodeling and gene activation

To determine if the newly established enhancers following E1AKD are in an accessible or inaccessible chromatin state prior to gaining H3 acetylation, we performed ATAC-seq (Buenrostro et al., 2013). Removal of E1A greatly increased ATAC-seq signal particularly ~300 bp up- or downstream of H3K27ac peaks (Fig. 3.5A), suggesting that TF binding in these regions generated increased chromatin accessibility. To identify the TFs involved in establishing the newly formed enhancers we performed HOMER motif analysis (Heinz et al., 2010) on E1AKD induced ATAC peaks (>5-fold increase in ATAC signal following E1AKD), and observed overwhelming enrichment for TEAD family TF binding motifs (Fig. 3.5B). Using ChIP-seq, TEAD1 and TEAD4 were found to be highly enriched at the E1AKD-induced ATAC peaks (Fig. 3.5C,D), implicating TEAD TFs in establishment of the newly formed enhancers in E1AKD293 cells.

For TEAD family TFs to activate gene expression they must associate with the closely related co-activators YAP and/or TAZ (Vassilev et al., 2001). Since YAP and TAZ are regulated through cytoplasmic restriction (Dong et al., 2007; Zhao et al., 2007) we determined whether or not their subcellular localization changed following E1AKD. Indeed, in control HEK293 YAP/TAZ are mostly restricted to the cytoplasm, and upon E1AKD they became concentrated in the nucleus (Fig. 3.5E, 3.4C). This nuclear localization was reversible. HEK293 cells were treated with siE1A for 4 days, then the media was replaced with media containing either siE1A or siCtrl for an additional 4 days. The E1AKD293 cells that had the siE1A replaced with siCtrl proliferated and had mostly cytoplasmic YAP with a reduction of F-actin filaments and a smaller surface area, similar to untreated HEK293 cells (Fig. 3.4D, 3.5E). Furthermore, E1A prevented

YAP nuclear accumulation in *dl*1500-infected IMR90 (Fig. 3.4E). Also, primary baby rat kidney (BRK) cells display mostly nuclear YAP, while Ad-transformed BRK cells have mostly cytoplasmic YAP (Fig. 3.4F). Taken together, these results suggest that E1A inactivation of YAP/TAZ by cytoplasmic sequestration is a general occurrence during adenovirus oncogenic transformation and infection.

To determine if nuclear YAP associates with chromatin at E1AKD-induced ATAC peaks, we performed YAP ChIP-seq. Indeed, following E1AKD YAP peaks coincided with 91% of E1AKD-induced ATAC peaks (Fig. 3.5F,G,H). Conversely, control HEK293 cells had much less, or no detectable YAP association at these sites. E1AKD-induced super-enhancers, such as those close to E1AKD-derepressed genes *IER3* and *AMOTL2* (Fig. 3.5H), had very low H3K27/18ac, ATAC signal or YAP association in control HEK293. However, following E1AKD, ATAC peaks were generated, all of which coincided with new peaks of YAP (Fig. 3.5H,I). H3K27/18ac peaks flanking YAP peaks first appeared after 1 day of E1AKD and continued to increase and spread across the entire super-enhancers following 4 days of E1AKD (Fig. 3.5H).

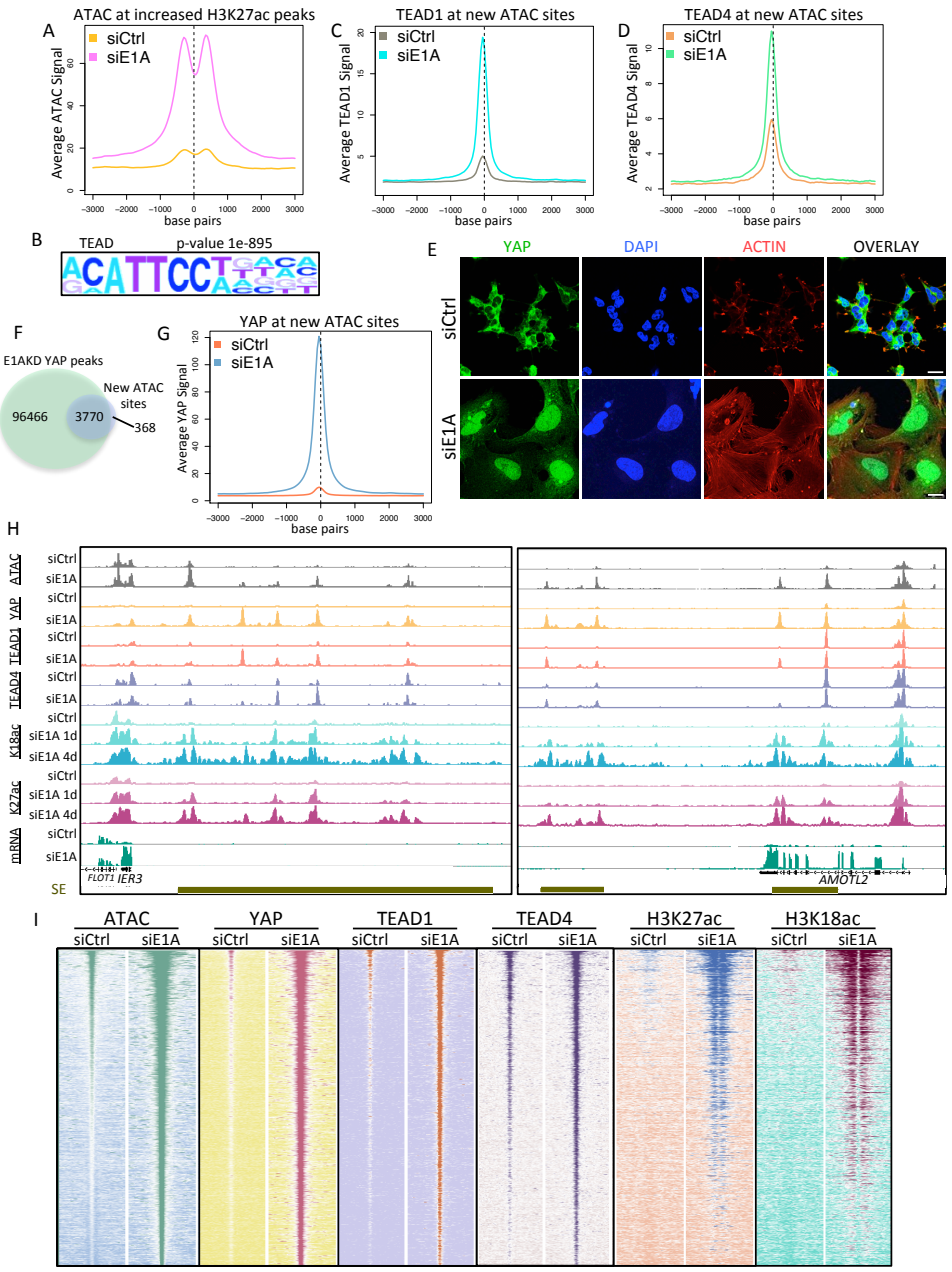

Figure 3.5 E1AKD induces YAP nuclear import and formation of TEAD/YAP complexes on chromatin at TEAD binding sites, establishing super-enhancers

(A) Average ATAC-seq signal centered at H3K27ac peaks that increased >5X following 4 days of E1AKD. **(B)** Sequence motif analysis (HOMER) showing most significantly enriched TF motif at all ATAC-seq peaks that increased >5X following E1AKD. **(C)** Average TEAD1 ChIP-seq signal centered at ATAC-seq peaks that increased >5X following 4 days of E1AKD. **(D)** Average TEAD4 ChIP-seq signal centered at ATAC-seq peaks that increased >5X following 4 days of E1AKD. **(E)** Confocal microscopy of 4 day siRNA transfected HEK293 cells fixed and immuno-stained with anti-YAP (DH81X) and stained with phalloidin-iFluor and DAPI. Scale bars represent 20µm. **(F)** Venn Diagram displaying number of overlapping or nonoverlapping ATAC-seq and YAP ChIP-seq peaks. **(G)** Average YAP ChIP-seq signal centered at ATAC-seq peaks that increased >5X following 4 days of E1AKD. **(H)** Genome browser plots (IGB) displaying indicated ChIP-, ATAC-, and mRNA-seq signal at super-enhancers (SE, gold bars) near E1AKD activated genes IER3 and AMOTL2. **(I)** Heat maps representing relative ATAC- or ChIP-seq read density centered at every E1AKD-induced ATAC-seq peak (increased >5X compared to siCtrl) from siRNA transfected HEK293 cells. Peaks are sorted by sum of ATAC-seq peak signal in siE1A. Base pair span is +/- 3kb from center of peak.

TEAD4 was found at many of the E1AKD-induced enhancers prior to E1AKD, indicating that these enhancers were marked with DNA-bound TEAD4 prior to their activation (Fig. 3.5D,H,I). However, H3K27/18ac and ATAC accessibility increased greatly when YAP was associated in E1AKD293 cells (Fig. 3.5A,H,I). H3K4me1 is found at both active enhancers and inactive, poised enhancers (Creyghton et al., 2010; Heintzman et al., 2009). In control HEK293, H3K4me1 was enriched at E1AKD induced ATAC peaks, but in E1AKD293 cells, H3K4me1 shifted to ~200-300 bp up- and downstream from the center of the ATAC peak (Fig. 3.6A, 3.6B). This finding suggests that chromatin remodeling occurred when YAP/TAZ associated with the DNA-bound TEAD TFs, resulting in nucleosome depleted regions detected as high ATAC peaks. Additionally, the level of TEAD4 and H3K4me1 correlated in control HEK293 (Fig. 3.6C), consistent with their co-occupancy at individual loci. Taken together, these data suggest that in HEK293 many of the E1AKD-induced enhancers are epigenetically pre-marked by DNA-bound TEAD4 and H3K4me1, but undergo chromatin remodeling following YAP binding to TEAD4, which induces chromatin accessibility and recruitment of additional transcriptional activators such as TEAD1.

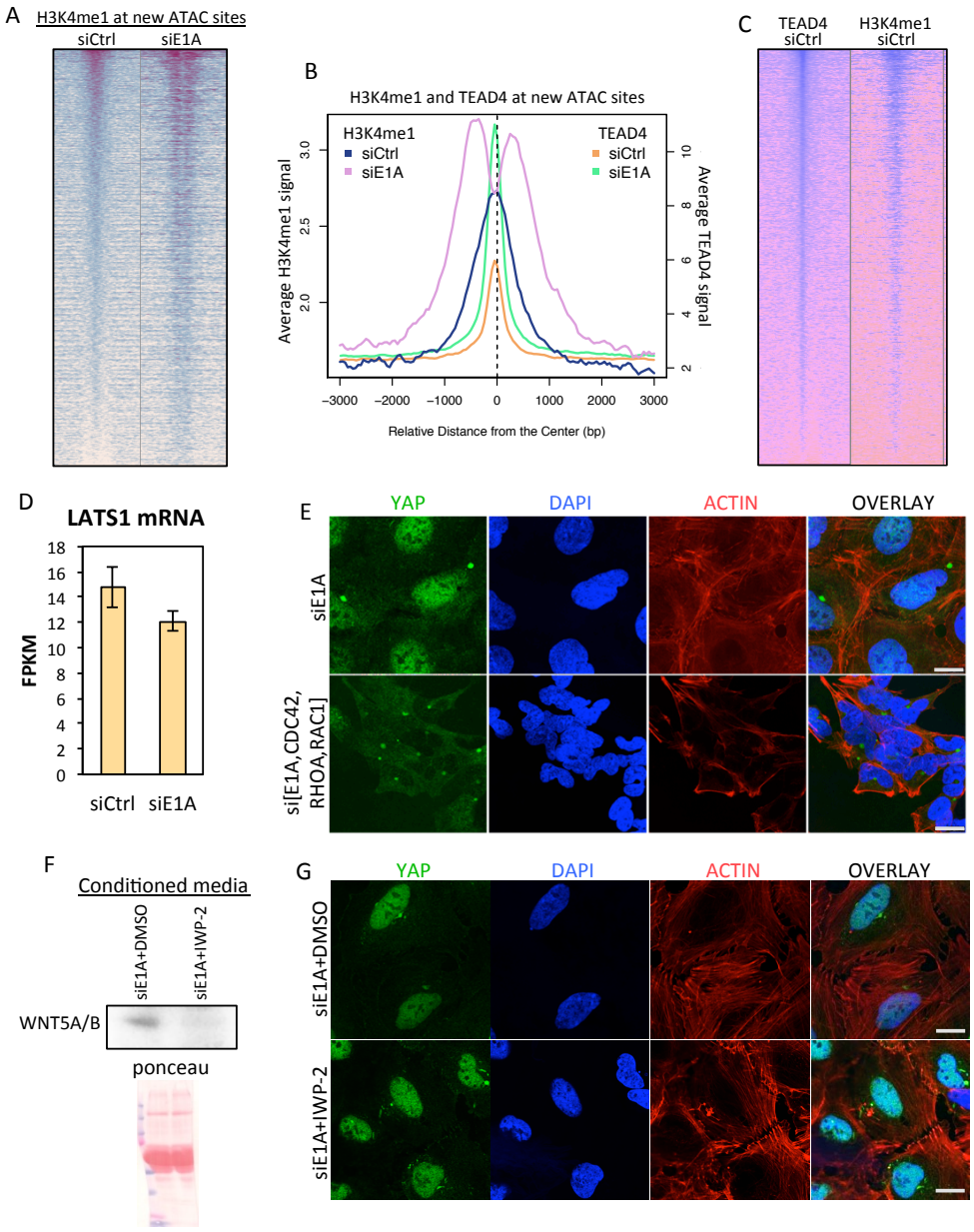

Figure 3.6 H3K4me1 and TEAD4 mark inactive enhancers and F-actin but not alternative Wnt signaling in E1AKD293 cells activates YAP

(A) Heatmap displaying relative signal for H3K4me1 ChIP-seq reads from HEK293 cells 4 days post siRNA transfection for at all ATAC-seq peaks that increased >5X with E1AKD (new ATAC sites) . Base pair span is +/- 3kb from the center of the ATAC peak. **(B)** Average ChIP-seq signal after transfection with the indicated siRNAs for 4 days centered at ATAC-seq peaks that increased >5X following 4 days of E1AKD. **(C)** Heatmap displaying relative signal for TEAD4 or H3K4me1 ChIP-seq reads in HEK293 cells 4 days post transfection at all ATAC-seq peaks that increased >5X with E1AKD (new ATAC sites). Peaks are sorted by amount of H3K4me1 signal in siCtrl HEK293 cells. Base pair span is +/-3 kb from center of peak. **(D)** Average expression level (FPKM) of LATS1 from 3 replicates of siRNA transfected HEK293 cells. **(E)** Confocal microscopy of 4 day siRNA transfected HEK293 cells fixed and immunostained with anti-YAP (DH81X), phalloidin-iFluor and DAPI. Scale bars represent 20µM. **(F)** Western blot for WNT5A/B using supernatant of E1AKD293 cell culture conditioned media following 4 days of transfection and DMSO or IWP-2 (2µM) treatment. Ponceau red of membrane serves as a loading control. **(G)** Confocal microscopy of HEK293 cells 4days after siRNA transfection and addition of either DMSO or IWP-2 in DMSO (2µM final media concentration). Cells were fixed and immunostained with anti-YAP (DH81X) and stained with phalloidin-iFluor and DAPI.

YAP activation requires F-actin and coincides with reduced Hippo signaling and AMOT re-localization

To determine if alterations in Hippo signaling account for YAP/TAZ activation when E1A is removed from HEK293 cells, we assayed protein levels and phosphorylation of YAP/TAZ and their upstream regulatory kinases LATS1/2. Nuclear YAP and TAZ are more stable than cytoplasmic YAP/TAZ (Yu et al. 2015). Consistent with this, the shift of YAP/TAZ from the cytoplasm into the nucleus in E1AKD293 cells was associated with substantial increases in YAP and TAZ (Fig. 3.7A). Unexpectedly, total LATS1 protein decreased considerably in E1AKD293 cells (Fig. 3.7A), while there was no significant decrease in LATS1 mRNA (Fig. 3.6D). This suggests post-transcriptional down-regulation of LATS1 following loss of E1A. Consistent with this, treatment with the drug MLN4924, an inhibitor of cullin neddylation required for activity of cullin-based ubiquitin ligases (Soucy et al., 2009), prevented the decrease in LATS1 (Fig. 4B). The level of LATS1 in control HEK293 cells was unaffected by MLN4924 suggesting ubiquitin-mediated degradation of LATS1 in E1AKD293 cells but not in HEK293 cells. In contrast, the protein level of LATS2 was unchanged before and after E1AKD (Fig. 3.7A). Activation by YAP/TAZ is promoted when LATS1 is in its inactive, hypophosphorylated state due to low activity of upstream Hippo pathway kinases. The level of T1079-phosphorylated, activated LATS1 in E1AKD293 cells was decreased compared to control siRNA-transfected HEK293 cells (Fig. 3.7A). The decrease in total LATS1 and phospho-T1079 LATS1 probably contribute to high YAP/TAZ activity in E1AKD293 cells.

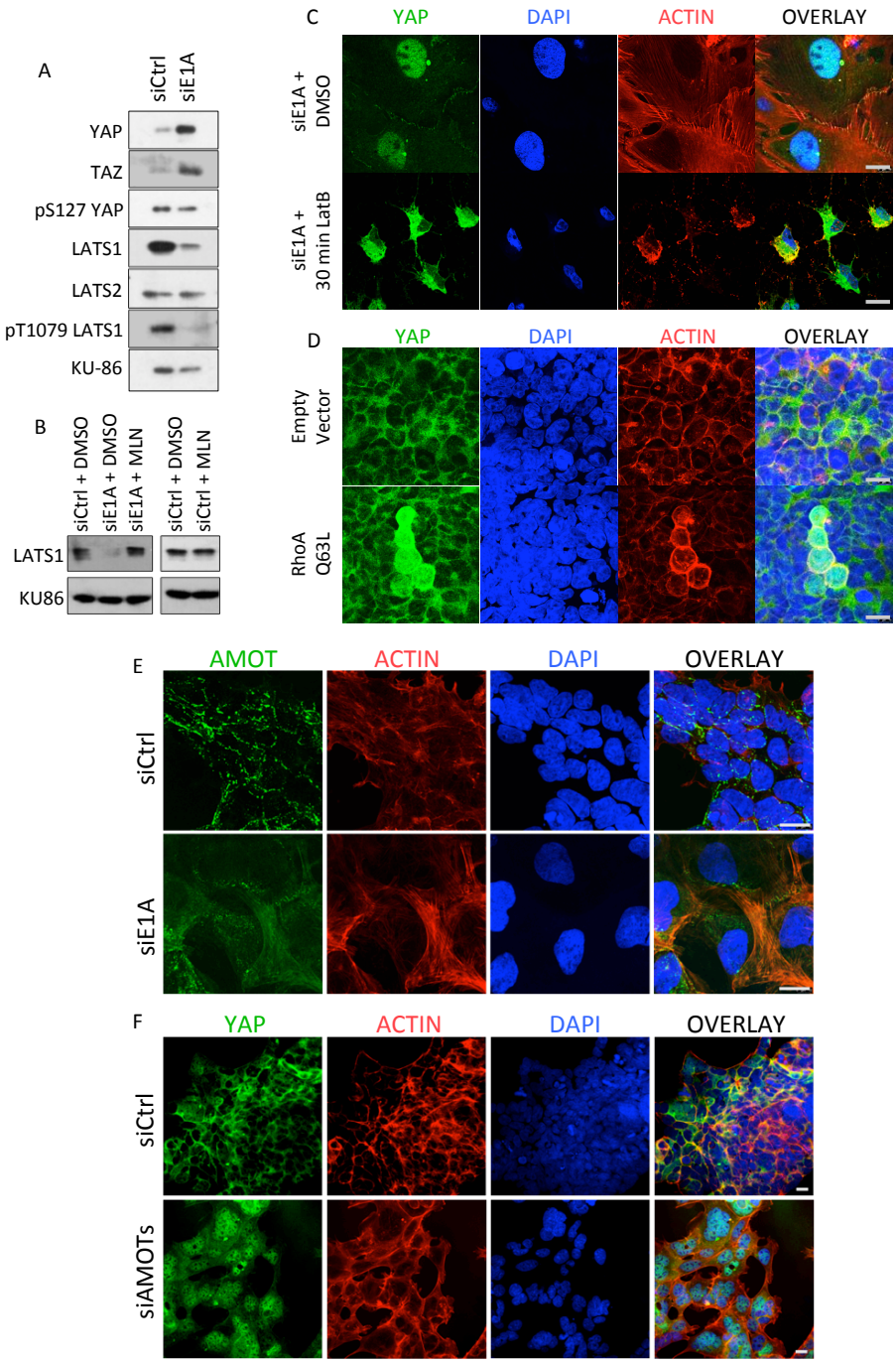

Figure 3.7 YAP nuclear import depends on F-actin and coincides with Hippo signaling and AMOT re-localization

(A) Protein levels and phosphorylation status of Hippo pathway proteins from 4 day siRNA transfected HEK293 cells. KU86 serves as a loading control. **(B)** LATS1 protein levels from HEK293 cells transfected for 3 days with either siCtrl or siE1A then treated with 5μM MLN4924 or DMSO control for 8 hours. **(C)** E1AKD293 cells treated with either DMSO or latrunculin B (LatB) for 30 minutes following 4 days of siE1A transfection. Cells were fixed and immuno-stained with anti-YAP (DH81X) and stained with phalloidin-iFluor and DAPI. **(D)** HEK293 cells were transfected with an empty vector plasmid or plasmid expressing RhoA Q63L for 3 days. Cells were fixed and immuno-stained with anti-YAP (DH81X) and stained with phalloidin-iFluor and DAPI. **(E)** Confocal microscopy of 4day siRNA transfected HEK293 cells fixed and immuno-stained with anti-AMOT and stained with phalloidin-iFluor and DAPI. **(F)** Same as in **E** except cells were immuno-stained with anti-YAP instead of anti-AMOT.

Since signals from the actin cytoskeleton activate YAP/TAZ (Dupont et al., 2011), and we observed robust F-actin assembly in E1AKD293 cells, we tested if F-actin is necessary for YAP activation by treating with latrunculin B, an inhibitor of actin polymerization. A 30 min treatment of E1AKD293 cells caused actin filament disassembly and YAP cytoplasmic localization (Fig. 3.7C). Consistent with a requirement for signaling from the actin cytoskeleton, knock-down of Rho-family small GTPases CDC42, RhoA, and RAC1 known to stimulate actin fiber assembly and dynamics, prevented YAP nuclear accumulation when E1A was knocked-down (Fig. 3.6E). To determine if F-actin formation in HEK293 cells is sufficient to force YAP into the nucleus, we transfected an expression vector for constitutively active RhoA Q63L, which promotes F-actin assembly (Caron and Hall, 1998). In cells with the brightest phalloidin signal indicating assembly of actin filaments, YAP was localized in the nucleus with a more intense signal (Fig. 3.7D), suggesting that F-actin assembly and/or RhoA signaling is sufficient for YAP nuclear import, even in the presence of E1A.

During trophectoderm differentiation in the 16-32 cell embryo, the correlation between F-actin assembly and nuclear YAP/TAZ can be attributed to AMOT family protein binding to newly formed F-actin in the apical cortex of surface cells (Hirate et al., 2013). This sequesters AMOTs, preventing them from directly inhibiting YAP/TAZ or from activating LATS1/2 at adherens junctions (Hirate et al., 2013; Sasaki, 2017). To test if AMOT is re-located similarly in E1AKD293 cells we performed AMOT immuno-staining. In siCtrl 293 cells AMOT was observed primarily in punctae often at cell peripheries or between cells, consistent with its association with adherens junctions (Fig. 3.7E) where it binds and activates LATS1/2, inhibiting YAP/TAZ. Upon E1AKD, most of the AMOT was co-localized with F-actin. Consequently, AMOT sequestration by F-actin in E1AKD293 cells likely contributes to YAP/TAZ nuclear

import. Indeed, siRNA KD of all three AMOTs was sufficient to induce YAP nuclear import and E1AKD-associated morphological changes in HEK293 cells even though E1A was still expressed (Fig. 3.7F). The association of AMOTs with F-actin is inhibited by their phosphorylation by LATS1 (Chan et al., 2013). Consequently, both the reduction in active phospho-LATS1 (Fig. 3.7A) and the large increase in polymerized actin that sequesters AMOTs can account for the re-localization of AMOT with F-actin following E1AKD, and likely also contributes to YAP/TAZ nuclear accumulation.

YAP/TAZ were recently shown to be downstream effectors for alternative Wnt signaling (Park et al., 2015). To determine if YAP/TAZ are being activated by the alternative Wnt pathway in E1AKD293 cells, we treated the cells with IWP-2, an inhibitor of Wnt processing/secretion (Chen et al., 2009). While IWP-2 prevented secretion of WNT5A/B, major activators of alternative Wnt-signaling (van Amerongen, 2012) (Fig. 3.6F), it did not prevent nuclear import of YAP (Fig. 3.6G), suggesting that alternative Wnt signaling is not necessary for E1AKD induced YAP nuclear import.

YAP/TAZ are required to establish enhancers for re-differentiating HEK293 after E1A is eliminated

To determine the extent to which E1AKD-induced gene de-repression is dependent on YAP/TAZ, we used siRNA to deplete YAP and TAZ simultaneously with E1A depletion (Fig. 3.8A). RNA-seq from triple KDs of E1A, YAP and TAZ revealed that most of the gene de-repression is dependent on YAP and TAZ (Fig. 3.9A). 1488/1890 (~80%) of E1AKD de-repressed genes (FPKM siE1A/siCtrl >2, $q<.05$) were defective ($p<.05$) for de-repression in E1AKD293 cells when YAP and TAZ were also knocked-down. Surprisingly, although YAP

and TAZ have been considered to be largely functionally redundant (Nishioka et al., 2009; Xin et al., 2013), many of the E1AKD-de-repressed genes, such as *COL1A1*, *SERPINE1*, *COL3A1*, *CTGF* and *MYOF*, depend on *both* YAP and TAZ for de-repression, indicating that YAP/TAZ have non-redundant functions required for expression of these genes (Fig. 3.9B, upper panel). However, some genes rely more on YAP or TAZ for expression when E1A is removed. When YAP or TAZ were individually knocked-down at the same time as E1A, a subset of genes de-repressed by E1AKD were >5X more dependent on TAZ than YAP (Table S1, e.g. *TGM2* (Fig. 3.9B lower panel left). The gene ontology of this subset of de-repressed genes is highly enriched (P=1.3E-15) for genes involved in synthesis of molecules in the extracellular space (Table S1 and Fig. 3.10). In contrast, the subset of genes de-repressed by E1AKD that were >5X more dependent on YAP than TAZ, e.g. *FGF18* (Fig. 3.9B, lower right), were enriched for gene ontologies "positive regulation of cell proliferation" (P=1.4E-06) and "cell growth" (P=2.7E-05) as well as gene ontologies related to "extracellular region" and "focal adhesions" (Fig. 3.10).

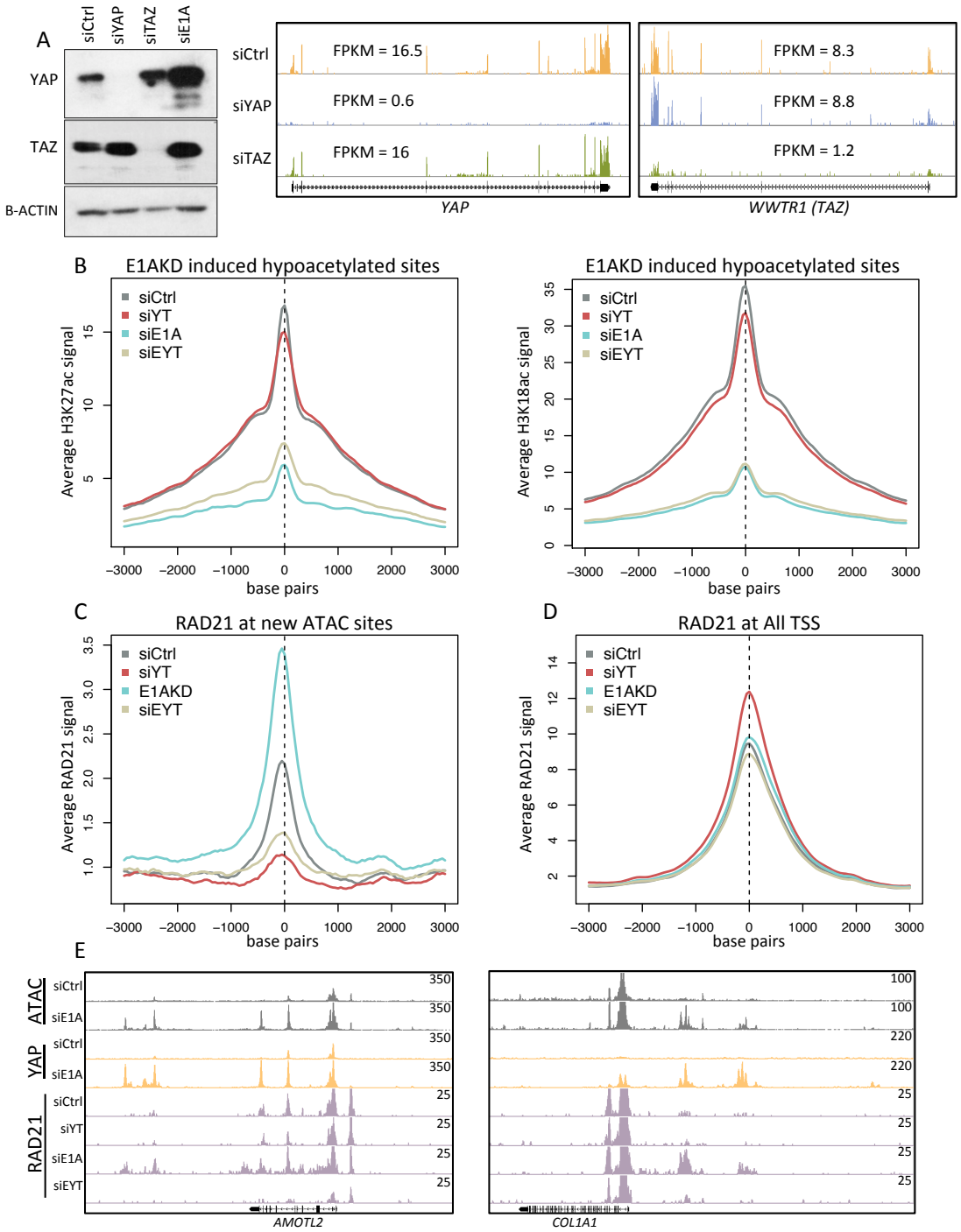

Figure 3.8 YAP and TAZ are necessary for cohesin loading at enhancers
(**A**) Left: protein levels of YAP and TAZ following indicated siRNA transfections for 2 days. β-ACTIN serves as a loading control. Right: Genome browser plots (IGB) displaying mRNA-seq signal of *YAP* and *WWTR1* (*TAZ*) following indicated siRNA treatment. (**B**) Average ChIP-seq signal after transfection with the indicated siRNAs for 4 days centered at H3K27ac peaks that decreased >2X following 4 days of E1AKD. (**C**) Average RAD21 ChIP-seq signal after transfection with the indicated siRNAs for 4days centered at ATAC-seq peaks that increased >5X (new ATAC sites) following 4days of E1AKD. (**D**) Average RAD21 ChIP-seq signal after transfection with the indicated siRNAs for 4 days centered at all TSSs. (**E**) Genome browser plots (IGB) displaying indicated ATAC- and ChIP-seq signal at super-enhancers near E1AKD de-repressed genes *AMOTL2* and *COL1A1*.

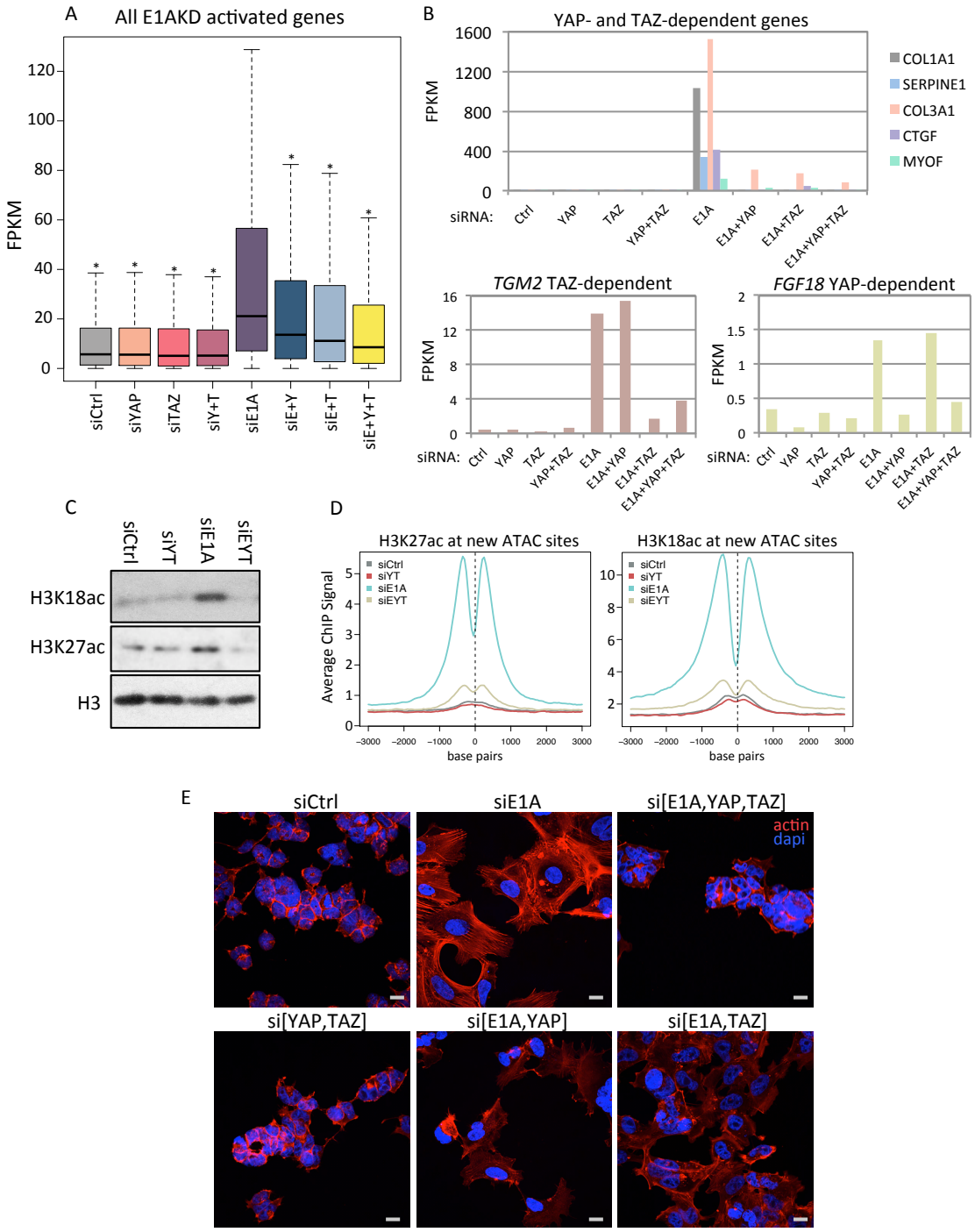

Figure 3.9 E1AKD induced re-differentiation of HEK293 cells requires YAP and TAZ
(**A**) Boxplots represent distribution of expression (FPKM) of E1AKD activated genes (>2X FPKM q<0.05) following 8 days of indicated siRNA transfections. E=E1A, Y=YAP, T=TAZ. * p<0.0000001 as compared to siE1A. (**B**) Bar graphs represent FPKM values of select genes that were defective for E1AKD activation when YAP and TAZ, YAP but not TAZ, or TAZ but not YAP were knocked down at the same time as E1A. (**C**) Total levels of H3K18ac or H3K27ac following indicated siRNA transfections for 2days. YT = YAP and TAZ. EYT = E1A and YAP and TAZ. (**D**) Average ChIP-seq signal after transfection with the indicated siRNAs for 4 days centered at ATAC-seq peaks that increased >5X following 4 days of E1AKD. Base pair span is +/-3kb from center of peak. (**E**) Confocal microscopy of siRNA transfected HEK293 cells for 4 days fixed and stained for phalloidin-iFluor or DAPI. Scale bar represents 20μM.

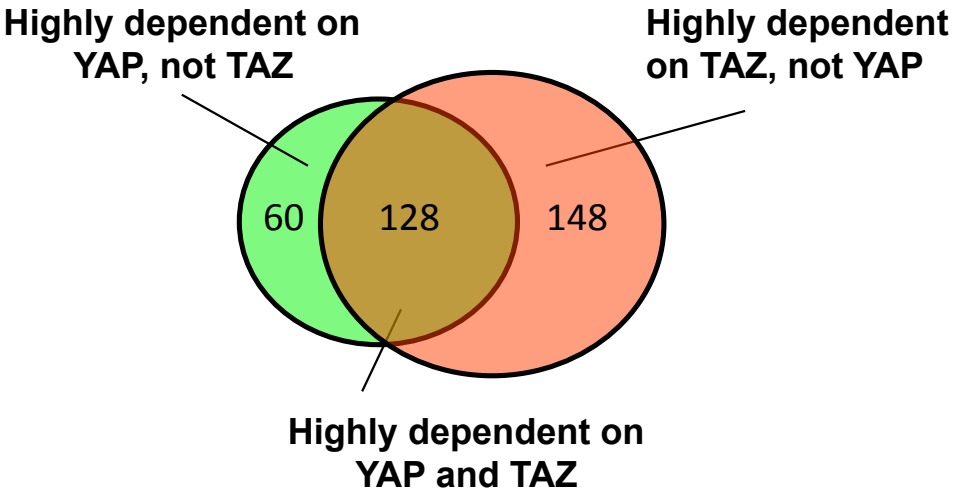

Highly dependent on YAP, not TAZ

	P-value	Benjamini
focal adhesion	3.2E-07	4.5E-05
positive regulation of cell proliferation	1.4E-06	1.1E-03
angiogenesis	5.3E-06	1.5E-03
extracellular region	2.2E-05	1.6E-03
cell growth	2.7E-05	5.5E-03

Highly dependent on TAZ, not YAP

extracellular space	1.3E-15	1.4E-13
proteinaceous extracellular matrix	3.1E-12	1.4E-14
extracellular matrix	3.8E-05	1.3E-03
heparin binding	1.3E-04	1.7E-02
calcium ion binding	4.0E-04	2.6E-02

Highly dependent on both YAP and TAZ

extracellular space	2.0E-13	2.0E-11
proteinaceious extracellular matrix	2.8E-10	1.4E-08
extracellular matrix structural constituent	3.7E-07	4.4E-05
collagen fibril organization	2.4E-06	1.5E-03
extracellular matrix	9.5E-06	3.2E-04

Figure 3.10 Genes highly dependent on YAP but not TAZ promote proliferation
Venn diagram and gene ontology (DAVID) enrichment terms for E1AKD activated genes (siE1A/siCtrl > 2X, q<0.05) that are highly dependent on YAP, not TAZ (si[E1A+YAP]/siE1A < 0.2), highly dependent on TAZ, not YAP (si[E1A+TAZ]/siE1A < 0.2), or highly dependent on YAP and TAZ (si[E1A+YAP]/siE1A < 0.2 and si[E1A+TAZ]/siE1A < 0.2).

Our observations that E1AKD in Ad-transformed cells induced an increase in total H3K27/18ac and that the genomic locations for these increases overlap new YAP peaks raised the question: How much of the increase in total cell H3K27/18ac in E1AKD293 cells results from activation by YAP and TAZ as opposed to all other activators in the cells? To address this question we analyzed total cell H3K27/18ac in HEK293 cells triply knocked down for YAP and TAZ as well as E1A. Western blots revealed that E1AKD-induced H3K27/18ac is entirely prevented when YAP and TAZ are additionally knocked-down (Fig. 3.9C). H3K27/18ac ChIP-seq demonstrated that the increase in H3K18/27ac at E1AKD-induced ATAC sites are almost completely lost in E1A/YAP/TAZ triple KD cells (Fig. 3.9D). In contrast, sites of E1AKD-induced H3 hypoacetylation (principally cell cycle genes regulated by E2Fs and Rbs) were largely unaffected by YAP/TAZ KD (Fig. 3.8B). These data suggest that most of the H3K27/18ac and gene de-repression resulting from elimination of E1A from HEK293 cells requires YAP/TAZ nuclear import to establish enhancers necessary for activating these genes.

Cohesin is necessary for many enhancer-promoter interactions (Kagey et al., 2010). Since YAP/TAZ are primarily regulating enhancers located distally from TSSs, we determined whether YAP/TAZ induce cohesin association at E1AKD-induced enhancers. The average association of cohesin subunit RAD21 with chromatin increased at E1AKD-induced ATAC sites following E1AKD, but fell below siCtrl levels when YAP and TAZ were knocked-down, both with and without E1AKD (Fig. 3.8C,E). These data suggest that YAP/TAZ are necessary for cohesin association at E1AKD-induced ATAC sites. The average RAD21 signal at all TSSs was largely unchanged by E1A and YAP/TAZ KDs (Fig. 3.8D), suggesting that YAP/TAZ-dependent cohesin association is specifically at enhancers, for example super-enhancers downstream of and within *AMOTL2* and upstream of *COL1A1* (Fig. 3.8E).

To determine the extent to which E1AKD-induced morphological changes are dependent on YAP/TAZ, we imaged DAPI and phalloidin stained HEK293 cells following siRNA KD. While YAP and TAZ KD did not have a readily apparent morphological consequence when E1A was present (Fig. 3.9E si[YAP,TAZ]), YAP and TAZ KD did inhibit the induced F-actin formation and cell surface area increase that result from E1AKD (Fig. 3.9E siE1A compared to si[E1A,YAP,TAZ]). KDs of only YAP or TAZ with E1A resulted in morphologies intermediate between siCtrl and E1AKD293 cells (Fig. 3.9E). These experiments show a co-dependence of the cell on YAP and TAZ for the striking change to a more differentiated morphology upon E1AKD. Consistent with this, YAP and TAZ KD in normal primary HBTEC and IMR90 cells caused a reduction of actin cytoskeletal fibers (Fig. 3.11). Consequently, YAP and TAZ are required for E1AKD293 cells to assume a morphology similar to that of MSCs.

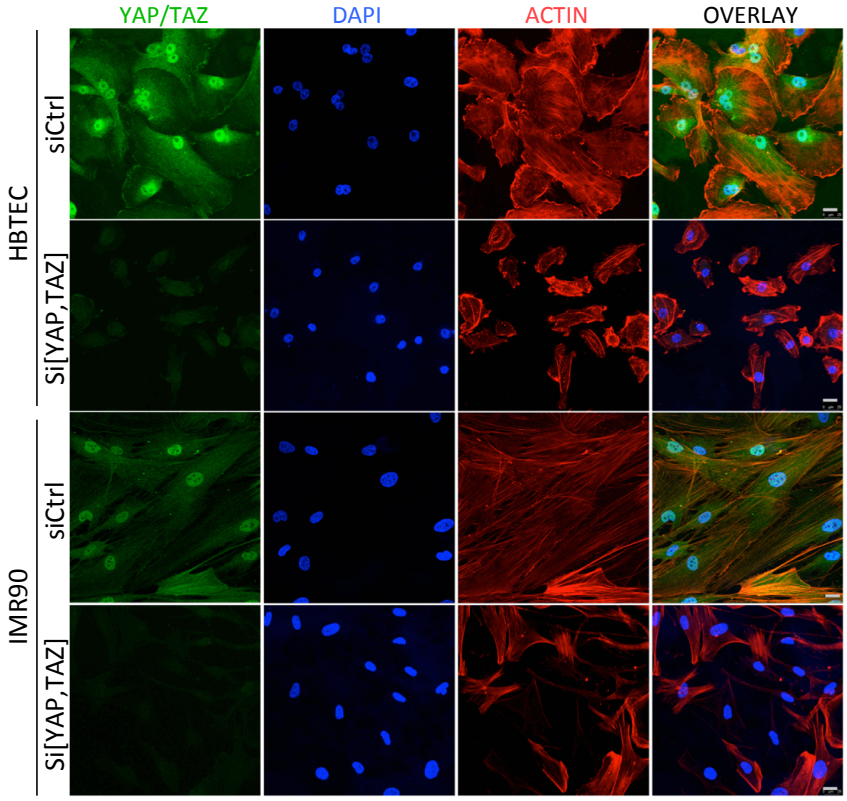

Figure 3.11 YAP and TAZ are necessary for normal F-ACTIN in primary cells
Confocal microscopy of HBTEC or IMR90 cells after 4day siRNA transfection. Fixed and immunostained with anti-YAP (DH81X) and anti-TAZ (CL0371) stained with phalloidin-iFluor and DAPI. Scale bar represents 20μM.

Methods

Cell Culture

Cells were maintained at 37°C in a 5% CO_2 incubator. HEK293 (human embryonic kidney cell line), IMR90 (primary human fetal lung fibroblasts), HFF (human foreskin fibroblasts), BRK (baby rat kidney cells) and BRK E1A and E1B-transformed cells were grown in Dulbecco's Modified Eagle Medium (DMEM) with 10% fetal bovine serum. Human Bronchial/Tracheal Epithelial Cells (HBTEC, Lifeline Cell Technology Cat# FC-0035; lot# 02196) in BronchiaLife Medium Complete Kit (Lifeline Cell Technology catalog number: LL-0023).

RNA-seq Procedure and Data Analysis

$1X10^6$ HEK293 were transfected with indicated siRNAs for 4, 8, or 16 days. RNA was isolated using QIAGEN RNeasy Plus Mini Kit. Eluted RNA was treated with Ambion DNA-free™ DNA Removal Kit and then Ambion TRIzol reagent, precipitated with isopropanol, and dissolved in sterile water. RNA concentration was measured with a Qubit fluorometer. One microgram of RNA was fragmented and copied into DNA then PCR amplified with bar-coded primers for separate samples to prepare sequencing libraries using the Illumina TruSeq RNA Sample Preparation procedure. Libraries were sequenced using the Illumina HIseq-2000 to obtain single end 50-base-long reads. Sequences were aligned to the hg19 human genome sequence using TopHat v2. FPKM (fragments per kb per million mapped reads) for each annotated hg19 RefSeq gene ID was determined using Cuffdiff v2 from Cufflinks RNA-Seq analysis tools at http://cufflinks.cbcb.umd.edu. All RNA-seq was performed using biological duplicates and FPKM values represent normalized averages of duplicates. Published RNA-seq datasets from

infected IMR90 (Ferrari et al. 2014) and infected HBTEC (Zemke and Berk 2017) are available on GEO: GSE59688 & GSE105039. RNA-seq from infected HFF was generated similarly as above except confluent HFF cells were infected at an MOI of 60 with a small E1A expressing Ad5 vector described below for 24 hours prior to RNA preparation. Gene ontology analysis was performed using DAVID Functional Annotation Tool (Huang et al., 2009a, 2009b). The web-based tool, SaVanT (Lopez et al., 2017) was used to determine the cell types with expression signatures most closely resembling expression from 16 day E1AKD HEK293.

ChIP-Seq

ChIP-seq was performed using $1x10^7$ siRNA transfected HEK293. Cells were transfected for 1 or 4 days for H3K18ac (814) and H3K27ac (Active Motif) ChIP, 4 days for H3K4me1 (abcam), RAD21 (abcam), and 8 days for YAP (CST D8H1X), TEAD1 (BD Transduction Laboratories), and TEAD4 (Santa Cruz N-G2). For H3K18ac, H3K27ac, H3K4me1 and RAD21 ChIP-seqs cells were cross-linked for 1% formaldehyde for 10 minutes at room temperature on rotator. Formaldehyde crosslinking was quenched with 0.14M glycine for 30 minutes at room temperature on rotator. Cells were washed with PBS and scraped from plates in PBS with Roche protease inhibitor cocktail. Cells were pelleted and lysed in 400uL lysis buffer (1% SDS, 50mM Tris-HCl pH8, 20mM EDTA, Roche complete protease inhibitors) and sonicated at 4°C using the Qsonica Q800R2 at 20% amplitude 10s on 30s off until DNA fragments from sheared chromatin were mostly between the sizes of mostly ~200-600 base pairs. Samples were normalized for equal amounts of DNA as measured by Qubit fluorometer in sonicated, cross-linked chromatin prior to pre-clear and IP. Up to 100uL of sonicated chromatin was diluted in 10X lysis dilution buffer (16.7 mM Tris-HCl, 1.1% Triton X-100, 1.2mM EDTA, 167mM NaCl)

and precleared for 1h 4°C with 30uL of protein A dynabeads washed 10X lysis dilution buffer on nutator. IPs were performed O/N at 4°C on nutator with precleared chromatin and 2ug of antibody or 5uL of H3K18ac anti-rabbit sera. 50uL of protein A dynabeads were added for 4h on nutator at 4°C. Bead-immunocomplexes were washed for 5min 2X with each of the following buffers in order: wash buffer A (50mM Hepes pH 7.9, 0.1% SDS, 1% Triton X-100, 0.1% Deoxycholate, 1mM EDTA, 140mM NaCl), wash buffer B (50mM Hepes pH 7.9, 0.1% SDS, 1% Triton X-100, 0.1% Deoxycholate, 1mM EDTA, 500mM NaCl), LiCl buffer (20mM Tris-HCl pH8, 0.5% NP-40, 0.5% Deoxycholate, 1mM EDTA, 250mM LiCl), TE (50mM Tris-HCl pH8, 1mM EDTA). Elution was performed in 150uL of elution buffer (50mM Tris HCl pH8, 1mM EDTA, 1% SDS) then ChIP samples and inputs (10uL of precleared chromatin lysis plus 140uL elution buffer) were reverse crosslinked O/N at 65°C. Samples were RNase A treated for 1h at 37°C and DNA was purified and extracted with phenol/chloroform and ethanol precipitated. DNA pellets were resuspended in 12uL of TE and measured using Qubit fluorometer. YAP, TEAD1, and TEAD4 ChIP-seqs were performed similarly with the following modifications: cells were double-crosslinked with 4mM DSG in PBS for 30min then 1% formaldehyde for 10 min, crosslinking was quenched in 500mM Tris pH7.9 for 20min and cell pellets were lysed in 1mL lysis buffer 1 (50mM HEPES-KOH, pH 7.5, 140mM NaCl, 1mM EDTA, 10% glycerol, 0.5% NP-40, 0.25% Triton X-100, Roche cOmplete protease inhibitors) for 10min on ice. Lysate was pelleted at 3000 rpm 5min 4°C then resuspended in 1mL lysis buffer 2 (10mM Tris-HCl, pH 8.0, 200mM NaCl, 1mM EDTA, 0.5mM EGTA, Roche complete protease inhibitors) and placed on nutator 10min 4°C and pelleted as before, then resuspended in 125uL of lysis buffer 3 (10mM Tris-HCl, pH 8.0, 100mM NaCl, 1mM EDTA, 0.5mM EGTA, 0.1% Na-Deoxycholate, 0.5% N-lauroylsarcosine, Roche complete protease inhibitors) and

sonicated, 2ug of antibody was used, magnetic beads were washed and blocked in 0.5% BSA in PBS. Sequencing libraries were constructed from 1ng of immunoprecipitated and input DNA using the KAPA Hyper Prep Kit from KAPA Biosystems and NEXTflex ChIP-Seq barcodes purchased from Bioo Scientific.

Data Analysis of ChIP-seq

ChIP-seq libraries were sequenced using Hiseq-2000 or 4000 systems for single-end 50 base pair reads. Reads were mapped to the hg19 human genome reference using Bowtie2 software. Only reads that aligned to a unique position in the genome with no more than two sequence mismatches were retained for further analysis. Duplicate reads that mapped to the same exact location in the genome were counted only once to reduce clonal amplification effects. A custom algorithm executed by MATLAB was used for further processing including peak calling (p-value $< 10^{-6}$ were considered significant). The genome was tiled into 50 base pair windows and each read was extended by 150 bases and was counted as one read to each window to which it partially or fully matched. The total counts of the input and ChIP samples were normalized to each other. Samples were normalized for equal number of uniquely mapped reads. The input sample was used to estimate the expected counts in a window. Wiggle files were generated using a custom algorithm and present the data as normalized tag density as seen in all figures with genome browser shots. Metagene plots displaying normalized average relative ChIP-seq signals were generated using CEAS software. For determining super-enhancers with H3K27ac ChIP-seq in 4 day E1AKD293 cells we used ROSE software (Lovén et al., 2013; Whyte et al., 2013). Using the ROSE-generated list of super-enhancers we generated a list of super-enhancer associated genes in E1AKD HEK293 by assigning the closest TSS of an expressed gene (>1

FPKM) to the center of a super-enhancer.

ATAC-seq and data analysis

ATAC-seq (Omni-ATAC protocol) was performed as described in Corces et al. 2017. HEK293 cells siRNA transfected for 4 days were lifted from plates using Accutase (Innovative Cell Technologies, Inc.) and 50,000 viable cells were gently pelleted at 500 RCF 4°C for 5min and resuspended in 50 uL cold ATAC-Resuspension Buffer (RSB) containing 0.1% NP40, 0.1% Tween-20, and 0.01% Digitonin. Cells were incubated on ice for 3min then washed with 1 ml of cold ATAC-RSB containing 0.1% Tween-20 to lyse plasma membranes. Nuclei were gently pelleted at 500 RCF for 10min at 4°C and resuspended in 50 uL of transposition mixture: 25 uL 2x TD buffer and 2.5 uL transposase (both supplied in the Nextera DNA Library Prep Kit), 16.5 uL PBS, 0.5 uL 1% digitonin, 0.5 uL 10% Tween-20, 5 uL H2O. DNA was isolated using DNA Clean and Concentrator-5 Kit (Zymo cat# D4014) and eluted in 21uL of elution buffer. 20uL of eluted DNA was amplified for 5 cycles Amplify for 5 cycles using NEBNext 2x MasterMix with 25uM primer Ad1 + 25uM primer Ad2 or 25uM Ad1 + 25uM Ad3. Refer to Corces et al. 2017 for PCR protocol and primer sequences. 5uL of preamplified sample was used in qPCR to determine additional cycles needed. Libraries were sequenced using Hi-seq-4000 single-end 50bp reads. Reads were aligned to hg19 reference genome using bowtie2. Macs14 was used for calling peaks with the following parameters: --space=50 --keep-dup all --nomodel -p 1e-6. The summits of peaks were used as the location for the center of peaks when doing motif analysis and metagene profiling. Motif analysis was performed on ATAC-seq peaks that increased >5X in signal with siE1A treatment compared to siCtrl using Homer (http://homer.salk.edu/homer PMID: 20513432) to search for enriched motifs +/- 300 bp from peak summits.

Confocal microscopy

250,000 cells were plated on fibronectin coated glass cover slips in 6-well plates. Cells were transfected or infected as indicated prior to fixing with 4% formaldehyde in PBS for 10min. Cells were then permeabilized with 0.1% Triton-X 100 in PBS for 10min. Next, cells were incubated in block buffer (1% BSA, 0.1% Tween 20 in PBS) for 30 min. Cells were incubated with primary antibody, YAP (CST D8H1X), TAZ (Thermo CL0371), AMOT (CST D2O4H) at 1:200 dilutions and incubated for 1h. Cells were washed 3X with PBS then incubated with secondary Anti-rabbit IgG (H+L), F(ab')2 Fragment (Alexa Fluor® 488 Conjugate) Cat#4412 or Anti-mouse IgG (H+L), F(ab')2 Fragment (Alexa Fluor® 555 Conjugate) Cat#4409 (CST 1:1000) and if indicated Cytopainter phalloidin-ifluor 555 reagent (abcam ab176756, 1:1000) for 1h diluted in block buffer. DAPI was added for 5 minutes at 1 ug/mL. Slides were mounted with VECTASHIELD Hardset Antifade Mounting Medium (Vector Laboratories Cat. No: H-1400). Micrographs were taken using confocal scanning laser microscopy on a Leica TCS SP8 100X or 40X numerical aperture oil immersion objective. All scare bars represent 20 μm.

Ad Vector infections

*dl*1500, an Ad2 mutant vector containing a deletion removing the 13S E1A mRNA 5' splice site (Montell et al., 1984) or the ΔE1A vector *dl*312 (Jones and Shenk 1979) were used for a 4 day infection of IMR90 at an MOI of 10 prior to fixing for confocal microscopy (fig S2D). Ad5 small E1A vectors expressed Ad2 WT from the normal E1A promoter with the *dl*1500 deletion removing the 13S E1A mRNA 5' splice site (Ferrari et al. 2014). The vectors were constructed using the Ψ5 vector and in vivo Cre24 mediated recombination (Hardy et al., 1997), and

consequently contain an out of frame insertion of a LoxP site at the Bgl II site in the region encoding the carboxy-terminus of E1B-55K. These vectors were used to infect IMR90, HFF, and HBTEC for 24 hours at an MOI 40 in IMR90 (Ferrari et al. 2014), MOI 60 in HFF, and MOI 60 in HBTEC (Zemke and Berk 2017) prior to RNA-seq (fig S1A).

siRNA and plasmid Transfections and small molecule treatment

siRNA KD was performed in HEK293, HBTEC, and IMR90 using Invitrogen RNAiMAX reverse transfection protocol. Cells were plated in antibiotic free 10% FBS DMEM containing indicated Ambion/ThermoFisher Silencer Select siRNA for a final concentration of 10nM that was pre-incubated in 7.5uL of lipofectamine RNAiMAX reagent in 750uL of Opti-MEM in $6cm^2$. Media and reagents were scaled up accordingly for $15cm^2$ and scaled down when using 6-well plates based on surface areas. For a complete list of Ambion/ThermoFisher Silencer Select siRNAs used and sequences see key resources table. Ambion/ThermoFisher Silencer Negative Control no.1 AM4611 was used as a negative control (siCtrl). Double, triple and quadruple knock-downs were performed with a total siRNA concentration of 10nM. Any parallel knock-downs where cells were treated with fewer siRNAs they were used at the same concentration as any individual siRNA from the cells treated with the most number of siRNAs but were supplemented with negative control siRNA (siCtrl) to have the same total siRNA concentration of 10nM. pRK5-myc-RhoA-Q63L was a gift from Gary Bokoch (Addgene plasmid # 12964) pRK5-myc-RhoA-Q63L or a control empty vector, pAdlox, was transfected into HEK293. 2.5 ug of DNA was transfected into a HEK293 confluent monolayer in 6-well plates on glass coverslips. Plasmid DNA was pre-incubated with 10uL of lipofectamine 2000 transfection reagent from Invitrogen in 250 uL in Opti-MEM for 5 minutes before adding it to cells.

Transfections proceeded for 3 days prior to fixing and confocal microscopy (fig 4D). To block WNT signaling in E1AKD HEK293 cells were treated with 5uM IWP-2 or DMSO (negative control) for 4 days beginning at time of siRNA transfection. To block ubiquitin-mediated degradation HEK293 cells were treated with 5uM MLN4942 or DMSO (negative control) for 8 hours.

Western blot

Proteins were extracted from indicated cells by lysis in EBC (120 mM NaCl, 0.5% NP-40, 50 mM Tris-Cl pH 8.0, and Roche cOmplete protease inhibitors). Protein concentration was quantified by Bradford assay and normalized in Laemmli buffer and heated for 10min at 65°C then resolved in a 9% SDS-polyacrylamide gel. Proteins were electrotransferred to a polyvinylidene difluoride (PVDF) membrane then blocked in 5% milk in TBS-Tween 0.1% (blocking buffer) for 30 minutes. Primary antibody (M58 (anti-E1A), anti-H3K18ac (814), anti-H3K27ac, anti-KU-86 (H-300), anti-Beta-Actin anti-YAP (D8H1X), anti-TAZ (D3I6D), anti-Phospho-YAP (D9W2I), anti-LATS1 (C66B5), anti-LATS2 (D83D6), anti-Phospho-LATS1 (D57D3), or anti-Wnt5a/b (C27E8)) was added at manufacturer recommended dilutions for 1h at room temperature or O/N at 4°C. Membranes were washed 3X in TBS-Tween (0.1%) then HRP conjugated anti-mouse or anti-rabbit secondary antibodies were added for 1h room temperature in blocking buffer. Membranes were then washed 3X in TBS-Tween (0.1%) prior to addition of ECL reagent for detection of chemiluminescence. Western blots were validated with replicates of two or more with representative western blots presented.

KEY RESOURCES TABLE

REAGENT or RESOURCE	SOURCE	IDENTIFIER
Antibodies		
Rabbit polyclonal anti-H3K27ac	Active Motif	Cat#39133; RRID: AB_2561016; Lot#31814008
Rabbit polyclonal anti-H3K18ac (814)	Grunstein/Kurdistani laboratories	(Suka et al., 2001)
Mouse monoclonal anti-E1A (M58) hybridoma supernatant	Produced in house	(Harlow et al., 1985)
Mouse monoclonal anti-WWTR1 (TAZ) (CL0371)	ThermoFisher	Cat#MA5-24604
Rabbit polyclonal anti-Beta-Actin	GeneTex	Cat#GTX16039; RRID: AB_367276
Rabbit polyclonal anti-KU-86 (H-300)	Santa Cruz	Cat#sc-9034; RRID: AB_2218743
Mouse monoclonal anti-TEF-3 a.k.a. TEAD4 (N-G2)	Santa Cruz	Cat#sc-101184
Rabbit polyclonal anti-H3K4me1	abcam	Cat#ab8895
Mouse monoclonal anti-TEF1 a.k.a. TEAD1 (31/TEF1)	BD Transduction Laboratories	Cat#610922
Rabbit polyclonal anti-RAD21	abcam	Cat#ab992
Rabbit monoclonal anti-YAP (D8H1X)	Cell Signaling Technology	Cat#14074
Rabbit monoclonal anti-Wnt5a/b (C27E8)	Cell Signaling Technology	Cat#2530
Rabbit monoclonal anti-Angiomotin (D2O4H)	Cell Signaling Technology	Cat#43130
Rabbit monoclonal anti-Phospho-YAP (Ser127) (D9W2I)	Cell Signaling Technology	Cat#13008
Rabbit monoclonal anti-LATS1 (C66B5)	Cell Signaling Technology	Cat#3477
Rabbit monoclonal anti-LATS2 (D83D6)	Cell Signaling Technology	Cat#5888
Rabbit monoclonal anti-TAZ (D3I6D)	Cell Signaling Technology	Cat#70148
Rabbit monoclonal anti-Phospho-LATS1 (Thr1079) (D57D3)	Cell Signaling Technology	Cat#8654
Anti-rabbit IgG (H+L), F(ab')2 Fragment (Alexa Fluor® 488 Conjugate)	Cell Signaling Technology	Cat#4412
Anti-mouse IgG (H+L), F(ab')2 Fragment (Alexa Fluor® 555 Conjugate)	Cell Signaling Technology	Cat#4409
Bacterial and Virus Strains		
e1aWT Ad5 recombinant vector	(Ferrari et al., 2014)	N/A

*dl*312	(Jones and Shenk, 1979)	N/A
*dl*1500	(Montell et al., 1984)	N/A
Chemicals, Peptides, and Recombinant Proteins		
IWP-2 Wnt Antagonist II, CAS 686770-61-6 Calbiochem	EMD Millipore	Cat#681671
MLN4924 NEDD8 E1 Activating Enzyme Inhibitor (NAE Inhibitor)	R&D Systems, Inc.	Cat#I-502-01M
Proteinase K	Roche/Sigma-Aldrich	Cat#3115887001
RNase A	Roche/Sigma-Aldrich	Cat#10109142001
Lipofectamine RNAiMAX Transfection Reagent	ThermoFisher	Cat#13778075
Lipofectamine 2000 Transfection Reagent	ThermoFisher	Cat#11668019
Complete Protease inhibitor Cocktail	Roche	Cat#04693132001
Critical Commercial Assays		
TruSeq Stranded mRNA Library Prep Kit	illumina	Cat#RS-122-2101
Kapa Hyper Prep Kit	Kapa biosystems	Cat#KK8504
NEXTflex ChIP-Seq barcodes	BIOO	Cat#NOVA-514121
RNeasy Plus Mini Kit	Qiagen	Cat#74134
FastStart Universal SYBR Green Master (Rox)	Roche	Cat#04913850001
Dynabeads Protein A	ThermoFisher	Cat#10001D
DNA-free™ DNA Removal Kit	Ambion/ThermoFisher	Cat#1906
DNA Clean and Concentrator-5 Kit	Zymo Research	Cat#D4014
Nextera DNA Library Prep Kit	illumina	Cat#FC-121-1030
NEBNext® High-Fidelity 2X PCR Master Mix	New England BioLabs	Cat#M0541S
Cytopainter phalloidin-ifluor 555 reagent	abcam	Cat#ab176756
Experimental Models: Cell Lines		
Male Human Bronchial/Tracheal Epithelial Cells (HBTEC)	Lifeline Cell Technologies	Cat#FC-0035; lot# 02196
HEK293 cell line	Graham et al. 1977	RRID: CVCL_0045
IMR-90 Female human fetal lung fibroblasts	ATCC	Cat#CCL-186 RRID: CVCL_0347
Human foreskin tissue (source of HFF human foreskin fibroblasts)	NDRI	Lot#ND03285
Oligonucleotides		

Silencer Select siRNA YAP1 Sense: AGAUACUUCUUAAAUCACAtt Antisense: UGUGAUUUAAGAAGUAUCUct	ThermoFisher	Assay ID: s534572
Silencer Select siRNA CDC42 Sense: AGAUCUAGUUUAGAAAACAtt Antisense: UGUUUUCUAAACUAGAUCUag	ThermoFisher	Assay ID: s227090
Silencer Select siRNA WWTR1 (TAZ) Sense: AAACACCCAUGAACAUCAAtt Antisense: UUGAUGUUCAUGGGUGUUUgt	ThermoFisher	Assay ID: s24788
Silencer Select siRNA RHOA Sense: CACAGUGUUUGAGAACUAUtt Antisense: AUAGUUCUCAAACACUGUGgg	ThermoFisher	Assay ID: s758
Silencer Select siRNA RAC1 Sense: ACAGAUUAAUUUUUCCAUAtt Antisense: UAUGGAAAAAUUAAUCUGUaa	ThermoFisher	Assay ID: s11712
Silencer Select siRNA AMOTL1 Sense: CAACUUUUCUUCCACGGAAtt Antisense: UUCCGUGGAAGAAAAGUUGtt	ThermoFisher	Assay ID: s45895
Silencer Select siRNA AMOT Sense: CAUCGUUUGUCUAUACCAAtt Antisense: UUGGUAUAGACAAACGAUGtg	ThermoFisher	Assay ID: s45887
Silencer Select siRNA AMOTL2 Sense: AGACCAUGCGGAACAAGAUtt Antisense: AUCUUGUUCCGCAUGGUCUtc	ThermoFisher	Assay ID: s28109
Custom Select siRNA E1A Sense: GGUACUGGCUGAUAAUCUUtt Antisense: AAGAUUAUCAGCCAGUACCtt	ThermoFisher	Design ID: ADLJIAM
Silencer™ Negative Control No. 1 siRNA	ThermoFisher	Cat#AM4611
Recombinant DNA		
pRK5-myc-RhoA-Q63L	Gary Bokoch Lab unpublished	Addgene Plasmid #12964
Software and Algorithms		
Bowtie2	http://bowtie-bio.sourceforge.net/bowtie2/index.shtml	RRID: SCR_005476
Samtools	http://samtools.sourceforge.net/	RRID: SCR_002105
Tophat2.2.1	https://ccb.jhu.edu/software/tophat/index.shtml	RRID: SCR_000691
HOMER	http://homer.salk.edu/homer	RRID: SCR_010881
CEAS	http://liulab.dfci.harvard.edu/CEAS/	RRID: SCR_010946

cuffdiff2.0.2	http://cole-trapnell-lab.github.io/cufflinks/cuffdiff/	RRID: SCR_001647
ROSE	http://younglab.wi.mit.edu/super_enhancer_code.html	(Whyte et al. 2013, Loven et al. 2013)

Bibliography

van Amerongen, R. (2012). Alternative Wnt pathways and receptors. Cold Spring Harb. Perspect. Biol. *4*.

Buenrostro, J.D., Giresi, P.G., Zaba, L.C., Chang, H.Y., and Greenleaf, W.J. (2013). Transposition of native chromatin for fast and sensitive epigenomic profiling of open chromatin, DNA-binding proteins and nucleosome position. Nat. Methods *10*, 1213–1218.

Bulger, M., and Groudine, M. (2011). Functional and mechanistic diversity of distal transcription enhancers. Cell *144*, 327–339.

Carey, M. (1998). The enhanceosome and transcriptional synergy. Cell *92*, 5–8.

Caron, E., and Hall, A. (1998). Identification of two distinct mechanisms of phagocytosis controlled by different Rho GTPases. Science (80-.). *282*, 1717–1721.

Chan, S.W., Lim, C.J., Chong, Y.F., Pobbati, A. V., Huang, C., and Hong, W. (2011). Hippo pathway-independent restriction of TAZ and YAP by angiomotin. J. Biol. Chem. *286*, 7018–7026.

Chan, S.W., Lim, C.J., Guo, F., Tan, I., Leung, T., and Hong, W. (2013). Actin-binding and cell proliferation activities of angiomotin family members are regulated by Hippo pathway-mediated phosphorylation. J. Biol. Chem. *288*, 37296–37307.

Chen, B., Dodge, M.E., Tang, W., Lu, J., Ma, Z., Fan, C.W., Wei, S., Hao, W., Kilgore, J., Williams, N.S., et al. (2009). Small molecule-mediated disruption of Wnt-dependent signaling in tissue regeneration and cancer. Nat. Chem. Biol. *5*, 100–107.

Creyghton, M.P., Cheng, A.W., Welstead, G.G., Kooistra, T., Carey, B.W., Steine, E.J., Hanna, J., Lodato, M.A., Frampton, G.M., Sharp, P.A., et al. (2010). Histone H3K27ac separates active from poised enhancers and predicts developmental state. Proc. Natl. Acad. Sci. *107*, 21931–21936.

DeCaprio, J.A. (2009). How the Rb tumor suppressor structure and function was revealed by the study of Adenovirus and SV40. Virology *384*, 274–284.

Dong, J., Feldmann, G., Huang, J., Wu, S., Zhang, N., Comerford, S.A., Gayyed, M.F., Anders, R.A., Maitra, A., and Pan, D. (2007). Elucidation of a Universal Size-Control Mechanism in Drosophila and Mammals. Cell *130*, 1120–1133.

Dupont, S., Morsut, L., Aragona, M., Enzo, E., Giulitti, S., Cordenonsi, M., Zanconato, F., Le Digabel, J., Forcato, M., Bicciato, S., et al. (2011). Role of YAP/TAZ in mechanotransduction. Nature *474*, 179–184.

Ferrari, R., Su, T., Li, B., Bonora, G., Oberai, A., Chan, Y., Sasidharan, R., Berk, A.J., Pellegrini, M., and Kurdistani, S.K. (2012). Reorganization of the host epigenome by a viral oncogene. Genome Res. *22*, 1212–1221.

Ferrari, R., Gou, D., Jawdekar, G., Johnson, S.A., Nava, M., Su, T., Yousef, A.F., Zemke, N.R., Pellegrini, M., Kurdistani, S.K., et al. (2014). Adenovirus small E1A employs the lysine acetylases p300/CBP and tumor suppressor Rb to repress select host genes and promote productive virus infection. Cell Host Microbe *16*, 663–676.

Frisch, S.M., and Mymryk, J.S. (2002). Adenovirus-5 E1A: paradox and paradigm. Nat. Rev. Mol. Cell Biol. *3*, 441–452.

Graham, F.L., Smiley, J., Russell, W.C., and Nairn, R. (1977). Characteristics of a human cell line transformed by DNA from human adenovirus type 5. J. Gen. Virol. *36*, 59–74.

Hardy, S., Kitamura, M., Harris-Stansil, T., Dai, Y., and Phipps, M.L. (1997). Construction of adenovirus vectors through Cre-lox recombination. J. Virol. *71*, 1842–1849.

Harlow, E., Franza, B.R., and Schley, C. (1985). Monoclonal antibodies specific for adenovirus early region 1A proteins: extensive heterogeneity in early region 1A products. J. Virol. *55*, 533–546.

Heintzman, N.D., Hon, G.C., Hawkins, R.D., Kheradpour, P., Stark, A., Harp, L.F., Ye, Z., Lee, L.K., Stuart, R.K., Ching, C.W., et al. (2009). Histone modifications at human enhancers reflect global cell-type-specific gene expression. Nature *459*, 108–112.

Heinz, S., Benner, C., Spann, N., Bertolino, E., Lin, Y.C., Laslo, P., Cheng, J.X., Murre, C., Singh, H., and Glass, C.K. (2010). Simple Combinations of Lineage-Determining Transcription Factors Prime cis-Regulatory Elements Required for Macrophage and B Cell Identities. Mol. Cell *38*, 576–589.

Heinz, S., Romanoski, C.E., Benner, C., and Glass, C.K. (2015). The selection and function of cell type-specific enhancers. Nat. Rev. Mol. Cell Biol. *16*, 144–154.

Hirate, Y., Hirahara, S., Inoue, K.I., Suzuki, A., Alarcon, V.B., Akimoto, K., Hirai, T., Hara, T., Adachi, M., Chida, K., et al. (2013). Polarity-dependent distribution of angiomotin localizes hippo signaling in preimplantation embryos. Curr. Biol. *23*, 1181–1194.

Hnisz, D., Abraham, B.J., Lee, T.I., Lau, A., Saint-André, V., Sigova, A.A., Hoke, H.A., and Young, R.A. (2013). Super-enhancers in the control of cell identity and disease. Cell *155*.

Horwitz, G.A., Zhang, K., McBrian, M.A., Grunstein, M., Kurdistani, S.K., and Berk, A.J. (2008). Adenovirus small e1a alters global patterns of histone modification. Science *321*, 1084–1085.

Huang, D.W., Sherman, B.T., and Lempicki, R.A. (2009a). Systematic and integrative analysis of large gene lists using DAVID bioinformatics resources. Nat. Protoc. *4*, 44–57.

Huang, D.W., Sherman, B.T., and Lempicki, R.A. (2009b). Bioinformatics enrichment tools: Paths toward the comprehensive functional analysis of large gene lists. Nucleic Acids Res. *37*, 1–13.

Jin, Q., Yu, L.R., Wang, L., Zhang, Z., Kasper, L.H., Lee, J.E., Wang, C., Brindle, P.K., Dent, S.Y.R., and Ge, K. (2011). Distinct roles of GCN5/PCAF-mediated H3K9ac and CBP/p300-mediated H3K18/27ac in nuclear receptor transactivation. EMBO J. *30*, 249–262.

Jones, N., and Shenk, T. (1979). Isolation of adenovirus type 5 host range deletion mutants defective for transformation of rat embryo cells. Cell *17*, 683–689.

Kagey, M.H., Newman, J.J., Bilodeau, S., Zhan, Y., Orlando, D.A., Van Berkum, N.L., Ebmeier, C.C., Goossens, J., Rahl, P.B., Levine, S.S., et al. (2010). Mediator and cohesin connect gene expression and chromatin architecture. Nature *467*, 430–435.

Kim, M., Kim, M., Lee, S., Kuninaka, S., Saya, H., Lee, H., Lee, S., and Lim, D.S. (2013). CAMP/PKA signalling reinforces the LATS-YAP pathway to fully suppress YAP in response to actin cytoskeletal changes. EMBO J. *32*, 1543–1555.

Levine, M. (2010). Transcriptional enhancers in animal development and evolution. Curr. Biol. *20*.

Little, M.H., and McMahon, A.P. (2012). Mammalian kidney development: Principles, progress, and projections. Cold Spring Harb. Perspect. Biol. *4*, 3.

Lopez, D., Montoya, D., Ambrose, M., Lam, L., Briscoe, L., Adams, C., Modlin, R.L., and Pellegrini, M. (2017). SaVanT: A web-based tool for the sample-level visualization of molecular signatures in gene expression profiles. BMC Genomics *18*.

Lovén, J., Hoke, H.A., Lin, C.Y., Lau, A., Orlando, D.A., Vakoc, C.R., Bradner, J.E., Lee, T.I., and Young, R.A. (2013). Selective inhibition of tumor oncogenes by disruption of super-enhancers. Cell *153*, 320–334.

Meng, Z., Qiu, Y., Lin, K.C., Kumar, A., Placone, J.K., Fang, C., Wang, K.C., Lu, S., Pan, M., Hong, A.W., et al. (2018). RAP2 mediates mechanoresponses of the Hippo pathway. Nature *560*, 655–660.

Montell, C., Courtois, G., Eng, C., and Berk, A. (1984). Complete transformation by adenovirus 2 requires both E1A proteins. Cell *36*, 951–961.

Nishioka, N., Yamamoto, S., Kiyonari, H., Sato, H., Sawada, A., Ota, M., Nakao, K., and Sasaki, H. (2008). Tead4 is required for specification of trophectoderm in pre-implantation

mouse embryos. Mech. Dev. *125*, 270–283.

Nishioka, N., Inoue, K. ichi, Adachi, K., Kiyonari, H., Ota, M., Ralston, A., Yabuta, N., Hirahara, S., Stephenson, R.O., Ogonuki, N., et al. (2009). The Hippo Signaling Pathway Components Lats and Yap Pattern Tead4 Activity to Distinguish Mouse Trophectoderm from Inner Cell Mass. Dev. Cell *16*, 398–410.

Park, H.W., Kim, Y.C., Yu, B., Moroishi, T., Mo, J.S., Plouffe, S.W., Meng, Z., Lin, K.C., Yu, F.X., Alexander, C.M., et al. (2015). Alternative Wnt Signaling Activates YAP/TAZ. Cell *162*, 780–794.

Pelka, P., Ablack, J.N.G., Fonseca, G.J., Yousef, A.F., and Mymryk, J.S. (2008). MINIREVIEW Intrinsic Structural Disorder in Adenovirus E1A: a Viral Molecular Hub Linking Multiple Diverse Processes. J. Virol. *82*, 7252–7263.

Roy, N., and Hebrok, M. (2015). Regulation of Cellular Identity in Cancer. Dev. Cell *35*, 674–684.

Sansores-Garcia, L., Bossuyt, W., Wada, K.I., Yonemura, S., Tao, C., Sasaki, H., and Halder, G. (2011). Modulating F-actin organization induces organ growth by affecting the Hippo pathway. EMBO J. *30*, 2325–2335.

Sasaki, H. (2017). Roles and regulations of Hippo signaling during preimplantation mouse development. Dev. Growth Differ. *59*, 12–20.

Soucy, T.A., Smith, P.G., Milhollen, M.A., Berger, A.J., Gavin, J.M., Adhikari, S., Brownell, J.E., Burke, K.E., Cardin, D.P., Critchley, S., et al. (2009). An inhibitor of NEDD8-activating enzyme as a new approach to treat cancer. Nature *458*, 732–736.

Stein, R.W., Corrigan, M., Yaciuk, P., Whelan, J., and Moran, E. (1990). Analysis of E1A-mediated growth regulation functions: binding of the 300-kilodalton cellular product correlates with E1A enhancer repression function and DNA synthesis-inducing activity. J. Virol. *64*, 4421–4427.

Suka, N., Suka, Y., Carmen, A.A., Wu, J., and Grunstein, M. (2001). Highly specific antibodies determine histone acetylation site usage in yeast heterochromatin and euchromatin. Mol. Cell *8*, 473–479.

Varelas, X. (2014). The Hippo pathway effectors TAZ and YAP in development, homeostasis and disease. Development *141*, 1614–1626.

Vassilev, A., Kaneko, K.J., Shu, H., Zhao, Y., and DePamphilis, M.L. (2001). TEAD/TEF transcription factors utilize the activation domain of YAP65, a Src/Yes-associated protein localized in the cytoplasm. Genes Dev. *15*, 1229–1241.

Wang, Y., Xu, X., Maglic, D., Dill, M.T., Mojumdar, K., Ng, P.K.-S., Jeong, K.J., Tsang, Y.H.,

Moreno, D., Bhavana, V.H., et al. (2018). Comprehensive Molecular Characterization of the Hippo Signaling Pathway in Cancer. Cell Rep. *25*, 1304–1317.e5.

Whyte, W.A., Orlando, D.A., Hnisz, D., Abraham, B.J., Lin, C.Y., Kagey, M.H., Rahl, P.B., Lee, T.I., and Young, R.A. (2013). Master transcription factors and mediator establish super-enhancers at key cell identity genes. Cell *153*, 307–319.

Winberg, G., and Shenk, T. (1984). Dissection of overlapping functions within the adenovirus type 5 E1A gene. EMBO J. *3*, 1907–1912.

Xin, M., Kim, Y., Sutherland, L.B., Murakami, M., Qi, X., McAnally, J., Porrello, E.R., Mahmoud, A.I., Tan, W., Shelton, J.M., et al. (2013). Hippo pathway effector Yap promotes cardiac regeneration. Proc. Natl. Acad. Sci. *110*, 13839–13844.

Yagi, R., Kohn, M.J., Karavanova, I., Kaneko, K.J., Vullhorst, D., DePamphilis, M.L., and Buonanno, A. (2007). Transcription factor TEAD4 specifies the trophectoderm lineage at the beginning of mammalian development. Development *134*, 3827–3836.

Yu, F.X., Zhao, B., and Guan, K.L. (2015). Hippo Pathway in Organ Size Control, Tissue Homeostasis, and Cancer. Cell *163*, 811–828.

Zhao, B., Wei, X., Li, W., Udan, R.S., Yang, Q., Kim, J., Xie, J., Ikenoue, T., Yu, J., Li, L., et al. (2007). Inactivation of YAP oncoprotein by the Hippo pathway is involved in cell contact inhibition and tissue growth control. Genes Dev. *21*, 2747–2761.

Zhao, B., Ye, X., Yu, J., Li, L., Li, W., Li, S., Yu, J., Lin, J.D., Wang, C.Y., Chinnaiyan, A.M., et al. (2008). TEAD mediates YAP-dependent gene induction and growth control. Genes Dev. *22*, 1962–1971.

Zhao, B., Li, L., Lu, Q., Wang, L.H., Liu, C.Y., Lei, Q., and Guan, K.L. (2011). Angiomotin is a novel Hippo pathway component that inhibits YAP oncoprotein. Genes Dev. *25*, 51–63.

CHAPTER 4

DISCUSSION

Assessing the functions of e1a's C-terminal interactions revealed undiscovered mechanism for e1a regulation of the innate immune response

We've identified a previously unrecognized anti-viral defense involving activation of a subset of interferon stimulated genes (ISGs) beginning 12h post adenovirus infection (see chapter 2). This is a much later time course than activation of ISGs by recognition of viral nucleic acids in endosomes during infection by the pathogen pattern receptors TLR7 and 9 (Ikushima et al., 2013). This late activation of ISGs was revealed by infection of primary human bronchial/tracheal epithelial cells (HBTEC) with adenovirus mutants expressing only the small e1a protein mutated at binding sites for host proteins and protein complexes in the C-terminal half of the 243 amino acid e1a protein. Infection with these mutants resulted in activation of a small subset (~50) of the hundreds of ISGs activated by the binding of an α- or β-IFN to the type I IFN receptor on the cell surface (Stark, 2007). This late activation of this subset of ISGs requires IRF3, which accumulates to high levels by 12h p.i. in cells expressing e1a C-terminal mutants, but not in cells expressing WT e1a (Fig. 4.1). Unexpectedly, the C-terminal mutants induce phosphorylation of IRF3 at its activating site Ser396 after accumulation of unphosphorylated IRF3 on chromatin. This is in contrast to the canonical view that nuclear import of IRF3 is regulated by phosphorylation (Lin et al., 1998). Complementation analysis in HBTEC coinfected with the mutants indicate that a single e1a molecule must interact via conserved regions in its C-terminal half with transcription factors FOXK1 or 2, the DCAF7 specificity factor of CLR4 ubiquitin-ligase complexes, and co-repressors CtBP1 or 2 in order to block activation of these ISGs. It is worth noting that only human adenovirus species C e1as contain the FOXK binding region (Cohen et al., 2013). Therefore this function of the e1a C-terminus may be limited to Ads in species C.

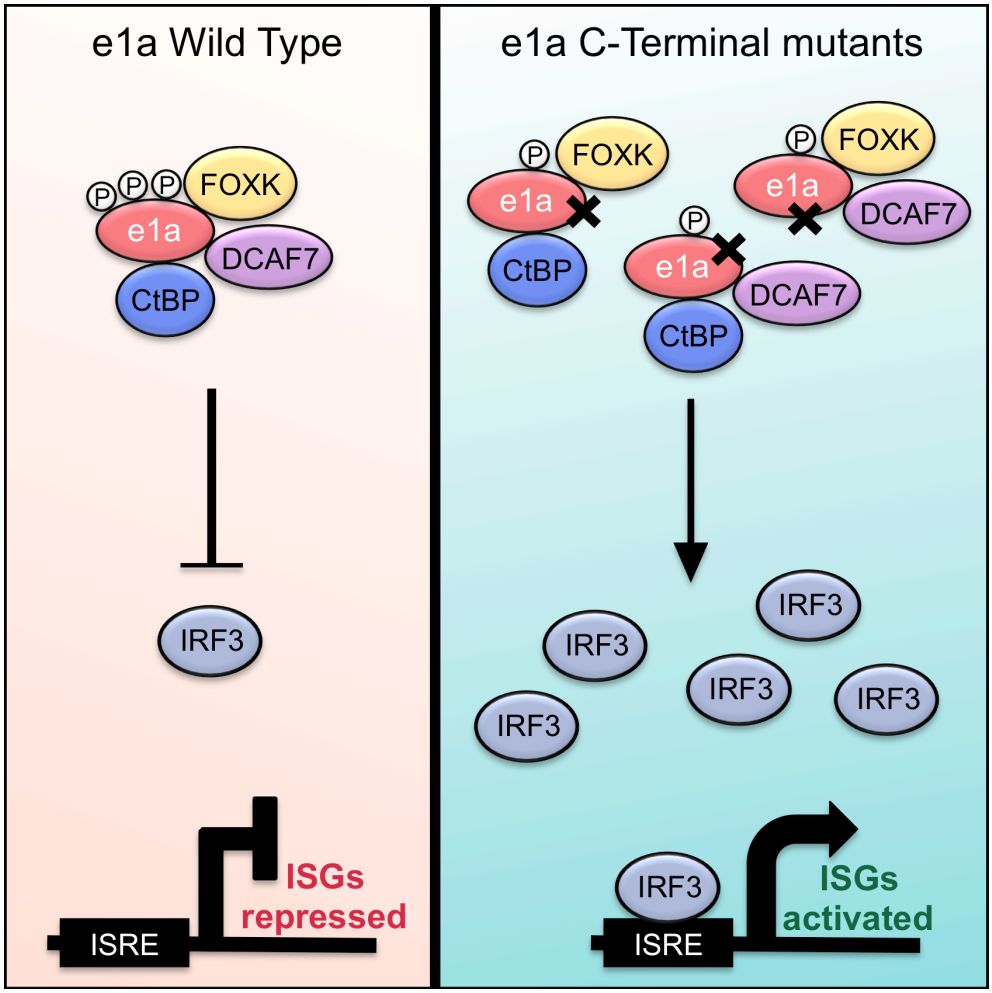

Figure 4.1 Model for a complex of FOXK, DCAF7, CtBP and e1a in regulation of IRF3 activation of a subset of ISGs

Similarly to the genes activated by mutations in e1a's C-terminal region, the genes repressed by these mutations had a high degree of overlap between the three different e1a C-terminal mutants (Fig. 2.4C,D). Surprisingly, these genes are enriched for the *HRAS* oncogenic signature. Repression of the Ras pathway by these mutants was unexpected considering oncogenic Ras cooperative co-transformation assays with e1a C-terminal mutants result in a larger number of transformed colonies compared to WT e1a (Boyd et al., 1993). Perhaps the C-terminal mutations increase the number of transformed foci in e1a-G12V *HRAS* co-

transformation assays (Boyd et al. 1993; Cohen et al. 2013) because they lower gene activation by oncogenic RAS to a level that is more compatible with cell survival and replication. In this regard, it is well-established that high level RAS signaling induces senescence (Serrano et al., 1997).

Cells coinfected with all three e1a C-terminal mutant expressing Ad vectors caused increased expression of *IFIT2*, *ISG15* and *OASL* similarly to infections with any of the individual mutants (Fig. 2.5B, 2.7A). This observation suggests that all three e1a C-terminal binding events must occur on the same e1a molecule to prevent induction of these ISGs. Some evidence supporting a multimeric e1a C-terminal region complex comes from a proteomic analysis of DYRK1A and DYRK1B complexes in the E1A expressing HEK293 cells (Varjosalo et al., 2013). The authors detected FOXK1 and CtBP2 as well as other major E1A binding proteins such as p300, RBs and p400 in complexes with DYRK1A and DYRK1B. In support of a possible multimeric complex with e1a and its C-terminal region binding partners, these proteins partially co-elute in size exclusion gel filtration column fractions from infected HeLa cell nuclear extract (Fig. 2.6B). Additionally, p300-associated e1a complexes were distinct from those containing FOXK1 and CtBP1, while DCAF7 and DYRK1A eluted in all e1a-containing fractions. Also, phosphorylation of e1a Ser89 causing a reduction in mobility in SDS-PAGE, varied between size-fractionated complexes (Fig. 2.6B). These results indicate that there are multiple different e1a-containing complexes in the cell, probably with distinct functions.

e1a co-eluting with FOXK1 was hyperphosphorylated (Fig. 2.6B, upper band), consistent with the notion that FOXKs bind e1a through their FHA domains that bind phosphoserine/threonine (Li et al., 2000). DYRK1A was recently reported to phosphorylate E1A in vivo (Glenewinkel et al., 2016). Consequently, the decrease in the slower migrating form of

e1aDCAF7b^{-} may be explained if one or more of the protein kinases associated with the DCAF7 complex, DYRK1A, DYRK1B, or HIPK2, is responsible for phosphorylating e1a Ser89.

Since our list of 52 e1a C-terminal mutant induced genes had a high degree of overlap with genes activated by the U-ISGF3 complex generated very late in response to β-interferon (Cheon and Stark, 2009; Cheon et al., 2013) (Fig. 2.9A), we asked if U-ISGF3 components, U-STAT1, U-STAT2 and IRF9, increase following expression of e1a C-terminal mutants. Indeed, we found much higher levels of these proteins in cells expressing the e1a C-terminal mutants (Fig. 2.10A). However, the e1a C-terminal mutants continued to induce these ISGs in IRF9 mutant cells. We found that another IRF, IRF3, was necessary, as a siRNA KD of IRF3 prevented activation of these ISGs (Fig. 2.10C,D). IRF3, STAT1/2 and IRF9 proteins increased greatly, yet the mRNAs encoding them did not increase more than 2-fold (Fig. 2.13B). IRF3 was found to increase as a result of protein stabilization in cells expressing e1aDCAF7b-. Similarly, the e1a C-terminal binding mutants may influence the stability of IRF9 and STAT1/2 proteins.

Relevant to our observation that the e1a C-terminal mutant induces stabilization of IRF3, IRF3 stability is regulated by polyubiquitinylation by the E3 ubiquitin ligase RAUL (a.k.a. UBE3C). RAUL activity is increased by the Kaposi's sarcoma virus protein RTA to suppress an innate immune response (Yu and Hayward, 2010). Adenovirus e1a may also be regulating an IRF3 ubiquitin ligase by a mechanism dependent on all three C-terminal interactions to prevent IRF3 protein from accumulating in response to adenovirus infection. Interestingly, an analysis of the interacting partners of e1aWT and all three e1a C-terminal binding by Multi-Dimensional Protein Identification Technology (MuDPIT), applying mass spectrometry to immunoprecipitated e1a complexes from A549 cell extracted previously infected with our mutant Ad5 vectors, revealed that the most significantly decreased protein with all three e1a C-

terminal mutants compared to e1aWT is DCAF10, a substrate receptor for the CUL4-DDB1 E3 ubiquitin-protein ligase complex (Table 4-1).

	e1aWT A	e1aWT B	Mock A	Mock B	FOXKb-A	FOXKb-B	DCAF7b-A	DCAF7b-B	CtBPb-A	CtBPb-B
DCAF10	36	38	0	0	1	0	0	0	0	0

Table 4.1 MuDPIT of indicated e1aWT or e1a C-terminal binding mutant immunocomplexes with DCAF10 in duplicate (replicate A or B). Numbers represent normalized spectral counts.

It is not immediately obvious how e1a interactions with FOXK, DCAF7 and CtBP prevent the stabilization of transcription factors that activate a restricted set of ISGs. However, a recent RNAi screen in *Drosophila* revealed that *D.m.* FOXK1 is required for activation of antiviral genes following infection with RNA viruses in both *Drosophila* and mammalian cells (Panda et al., 2015). Relevantly, depletion of FOXK1 by siRNA knockdown in U2OS cells reduced expression from a virus-inducible ISRE-luciferase reporter. FOXK1 transcriptional activation of ISRE-containing promoters could be a direct link between e1a's FOXK binding and regulation of a subset of ISGs.

Downregulation of some ISGs by e1a has been attributed to its ability to bind the H2B E3 ubiquitin ligase complex hBre1/RNF20 via an N-terminal region including aa 4-25, inhibiting H2B ubiquitinylation (Fonseca et al., 2012). However, it is unlikely that the mutations made in e1a's C-terminal region affect its ability to bind hBre1 via amino acids 4-25. Another recent report suggested that e1a's C-terminal region binding to RuvBL1 contributes to the suppression of ISG activation (Olanubi et al., 2017). However the e1a mutants that were defective in RuvBL1 binding also have disrupted FOXK and DYRK1A binding (Komorek et al., 2010).

It is remarkable that these e1a mutants, defective for binding different host proteins with no known overlapping functions, result in a similar phenotypic cellular response. One unifying feature shared among these e1a mutants is their hypophosphorylation. The phosphorylation(s)

absent in the three e1a C-terminal mutants might be required for e1a to form a complex that counteracts the increase in IRF3 and subsequent ISG activation. The mechanism by which these hypophosphorylated e1a C-terminal mutants activate a late IFN response by increasing IRF3 protein warrants further exploration.

Ad-transformed HEK293 cells retain the ability to re-differentiate upon E1A elimination

Compromised cellular differentiation is generally observed as cancer progresses, contributing to invasion of surrounding tissues and metastasis. E1A inhibition of differentiation has been appreciated for decades (Webster et al., 1988) and may be a useful model for understanding molecular mechanisms causing de-differentiation during oncogenic transformation, just as studies of E1A helped uncover control of cell cycling by the family of E2F transcription factors and the small family of retinoblastoma proteins that regulate them. The observation that E1A represses primarily cell type-specific genes in different primary human cells (Fig. 3.1A) led us to ask if removing E1A from a de-differentiated E1A-expressing transformed human cell line would reverse de-differentiation and activate cell type-specific gene expression. We found that when E1A was knocked-down to <1% the level in transformed human embryonic kidney HEK293 cells (Graham et al., 1977), thousands of genes were de-repressed resulting in gene expression most similar to mesenchymal stem cells (MSCs) and slightly less similar to fibroblasts which have similar gene expression to MSCs (Driskell and Watt, 2015) (Fig. 3.1E). This result demonstrates that HEK293 cells harbor the "memory" to re-differentiate even after hundreds of generations of E1A-induced de-differentiation. It appears that after elimination of E1A, the cells revert back to a gene expression program and morphology similar to the most

abundant cell type in the originally transfected embryonic kidney culture (Graham et al., 1977), an MSC (Little and McMahon, 2012).

YAP/TAZ inactivation promotes de-differentiation of Ad-transformed cells

The present study reveals that YAP and its paralog TAZ are inactivated by E1A in adenovirus-infected and transformed mammalian cells. The requirement for YAP/TAZ for maintenance of the normal morphology and actin-cytoskeleton of primary IMR90 fibroblasts and HBTEC epithelial cells (Fig. 3.11), and for re-differentiation of HEK293 cells when E1A is eliminated (Fig. 3.9E), together with the inactivation of YAP/TAZ by E1A can explain the block to differentiation in adenovirus transformed cells.

YAP/TAZ association with TEAD TFs establishes MSC-specific super-enhancers

The mechanism of YAP/TAZ-dependent re-differentiation of HEK293 cells after removal of E1A was investigated. We observed that after release from cytoplasmic anchors by E1AKD, YAP/TAZ associate with enhancers, as previously reported (Galli et al., 2015; Stein et al., 2015). However, by comparing sites of H3K27/18ac, chromatin accessibility, and YAP-association, together with RNA expression in response to YAP/TAZ activation by E1AKD in HEK293 cells, we could discern that >90% of MSC-specific enhancers are bound by YAP. YAP/TAZ knock-down showed that most of the increase in transcription from these genes requires active YAP/TAZ. This activates MSC and fibroblast (closely related to MSC (Driskell and Watt, 2015))-specific genes (Fig. 3.2C, 3.3F, 3.1E, 3.10). Upon recruitment to the nucleus following E1AKD, YAP associates with TEAD family DNA-binding proteins (TEAD1 through TEAD4), primarily distal to promoters, and induces H3K27/18ac and chromatin opening as detected by

accessibility to Tn5 transposase through ATAC-seq (Fig. 3.5H,I, 4.2). After 1 day of E1AKD there was a large increase in H3K27/18ac neighboring TEAD/YAP peaks, while after 4 days, acetylation spread between closely spaced peaks establishing super-enhancers (Fig. 3.5H). Interestingly, TEAD4, the most highly expressed TEAD family transcription factor in HEK293 cells, and H3K4me1 were detected at many of these YAP-dependent enhancer sites prior to E1AKD (Fig. 3.5H,I, 3.6A,B). Therefore, TEAD4 and H3K4me1 mark these inactive enhancers prior to YAP association. Furthermore, the association of TEAD4 at chromatin sites inaccessible to ATAC before E1AKD suggests a possible pioneer function for TEAD4 (Zaret and Mango, 2016). The gain in YAP-binding and chromatin accessibility after E1AKD correlated with a shift in the peak of H3K4me1-marked nucleosomes from centered over the TEAD4 peak to adjacent sites ~200-300 bp away, indicative of chromatin remodeling (Fig. 3.6A,B). We also observed YAP/TAZ- dependent cohesin association with these newly established super-enhancers (Fig. 3.8C,E), suggesting looping of an activated enhancer to its activated promoter.

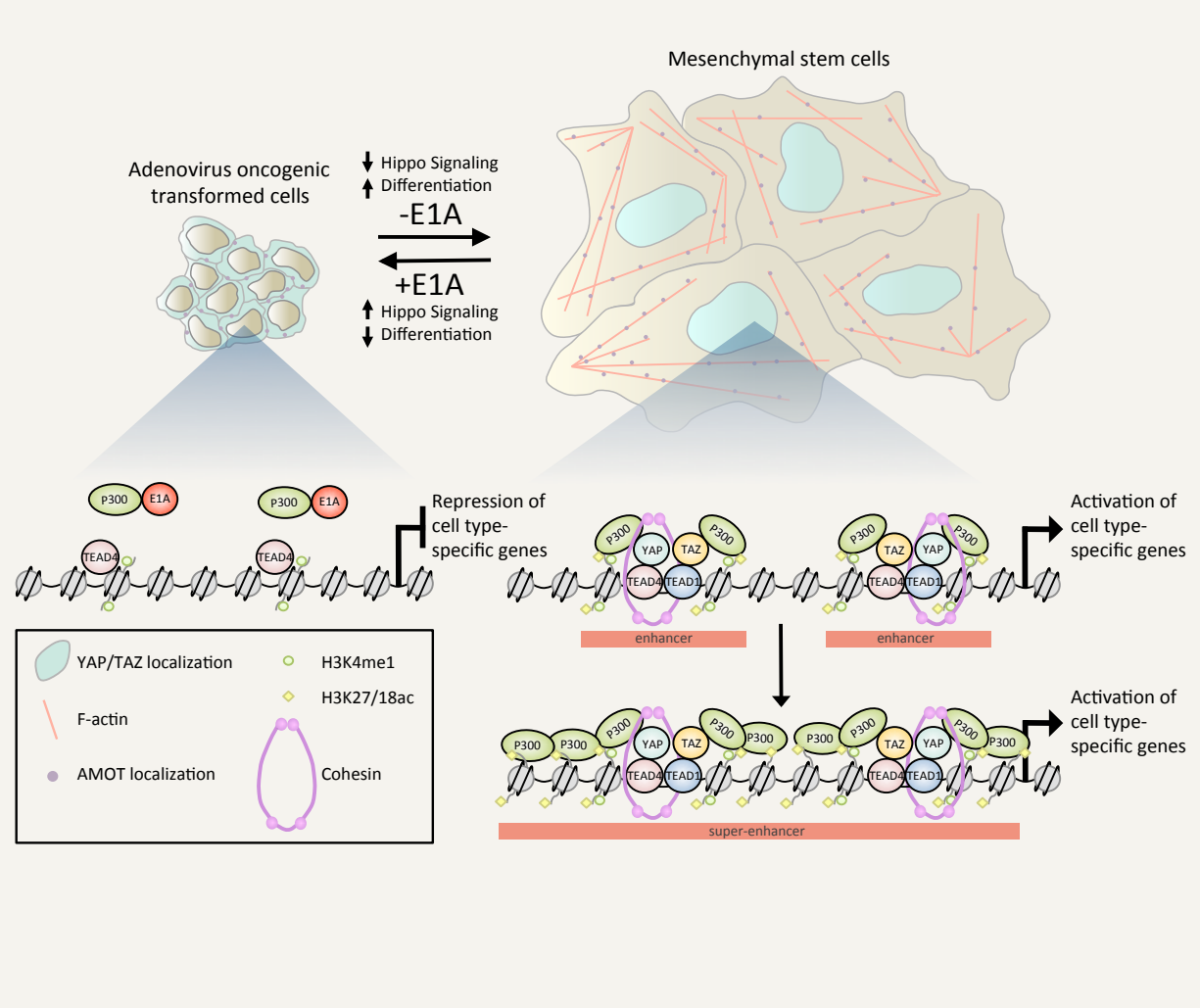

Figure 4.2 Model for E1A repression of cell type-specific genes to suppress differentiation in adenovirus transformed cells.

While KD of E1A causes a dramatic alteration in the morphology of HEK293 cells (Fig. 3.2D), knocking down YAP and TAZ in addition to E1A prevents this. Since YAP/TAZ are activated through sensors of the physical cellular microenvironment and control expression of genes necessary for differentiation, YAP/TAZ form a molecular link between a cell's spatial orientation within a tissue and its cellular identity. This link provides the potential for YAP/TAZ to transduce the necessary signals for a cell to undergo differentiation only after it senses a suitable physical environment (Fu et al., 2017; Sasaki, 2017; Totaro et al., 2018). This provides a

developmental checkpoint to prevent differentiation if a cell is not in the correct cellular and ECM environment.

Indirect regulation of YAP/TAZ nuclear import by E1A

Given the reliance on actin filaments for YAP activation in E1AKD293 cells, we propose that E1A inactivates YAP/TAZ indirectly by repressing actin genes (e.g. *ACTA1*, *ACTA2*, *ACTG1*, *ACTB*, and *ACTBL2*) and genes which stimulate actin filament assembly (e.g. *CDC42EP3* and *CDC42EP5*). Also, stimulation of cortical actin fiber assembly by dominant-active RhoA Q63L induced nuclear YAP in HEK293 cells without reducing E1A-expression (Fig. 3.7D). This explains how E1A regulates YAP/TAZ nuclear localization without interacting with them directly.

Recently Elosegui-Artola et al. (2017) indicated that the mechanism regulating nuclear import of YAP through mechanotransduction may involve generation of force by actomyosin fibers between focal adhesions and the nucleus, causing nuclear stretching that expands the cytoplasmic side of nuclear pores, reducing mechanical resistance to YAP import. Consistent with this, in E1AKD HEK293, we observe flattened nuclei that coincide with increased YAP nuclear import (Fig. 3.2D). Another recent report (Meng et al., 2018) ascribes regulation of YAP import by mechanotransduction to the small GTPase RAP2. At low ECM stiffness, RAP2-GTP activates LATS1/2, which phosphorylate YAP/TAZ causing their cytoplasmic sequestration. RAP2-GTP may be very low in E1AKD293 cells because of the low level of actin filaments, resulting in very low phospo-LATS1 (Fig. 3.7A) and YAP/TAZ nuclear localization.

YAP/TAZ activity required for most H3K27/18 acetylation

It is remarkable that knock-down of YAP and TAZ prevented the increase in total cell H3K27/18ac in HEK293 cells when E1A was knocked down (Fig. 3.9C). E1A has been considered to be a direct inhibitor of p300/CBP acetyltransferase activity, in part because the in vitro histone acetyltransferase activity of CBP was inhibited by recombinant E1A (Chakravarti et al., 1999). The reduction in total cell H3K27/18ac caused by E1A to ~30% the level in control cells also is consistent with the model of direct inhibition of CBP/p300 acetyl transferase activity by E1A (Ferrari et al., 2014; Horwitz et al., 2008). However, E1A K285 near the C-terminus is acetylated by CBP (Zhang et al., 2000), so the in vitro inhibition may have been competitive rather than allosteric. Also, E1A binds to the CBP TAZ2 domain (Ferreon et al., 2009) which is far from the CBP acetyltransferase domain (Delvecchio et al., 2013). Consequently, it is unclear how the E1A-CBP TAZ2 domain interaction would inhibit CBP acetyltransferase activity. We considered the model that E1A-binding to the CBP TAZ2 domain holds the E1A acetylation site(s) at high local concentration to the acetyltransferase catalytic domain, increasing competitive inhibition. However, mutations of K285 or all three E1A lysines, to alanine or arginine had no effect on E1A's inhibition of total cell H3K27/18ac (DG, AJB, unpublished results).

Two alternative related possible explanations for E1A-induced H3K27/18 hypoacetylation are raised by our observations: (1) most H3K27/18 acetylation in primary mammalian cells results from co-activator interactions with the YAP and TAZ activation domains as opposed to activation domains of all other TFs, or (2) YAP/TAZ may be required to initiate differentiation programs involving additional transcription factors that together result in

most H3K27/18ac. In either case, YAP/TAZ appear to be master regulators of MSC differentiation since they are required for the re-differentiation of E1AKD293 cells into MSC-like cells, and associate with ~90% of the new H3K27/18ac peaks that appear when re-differentiation is induced by E1AKD.

Functional differences between YAP and TAZ

YAP and TAZ share 46% identical and 60% similar sequence, both interact with DNA-bound TEAD TFs through similar interfaces (Kristal Kaan et al., 2017), and both are overexpressed individually (i.e. YAP but not TAZ, or TAZ but not YAP) in a variety of human cancers (Zanconato et al., 2016). However, the two proteins have distinctive features and probably activities (Wang et al., 2009). For example, both contain WW domains that mediate protein–protein interactions with LATS1/2 and AMOTs, but YAP contains two tandem WW domains, whereas TAZ has only one. An important example of the non-equivalence of YAP and TAZ was recently reported in a mouse model for basal cell carcinoma (BCC), the most common human cancer (Maglic et al., 2018). In this mouse model where BCC is initiated by abnormal Hedgehog-signaling, YAP becomes over-expressed in the emerging BCC cells. Importantly, YAP, but not TAZ, is required for initiation and progression of BCC (Maglic et al., 2018).

Plouffe et al. (2018) recently reported on deletion of YAP, TAZ, and both genes in a subline of 293 cells (293A). The effects of these gene deletions on the response to lysophosphatidic acid (LPA) demonstrated that YAP and TAZ are not completely functionally redundant as we observe in response to elimination of E1A from HEK293 cells. Although far fewer genes were significantly activated >2-fold by LPA in 293A cells (4 genes) than by knock-down of E1A in HEK293 cells (2584 genes), their results showed that LPA activation of

AMOTL2 and *FOSL1* was much more dependent on YAP than TAZ, as we also observed following de-repression by removal of E1A (Table S1). Moreover, far more genes were highly dependent (5-fold) on YAP and/or TAZ during re-differentiation of E1AKD293 cells (336 genes) than during the LPA response in 293A cells (6 genes), and the extent of de-repression for many genes was far greater (several hundred-fold). Consequently, the phenomena we observe in E1AKD293 cells are very different than the LPA response in 293A cells (Plouffe et al., 2018). The observation that genes highly dependent on YAP for their transcription in re-differentiating E1AKD293 cells and genes highly dependent on TAZ only partially overlap (Fig. 3.10) is relevant to the increased tumorigenicity of YAP compared to TAZ in the BCC model (Maglic et al., 2018). Genes strongly dependent on YAP but not TAZ with gene ontology term "positive regulation of cell proliferation" include *FOSL1, FGF18*, and *Endothelin 1*, a peptide that regulates cell proliferation, survival, motility, and angiogenesis (Battistini et al., 1993). TAZ and YAP likely compete for association with DNA-bound TEAD TFs since they bind the same surface of the TEADs. Consequently, the overexpression of YAP observed in many human cancers (Pan, 2013; Zanconato et al., 2016) may contribute to tumor progression by promoting expression of these genes that stimulate cell proliferation. Increased expression of these genes is not sufficient to cause cell cycling in E1AKD293 cells, probably in part because Rb proteins become active when E1A is eliminated. However, in tumor cells with inactive *RB1* (Hanahan and Weinberg, 2000), over-expression of these YAP-activated genes may contribute to progression of the oncogenic phenotype.

Bibliography

Battistini, B., Chailler, P., D'Orléans-Juste, P., Brière, N., and Sirois, P. (1993). Growth regulatory properties of endothelins. Peptides *14*, 385–399.

Boyd, J.M., Subramanian, T., Schaeper, U., La Regina, M., Bayley, S., and Chinnadurai, G. (1993). A region in the C-terminus of adenovirus 2/5 E1a protein is required for association with a cellular phosphoprotein and important for the negative modulation of T24-ras mediated transformation, tumorigenesis and metastasis. EMBO J. *12*, 469–478.

Braun, T., Bober, E., and Arnold, H.H. (1992). Inhibition of muscle differentiation by the adenovirus E1a protein: Repression of the transcriptional activating function of the HLH protein Myf- 5. Genes Dev. *6*, 888–902.

Chakravarti, D., Ogryzko, V., Kao, H.Y., Nash, A., Chen, H., Nakatani, Y., and Evans, R.M. (1999). A viral mechanism for inhibition of P300 and PCAF acetyltransferase activity. Cell *96*, 393–403.

Cheon, H., and Stark, G.R. (2009). Unphosphorylated STAT1 prolongs the expression of interferon-induced immune regulatory genes. Proc. Natl. Acad. Sci. U. S. A. *106*, 9373–9378.

Cheon, H., Holvey-Bates, E.G., Schoggins, J.W., Forster, S., Hertzog, P., Imanaka, N., Rice, C.M., Jackson, M.W., Junk, D.J., and Stark, G.R. (2013). IFNβ-dependent increases in STAT1, STAT2, and IRF9 mediate resistance to viruses and DNA damage. EMBO J. *32*, 2751–2763.

Cohen, M.J., Yousef, A.F., Massimi, P., Fonseca, G.J., Todorovic, B., Pelka, P., Turnell, A.S., Banks, L., and Mymryk, J.S. (2013). Dissection of the C-terminal region of E1A redefines the roles of CtBP and other cellular targets in oncogenic transformation. J. Virol. *87*, 10348–10355.

Delvecchio, M., Gaucher, J., Aguilar-Gurrieri, C., Ortega, E., and Panne, D. (2013). Structure of the p300 catalytic core and implications for chromatin targeting and HAT regulation. Nat. Struct. Mol. Biol. *20*, 1040–1046.

Driskell, R.R., and Watt, F.M. (2015). Understanding fibroblast heterogeneity in the skin. Trends Cell Biol. *25*, 92–99.

Ferrari, R., Gou, D., Jawdekar, G., Johnson, S.A., Nava, M., Su, T., Yousef, A.F., Zemke, N.R., Pellegrini, M., Kurdistani, S.K., et al. (2014). Adenovirus small E1A employs the lysine acetylases p300/CBP and tumor suppressor Rb to repress select host genes and promote productive virus infection. Cell Host Microbe *16*, 663–676.

Ferreon, J.C., Martinez-Yamout, M.A., Dyson, H.J., and Wright, P.E. (2009). Structural basis for

subversion of cellular control mechanisms by the adenoviral E1A oncoprotein. Proc. Natl. Acad. Sci. U. S. A. *106*, 13260–13265.

Fonseca, G.J., Thillainadesan, G., Yousef, A.F., Ablack, J.N., Mossman, K.L., Torchia, J., and Mymryk, J.S. (2012). Adenovirus evasion of interferon-mediated innate immunity by direct antagonism of a cellular histone posttranslational modification. Cell Host Microbe *11*, 597–606.

Fu, V., Plouffe, S.W., and Guan, K.L. (2017). The Hippo pathway in organ development, homeostasis, and regeneration. Curr. Opin. Cell Biol. *49*, 99–107.

Galli, G.G., Carrara, M., Yuan, W.C., Valdes-Quezada, C., Gurung, B., Pepe-Mooney, B., Zhang, T., Geeven, G., Gray, N.S., de Laat, W., et al. (2015). YAP Drives Growth by Controlling Transcriptional Pause Release from Dynamic Enhancers. Mol. Cell *60*, 328–337.

Glenewinkel, F., Cohen, M.J., King, C.R., Kaspar, S., Bamberg-Lemper, S., Mymryk, J.S., and Becker, W. (2016). The adaptor protein DCAF7 mediates the interaction of the adenovirus E1A oncoprotein with the protein kinases DYRK1A and HIPK2. Sci. Rep. *6*, 28241.

Graham, F.L., Smiley, J., Russell, W.C., and Nairn, R. (1977). Characteristics of a human cell line transformed by DNA from human adenovirus type 5. J. Gen. Virol. *36*, 59–74.

Hanahan, D., and Weinberg, R. (2000). The Hallmarks of Cancer. Cell *100*, 57–70.

Horwitz, G.A., Zhang, K., McBrian, M.A., Grunstein, M., Kurdistani, S.K., and Berk, A.J. (2008). Adenovirus small e1a alters global patterns of histone modification. Science *321*, 1084–1085.

Ikushima, H., Negishi, H., and Taniguchi, T. (2013). The IRF family transcription factors at the interface of innate and adaptive immune responses. Cold Spring Harb. Symp. Quant. Biol. *78*, 105–116.

Iwafuchi-Doi, M., and Zaret, K.S. (2016). Cell fate control by pioneer transcription factors. Development *143*, 1833–1837.

Komorek, J., Kuppuswamy, M., Subramanian, T., Vijayalingam, S., Lomonosova, E., Zhao, L.-J., Mymryk, J.S., Schmitt, K., and Chinnadurai, G. (2010). Adenovirus type 5 E1A and E6 proteins of low-risk cutaneous beta-human papillomaviruses suppress cell transformation through interaction with FOXK1/K2 transcription factors. J. Virol. *84*, 2719–2731.

Li, J., Lee, G.I., Van Doren, S.R., and Walker, J.C. (2000). The FHA domain mediates phosphoprotein interactions. J. Cell Sci. *113 Pt 23*, 4143–4149.

Lin, R., Heylbroeck, C., Pitha, P.M., and Hiscott, J. (1998). Virus-Dependent Phosphorylation of the IRF-3 Transcription Factor Regulates Nuclear Translocation, Transactivation Potential, and Proteasome-Mediated Degradation. Mol. Cell. Biol. *18*, 2986–2996.

Little, M.H., and McMahon, A.P. (2012). Mammalian kidney development: Principles, progress, and projections. Cold Spring Harb. Perspect. Biol. *4*, 3.

Maglic, D., Schlegelmilch, K., Dost, A.F., Panero, R., Dill, M., Calogero, R.A., and Camargo, F.D. (2018). YAP-TEAD signaling promotes basal cell carcinoma development via a c-JUN/AP1 axis. EMBO J. e98642.

Olanubi, O., Frost, J.R., Radko, S., and Pelka, P. (2017). Suppression of type I interferon signaling by E1A via RuvBL1/Pontin. J. Virol. JVI.02484-16.

Pan, D. (2013). Hippo signaling in development and cancer. Cancer Res. *73*, 172DUMMY.

Panda, D., Gold, B., Tartell, M.A., Rausch, K., Casas-Tinto, S., and Cherry, S. (2015). The transcription factor FoxK participates with Nup98 to regulate antiviral gene expression. MBio *6*.

Plouffe, S.W., Lin, K.C., Moore, J.L., Tan, F.E., Ma, S., Ye, Z., Qiu, Y., Ren, B., and Guan, K.L. (2018). The Hippo pathway effector proteins YAP and TAZ have both distinct and overlapping functions in the cell. J. Biol. Chem. *293*, 11230–11240.

Sasaki, H. (2017). Roles and regulations of Hippo signaling during preimplantation mouse development. Dev. Growth Differ. *59*, 12–20.

Serrano, M., Lin, A.W., McCurrach, M.E., Beach, D., and Lowe, S.W. (1997). Oncogenic ras provokes premature cell senescence associated with accumulation of p53 and p16(INK4a). Cell *88*, 593–602.

Stark, G.R. (2007). How cells respond to interferons revisited: From early history to current complexity. Cytokine Growth Factor Rev. *18*, 419–423.

Stein, C., Bardet, A.F., Roma, G., Bergling, S., Clay, I., Ruchti, A., Agarinis, C., Schmelzle, T., Bouwmeester, T., Schübeler, D., et al. (2015). YAP1 Exerts Its Transcriptional Control via TEAD-Mediated Activation of Enhancers. PLoS Genet. *11*.

Subramanian, T., Zhao, L. jun, and Chinnadurai, G. (2013). Interaction of CtBP with adenovirus E1A suppresses immortalization of primary epithelial cells and enhances virus replication during productive infection. Virology *443*, 313–320.

Tiainen, M., Spitkovsky, D., Jansen-Dürr, P., Sacchi, A., and Crescenzi, M. (1996). Expression of E1A in terminally differentiated muscle cells reactivates the cell cycle and suppresses tissue-specific genes by separable mechanisms. Mol. Cell. Biol. *16*, 5302–5312.

Totaro, A., Panciera, T., and Piccolo, S. (2018). YAP/TAZ upstream signals and downstream responses. Nat. Cell Biol. *20*, 888–899.

Varjosalo, M., Keskitalo, S., VanDrogen, A., Nurkkala, H., Vichalkovski, A., Aebersold, R., and Gstaiger, M. (2013). The Protein Interaction Landscape of the Human CMGC Kinase Group. Cell Rep. *3*, 1306–1320.

Wang, K., Degerny, C., Xu, M., Yang, X.-J., Wang, K., Yang, X.-J., Degerny, C., and Xu, M. (2009). YAP, TAZ, and Yorkie: a conserved family of signal-responsive transcriptional coregulators in animal development and human disease. Biochem. Cell Biol *87*, 77–91.

Webster, K.A., Muscat, G.E.O., and Kedes, L. (1988). Adenovirus E1A products suppress myogenic differentiation and inhibit transcription from muscle-specific promoters. Nature *332*, 553–557.

Weigel, R.J., and Nevins, J.R. (1990). Adenovirus infection of differentiated F9 cells results in a global shut-off of differentiation-induced gene expression. Nucleic Acids Res. *18*, 6107–6112.

Weigel, R.J., Devoto, S.H., and Nevins, J.R. (1990). Adenovirus 12S E1A gene represses differentiation of F9 teratocarcinoma cells. Proc. Natl. Acad. Sci. *87*, 9878–9882.

Yu, Y., and Hayward, G.S. (2010). The Ubiquitin E3 Ligase RAUL Negatively Regulates Type I Interferon through Ubiquitination of the Transcription Factors IRF7 and IRF3. Immunity *33*, 863–877.

Zanconato, F., Cordenonsi, M., and Piccolo, S. (2016). YAP/TAZ at the Roots of Cancer. Cancer Cell *29*, 783–803.

Zaret, K.S., and Mango, S.E. (2016). Pioneer transcription factors, chromatin dynamics, and cell fate control. Curr. Opin. Genet. Dev. *37*, 76–81.

Zhang, Q., Yao, H., Vo, N., and Goodman, R. (2000). Acetylation of adenovirus E1A regulates binding of the transcriptional corepressor CtBP. Proc. Natl. Acad. Sci. *97*, 14323–14328.